Technical University of Liberec

Faculty of Mechatronics, Informatics and Interdisciplinary Studies

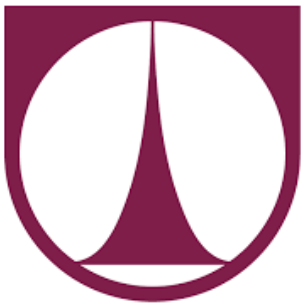

Functionalized Green and Sustainable Sponges based on Tree Gum Kondagogu: Preparation, Characterization, and Applications

Ph.D. Thesis

Liberec 2022 **Rohith Kunjiparambil Ramakrishnan**

TECHNICKÁ UNIVERZITA V LIBERCI
Fakulta mechatroniky, informatiky
a mezioborových studií

Thesis topic: Functionalized Green and Sustainable Sponges based on Tree Gum Kondagogu: Preparation, Characterization, and Applications

Study program: P3942 Nanotechnology

Field of Study: 3942V001 Nanotechnology

Author: Rohith Kunjiparambil Ramakrishnan

Supervisor: Dr. Vinod V.T. Padil, M.Sc., B.Ed., Ph.D.

Workplace: Institute for Nanomaterials, Advanced Technology and Innovation, Technical University of Liberec.

Declaration

I hereby certify, I, myself, have written my Ph.D. thesis as an original and primary work using the literature listed below and consulting it with my thesis supervisor.

I acknowledge that my Ph.D. thesis is fully governed by Act No. 121/2000 Coll., the Copyright Act, in particular Article 60 – School Work.

I acknowledge that the Technical University of Liberec does not infringe my copyrights by using my Ph.D. thesis for internal purposes of the Technical University of Liberec.

I am aware of my obligation to inform the Technical University of Liberec on having used or granted license to use the results of my Ph.D. thesis; in such a case the Technical University of Liberec may require reimbursement of the costs incurred for creating the result up to their actual amount. At the same time, I honestly declare that the text of the printed version of my Ph.D. thesis is identical with the text of the electronic version uploaded into the IS STAG.

I acknowledge that the Technical University of Liberec will make my Ph.D. thesis public in accordance with paragraph 47b of Act No. 111/1998 Coll., on Higher Education Institutions and on Amendment to Other Acts (the Higher Education Act), as amended.

I am aware of the consequences which may under the Higher Education Act result from a breach of this declaration.

Date:

Signature:

Acknowledgements

First and foremost, I would like to thank my respected supervisor, Dr. Vinod V.T. Padil, whose valuable guidance and professional attitude were appreciable in completing this thesis. I thankfully acknowledge the support and inspiration I received from Dr. Miroslav Černík. I am also thankful to Dr Stanisław Wacławek for providing the support to conduct this research work.

I would like to express my heartiest gratitude to Dr. Rani Joseph and Dr. A. V. Ramesh Kumar for introducing this scientific field to me. I also want to thank my colleagues, Daniele Silvestri, Dr. Abhilash Venkateshaiah, and Barbara Socha, for their help during my Ph.D. I thank all the colleagues and the personnel of the Institute for Nanomaterials, Advanced Technology and Innovation who were directly or indirectly involved in the success of this work. I would also like to thank the various projects that supported me during this study.

I am deeply grateful to my parents for their support and encouragement in my academic achievements. Finally, I would like to express my appreciation to my wife Sumitha N. S. for her love and motivational support throughout the research work.

Abstract

Tree gums are natural exudates of various tree species, making up a group of renewable and sustainable polymers. These abundantly available tree gums exhibit good biodegradability, non-toxicity, low cost, good physical and chemical qualities, and functional diversity. Nowadays, their processed exports open an enormous potential for income growth, and their production can promote further economic development and secure rural livelihoods, empower vulnerable groups, including women, and promote integration with natural resource management and climate change mitigation.

For many years, tree gum hydrocolloids have been used extensively in the food industry as stabilizers, thickeners, emulsifiers, and binders. However, only high-grade gums with better purity are suitable for the food industry, and low-grade gums are often discarded. It is a challenge to find a use for these low-grade biowastes, which account for about 60% of all gross production. In recent years, the use of these gums for non-food applications such as medications, energy, and the environment has sparked public attention.

This thesis investigates the potential of sponge fabrication by tree gum kondagogu (*Cochlospermum gossypium*), focusing on their use in environmental applications. Its sustainability, abundant availability, and biodegradability, combined with non-toxicity and low cost make this material suitable for environmental remediation. However, this exudate gum has inherent limitations, including high hydrophilicity, structural stability, and low mechanical properties for stable three-dimensional structures. Different strategies have been employed to overcome these limitations, including crosslinking, silylation, and nanocomposite formations. While the resulting sponges were still biodegradable, their physical and chemical, mechanical, and thermal qualities were vastly improved.

In addition, specific environmental remediation strategies have been evaluated. Hydrophilic gum sponges can be converted into hydrophobic and oleophilic by a simple chemical vapor deposition method and are excellent for selective oil/water separation. Ionically crosslinked sponges retain a low density and highly porous structure, which is highly efficient for dye adsorption. The gum conjugates emphasize the green synthesis of nanoparticles and, at the same time, embed these nanoparticles on the sponges for excellent catalytic application.

To summarize, this work emphasizes the functionalization of tree gum kondagogu-based sponges for environmental applications. The results demonstrate the great future opportunities of tree gum kondagogu for sponge production. In addition, the added value of gum waste may be a useful resource for the development of cutting-edge applications.

Keywords: tree gum kondagogu, sponges, environmental applications, biodegradability

Abstrakt

Stromové pryskyřice jsou přírodní exudáty převážně tropických druhů stromů, které lze považovat za skvělý zdroj obnovitelných a udržitelných polymerů. Tyto hojně dostupné suroviny vykazují dobrou biologickou odbouratelnost, nízkou toxicitu, nízkou pořizovací cenu, dobré fyzikální a chemické vlastnosti a rozmanitost funkčních skupin. Vývoz zpracovaných stromových pryskyřic otevírá v současné době obrovský potenciál pro růst příjmů znevýhodněných komunit a jejich produkce může podpořit hospodářský rozvoj venkova, posílit socioekonomické postavení zranitelných skupin včetně žen, podpořit udržitelný management přírodních zdrojů a přispět ke zmírňováním změny klimatu.

Hydrokoloidy ze stromových pryskyřic se již mnoho let hojně používají v potravinářském průmyslu jako stabilizátory, zahušťovadla, emulgátory a pojiva. Pro potravinářský průmysl jsou však vhodné pouze vysoce kvalitní pryskyřice s vyšší čistotou a nekvalitní pryskyřice jsou často považovány za odpad. Je výzvou najít využití pro tyto méně kvalitní bioodpady, které tvoří přibližně 60 % veškeré produkce. V posledních letech vzbudilo pozornost veřejnosti využití těchto gum pro nepotravinářské účely, např. ve farmacii, energetice a v ochraně životního prostředí.

Tato práce zkoumá potenciál výroby porézních hub z pryskyřice guma kondagogu, jejímž zdrojem je strom *Cochlospermum gossypium*. Zaměřená je na jejich využití v environmentálních aplikacích. Ekologicky udržitelná produkce, hojná dostupnost a biologická odbouratelnost, spolu s nízkou toxicitou a nízkou cenou činí tento materiál vhodným pro použití při sanacích životního prostředí. Tato exudátová guma má však svá inherentní omezení, včetně vysoké hydrofility, nízké strukturní stability a nedostatečných mechanických vlastností pro tvorbu stabilních trojrozměrných útvarů. K překonání těchto omezení byly použity různé strategie, včetně síťování, silylace a tvorby nanokompozitních směsí. Výsledné houby byly

sice stále biologicky odbouratelné, ale jejich fyzikální, chemické, mechanické a tepelné vlastnosti se výrazně zlepšily.

Kromě toho byly vyhodnoceny konkrétní strategie sanace životního prostředí. Hydrofilní polymerní houby mohou být jednoduše přeměněny na lipofilní za pomocí jednoduché metody chemické depozice par a jsou vynikající pro selektivní separaci olej/voda. Iontty zesítěné houby si zachovávají nízkou hustotu a vysoce porézní strukturu, která je vysoce účinná pro adsorpci barviv. Konjugáty gum jsou umožňují ekologickou syntézu nanočástic a zároveň tyto nanočástice ukotvují do porézní houby pro vynikající katalytické vlastnosti.

Souhrnně lze říci, že stěžejním bodem této práce je funkcionalizace polymerních hub na bázi stromové pryskyřice guma kondagogu pro environmentální aplikace. Výsledky ukazují vysokou vhodnost gumy kondagogu pro výrobu polymerních hub. Velkým přínosem je možnost přeměny jinak odpadního materiálu v užitečný nástroj pro vývoj špičkových aplikací.

Klíčová slova: guma kondagogu, polymerní houby, environmentální aplikace, biologická rozložitelnost.

Contents

1. Abbreviations

BET - Brunauer-Emmett-Teller

EMI - Electromagnetic Interference

FAO - Food and Agriculture Organization

FD - Freeze-Drying

HA - Hyaluronic Acid

PCL- Polycaprolactone

PLA- Polylactic Acid

SCD - Supercritical Drying

SEM - Scanning Electron Microscopy

T - Temperature

TD - Thermal Drying

UV - Ultraviolet

BOD - Biological Oxygen Demand

2. Introduction

Lightweight materials with favorable properties have always intrigued the scientific world. The scientific community sees lightweight sponges as a "*future material*". These forms, which are inspired by nature, have a variety of intellectual properties. Research of sponges with superior functional and structural performances has been inspired by the hierarchical natural structure of wood and bones. Over the past nine decades, sponges have grown into a class of very enticing lightweight open cellular structures that have presented both a challenge and an opportunity in advanced chemistry and material science. Research of sponges can help accelerate this exciting development and expand the possibilities for innovative materials and their engineering.

Figure 1. Low-density bio sponge on foxtail grass.

As shown in Figure 1, sponges are macroporous (>50 nm) cells, with a very low density (<100 mg/cm^3), open cellular structure, and very high specific surface area. Sponge structures have common characteristics of reversible compressibility, mechanical integrity, breathability, high porosity, and good fluid absorption capacity, which broadens their practical usage. Such exciting features help to develop a variety of environmental applications. In many publications, the term aerogel has been used to describe sponges.

However, The Gold Book of the International Union's Pure and Applied Chemistry (IUPAC) defines aerogel as a microporous (pore width of less than 2 nm) solid. Nevertheless, the definitions do not necessarily apply to all aspects of advanced open cellular materials. Therefore, such open cellular materials are also called aerogels and foams in the literature.

In the succeeding decades, inorganic sponges [1], carbon-based sponges [2], graphene oxide sponges [3], and organic sponges are often used for environmental purposes. Sponges made of polymers produced from petroleum are utilized in various fields from household cleaning to aerospace applications. Polymers are commonly based on imide [4]–[6], polyurea [7], polystyrene [8], [9], polyurethane [10]–[13], polyethylene [14], [15], polypropylene [16], [17], and polyvinyl alcohol [18], [19]. The characteristics of these sponges make them ideal for many applications, such as tissue engineering, drug delivery, packaging, catalysis, filtration, thermal insulation, supercapacitor, battery applications, and EMI shielding. Synthesis of these polymeric sponges involves expensive equipment, harsh processing, hazardous chemicals, and complex technologies [20], [21]. Furthermore, due to their chemical precursors, non-biodegradability, and hazardous decomposition products. Synthetic polymer-based sponges are inadequate for sustainability. In this context, the importance of sponge fabrication using green and sustainable biopolymers has been revealed.

2.1. Biopolymer Sponges

Recent research of biopolymeric materials for sponge fabrication has focused on more than just petroleum-based materials. The famous concept of sustainability, "*Meeting the needs of the present without compromising the ability of future generations to meet their*

own needs" (Brundtland Commission report, United Nations, 1987), motivates the research of sustainable biopolymeric materials [1]. The biopolymers of chitosan, cellulose, alginate, lignin, gelatin, starch, PLA, and PCL are abundant, non-toxic and highly biodegradable, and suitable for bio-sponges. In addition, biopolymers generally contain an abundance of surface functional groups, allowing them to be functionalized to enhance their inherent properties and expand their applications. Each biopolymer-based sponge seems unique due to its differences in terms of crystallinity, topology, composition, molecular weight distribution, and its peculiar and often multiple gelation mechanisms.

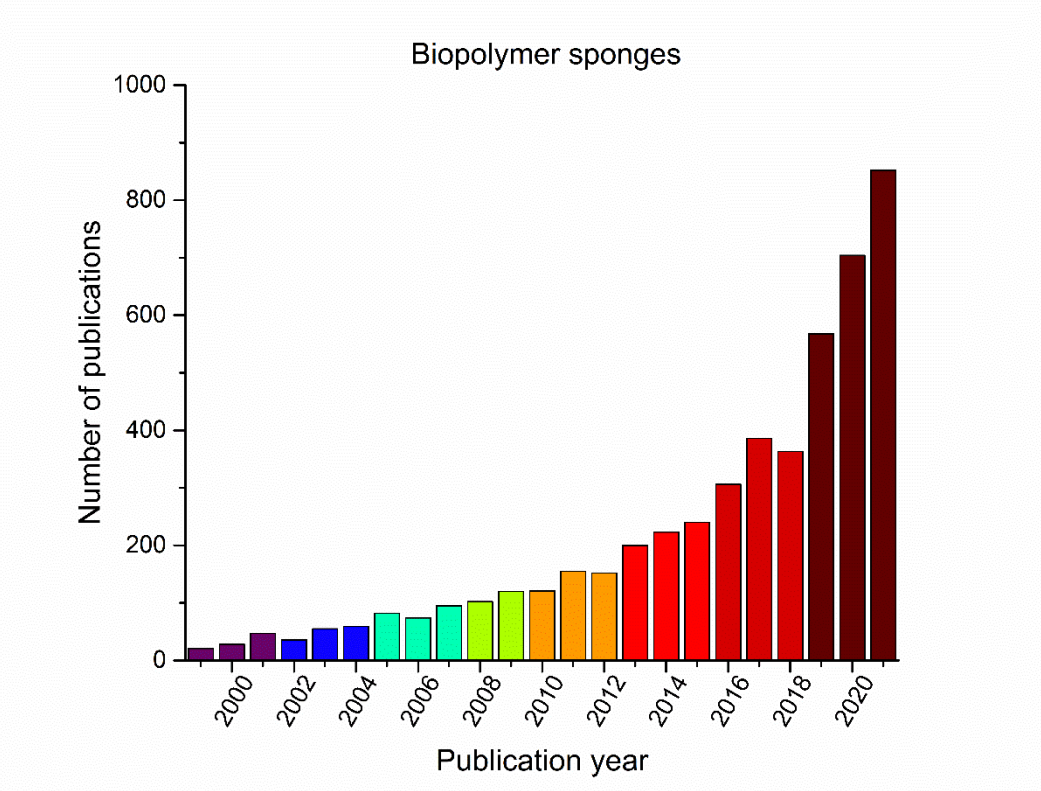

Figure 2. Number of scientific publications (ScienceDirect record) during the last 22 years containing "*Biopolymer sponge*" in the content.

Early in the 1930s, Kistler developed the first aerogels, including a variety of biopolymers comprised of gelatin, cellulose, agar, and albumin [22]. In recent years, the scientific community's interest in biopolymer sponges has significantly accelerated. This is also

evident from the number of publications on biopolymer sponges between 1999 and 2021 (see Figure 2). To date, cellulose, chitosan, alginate, and their derivatives have dominated in open cellular structure research due to their inherent features. Although cellulose sponges make up around half of the articles on biopolymer sponges, research of sponges made from other biopolymers has also performed better. Such reported biopolymer-based sponges are highly porous (90–99%), lightweight (0.07–0.46 g cm^{-3}), and have a high surface area (70–680 m^2 g^{-1}) [23]. Consequently, biopolymer sponges highlight their applications as adsorbents, thermal insulators, catalysts, sensors, drug delivery systems, tissue engineering, and regenerative medicines. Modern research groups have mainly focused on the assemblies and chemical modifications of biopolymer sponges.

The current Ph.D. research thesis is focused on the preparation and functionalization of tree gum-based sponges, which led to publications in four international peer-reviewed journals.

According to my research thesis, significant volumes of tree gums that disintegrate as bio-waste can be turned into an asset with added value in an efficient and affordable manner. In the current study, it was demonstrated that it is feasible to produce a green and sustainable sponge, which demonstrates promising results when used in a variety of environmental remediation processes.

3. Theoretical Part

3.2. Preparation of Sponges

Biopolymer sponges can be produced in two main ways:

i) By the production of colloids from molecules, such as alginate, pectin, or chitosan. In this method, gel structures are generated from biopolymer molecule solutions. The majority of the biopolymers that are used to make bio-sponges have the ability to create molecular colloids, and their solvents can either be water, an organic solvent, or a mixture. The type of interactions created between the polymeric chains determines the gelation kinetics and final structure of biopolymer sponges.

ii) Through the use of abbreviated particle-based precursors, for example, protein nanofiber aggregates, chitin nanofibrils, or nanofibrous cellulose. Here, a colloidal route is used to form the network through controlled aggregation of nano- or microparticles. The resulting gel is most often a physically cross-linked particle network, although chemical crosslinks have also been employed.

For both methods, the properties of the sponge are primarily dictated by the concentration and functional groups of the precursors, the pH of the solution, the type and density of the cross-linkers, the gelation process, and the drying procedure. Commonly, “gelation” refers to the creation of physical entanglements, such as van der Waals force, electronic interactions, hydrogen bonding, and chemical cross-links, which provide a stable structure, adequate swelling, and high rigidity [24]. Depending on the raw materials and desired applications, biopolymer sponges can be manufactured using various techniques, such as the blowing method, the sol-gel process, template growth, freeze drying, self-assembly, and 3D printing.

3.1.1 The Blowing Method

The blowing method is a well-established technique that involves the formation of open or closed cell-shaped polymer foams using physical or chemical blowing agents. The fundamental reaction of this method is the expansion of gas that has been entrapped or chemically produced in a polymer matrix. Baking is considered to be the oldest man-made blowing process. Selection of the blowing agents is depending on the nature of the material and the conditions under which it is applied. In general, these microcellular foams usually have a closed cell structure. The blowing method is used to create a wide range of biobased polymeric porous and cellular structures, which were detailed in a book published by Iannace and Park [25]. For example, alginate cellular structures were developed by Barbetta et al., with a well-defined morphology and interconnected pores using different blowing agents such as pluronic, polyquaternium, sodium dodecylsulfate, tyloxapol, and triton [26]. Sjöqvist & Gatenholm fabricated low-density starch foams with water as a blowing agent [27]. In another study, Zhang et al., elucidated that low-density cellulose aerogels with interconnected pores were obtained with physical (sodium sulfate anhydrous) and chemical (p-toluenesulfonyl hydrazide) blowing agents resulting in a honeycomb structure with excellent oil absorption and oil spillage clean-up properties [28]. Microcellular PLA foams with a high expansion ratio were recently developed using CO_2 as a blowing agent [29]–[31]. Sodium hydrogen carbonate is used as a forming agent for a stable porous scaffold developed from gelatin [32]. In this scenario, the blowing chemicals and their by-products must be compatible with the polymer.

3.1.2 The Sol-Gel Process

The sol-gel process is an important wet chemical synthesis process used to form a spongy structure from hydrocolloids (see Figure 3). The first step is to create a colloidal

suspension by dispersing biopolymers or particles in a dispersing solvent. The solvent used in this step could be water or organic liquids. These hydrocolloids interconnected to form a three-dimensional network (gel) by polycondensation in the presence of a crosslinker or by the physical interaction. The next step is the drying process, which removes the solvent of the gel replaced by air without compromising the structural integrity. The structure of the sponges produced in this way varies mainly depending on the drying method. The three most common drying methods are thermal drying (TD), supercritical drying (SCD), and freeze drying (FD). The TD method is safe and inexpensive for large-scale production, but this method is usually very time consuming and difficult to maintain in 3D structures. This drying process has been used to produce 3D structures with densities of more than 0.1 g cm^{-3}, and it cannot be use with fragile and hydrophilic matrices.

Another form of drying, known as SCD, can be divided into two categories, high temperature SCD (>100 °C and 50-100 atm) and low temperature SCD (31.2 °C and 72.79 atm). The high temperature SCD method is generally incompatible with biopolymers, as the temperature is above 100 °C. Under this condition, the properties of the biopolymers deteriorate, and they react with the solvent creating a high risk of explosion and hazardous contamination. Due to its low supercritical temperature and lack of toxicity, the low-temperature SCD method is frequently employed to build polymeric cellular structures by eliminating solvents with the use of safe and non-flammable supercritical liquid carbon dioxide (CO_2). This method is compatible with all types of biopolymers and is commonly used to produce structurally stable aerogels with nano/macro size pores.[33] In this method, when the drying medium is in the critical condition the gas-liquid interface disappears, and the liquid phase converts to a gas phase without destroying the network structure of hydrogel. Chitin aerogels developed in this way have a very low density

(0.039-0.063 g L^{-1}) and high porosity (84.1-90.2%). Based on these characteristics, the obtained sponges may be used as biomaterials for biomedical applications [34].

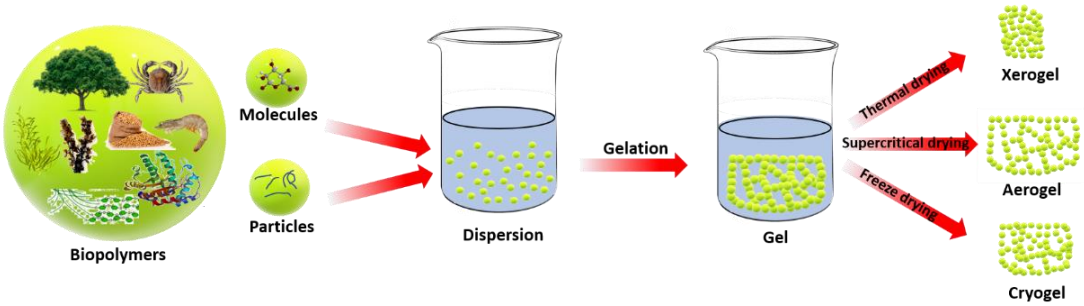

Figure 3. Synthesis of biopolymer sponges through the sol-gel process

In the FD process, the liquid phase of the polymeric gel is frozen to create continuous solvent crystallization, which is subsequently removed by sublimation to make stable sponges. This gives a regular interconnected macroporous morphology with significantly better mechanical integrity. This method is a simple, more economical, and environmentally friendly process than FD and SCD. Drying procedures have a great impact on the final structure and properties of biopolymer sponges such as bulk density, porosities, and pore size distribution. Compared to SCD, the high volume of macroporosity, a significant amount of shrinkage, and low specific surface area are more developed.

3.1.3 The Template Growth Method

Template growth is a method for creating sponges using sacrificial templates. Once the sponge structure has been created, the templates will be removed by one or more possibilities such as etching, leaching, FD, or pyrolysis. The widely used sacrificial templates are made by natural and synthetic polymers, salts, liquids, metals, and ceramics. In the early days, this method was used to make macroporous ceramics. Particulate

leaching is a template-based method for producing tissue engineering scaffolds utilizing biodegradable polymer sponges [35]–[37]. Here, the sponge-forming polymer matrix is mixed with soluble and easily removable particulates and then selectively removed. The porosity and cellular structure are controlled according to the amount of salt and crystallite size [38].

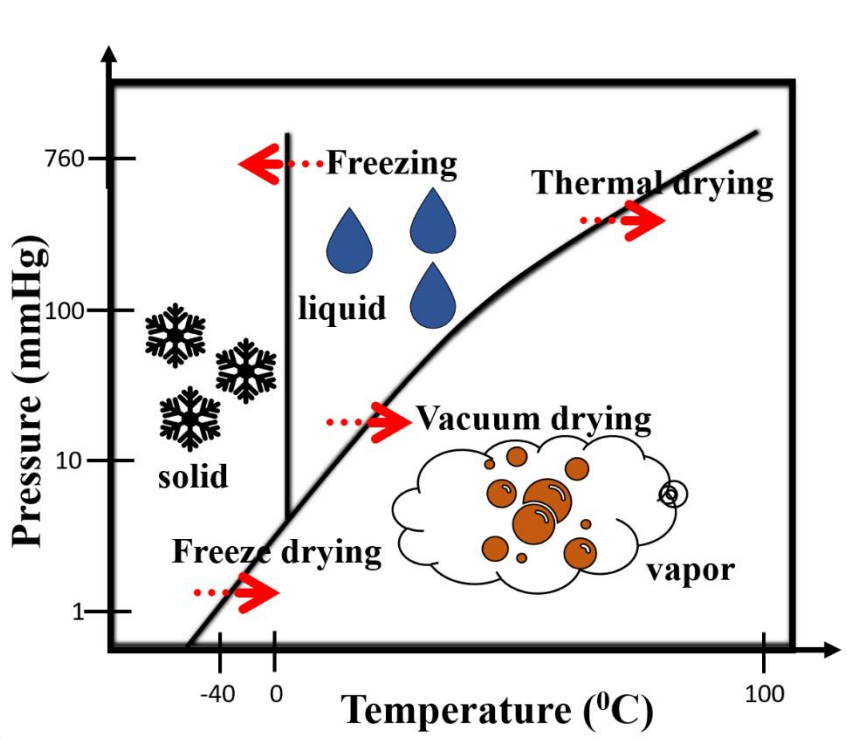

Figure 4. A phase diagram of the temperature-pressure paths for drying.

Ice is utilized as a sacrificial template for biopolymer sponges, and the template is removed by freeze drying once the structure is formed. Such sponges have pore interconnectivity of more than 99%, porosity of up to 95%, and density of 25 mg cm^{-3}. In this method, it is possible to construct ultralight, mechanically strong bio-sponges using renewable resources. The critical characteristics of pore size and morphology are controlled by the freezing temperatures and directly affect the mechanical properties. FD is the most widely used drying method for low-density porous 3D sponges. Its function

is to freeze the polymeric solution at temperatures between -20 °C and -196 °C, allowing ice crystals to grow and subsequent removing the water by lyophilization. For instance, a quick-freezing rate frequently produces small ice crystals, which leads to products with small pore sizes and large pore surface area. On the other hand, a slow freezing rate results in the development of large ice crystals, which produces a sponge with large pore sizes. The typical temperature–pressure phase diagram shown in Figure 4 can be used to explore the drying methods.

3.1.4 The Self-Assembly Method

Self-assembly is another common technique for making sponges with hierarchical pore structures. They can be obtained from nanosheets, nanofibers/microfibers, and zero-dimensional particles. Depending on the raw materials, the driving force for the construction of 3D structures can be hydrogen bonding, electrostatic interactions, or redox reactions. Cellulose, silks, chitins, and peptide molecules contain functional groups, such as hydroxyl groups (-OH) and amide groups (-CONH-), that can form intermolecular H-bond interactions. Self-assembled sponges have a high specific surface area and excellent mechanical properties. Throughout the procedure, nanoparticles and nanofibers in aqueous media consolidate to form nanochains, and the self-assembling network is produced by interconnection and interpenetration. Different one-dimensional fibers, including nanofibers, microfibers, and short electrospun fibers make three-dimensional structures using this method. Moreover, the chemical vapor deposition method is also classified as self-assembly method.

3.1.5 3D Printing

3D printing has recently gained popularity as a viable method for producing spongy materials with a predetermined structure and with a controlled pore size, shape, and interconnectivity. This approach has been widely employed to create 3D structures for biomedical applications such as tissue engineering scaffolds. This method can directly control the micro- and macro-architecture of the 3D structures. The emergence of modern 3D printing techniques using biomaterials such as chitosan, alginate, PLA, and cellulose acetate has already led various research groups to various applications. 3D printing ensures better control over porosity and pore structure. In various 3D printing methods, the direct-inking or gel-inking method is mainly used to produce biopolymer sponges. In this process, the liquid ink is usually a colloidal, nanoparticle-filled, or sol-gel-like biopolymer mixture. After the deposition of a printing ink on a printing board, it undergoes further solidification by gelation, evaporation, or drying. 3D printing has a great potential for the development of bio-based, reusable, custom-optimized, and scalable sponges suitable for biomedical and environmental applications.

There have also been reports of hybrid techniques for creating 3D constructions that combine the sol-gel method, template approach, and self-assembly.

3.2 Properties of Sponges

The characteristics of biopolymer sponges are dictated by the type of precursors used (molecules or the particles), the drying method, the gelation, and the conjugation. The primary properties of sponges include low density, high surface area, microstructure, pore size distribution, mechanical capabilities, and high sorption capacity. As a result of these characteristics, biopolymer sponges have the capability to be employed in a wide variety

of applications. Figure 5 presents an illustration of bio-sponges with the specific critical qualities that are presented here.

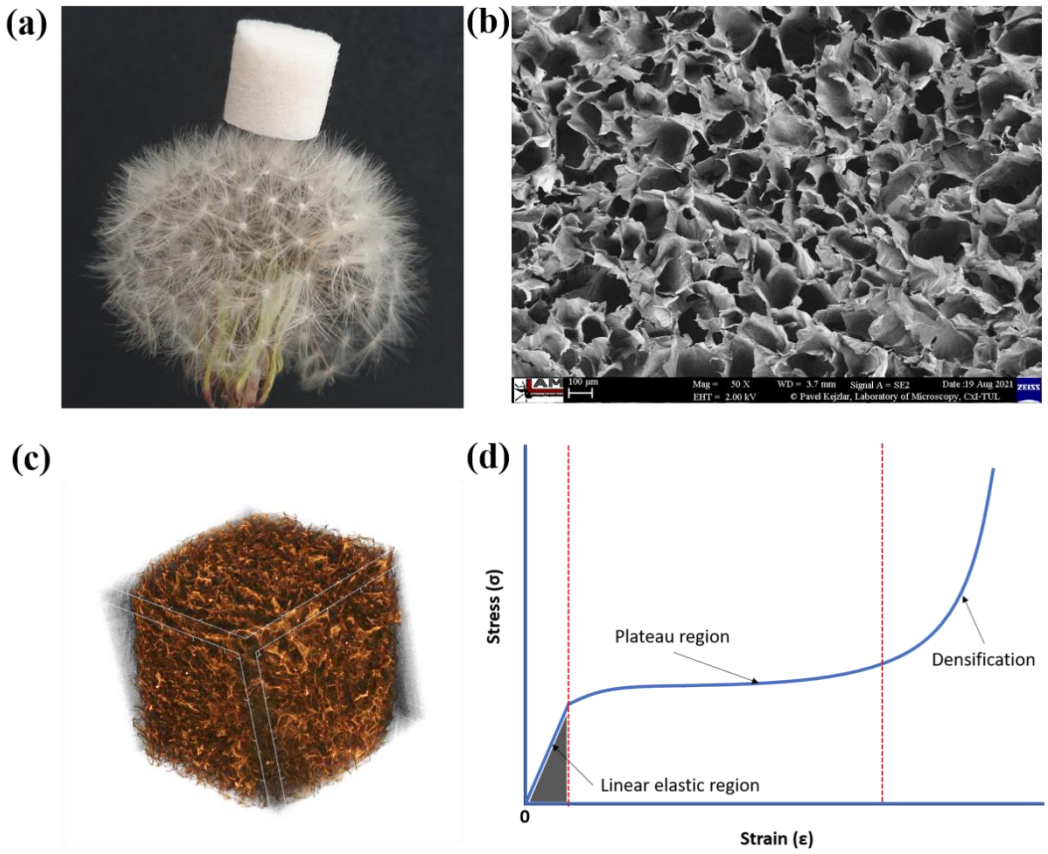

Figure 5. A lightweight sponge on a dandelion flower (a), SEM image (b), Micro-CT image (c) of a sponge and the stress-strain curve of a sponge with important parameters (d).

A sponge's main attraction and most crucial quality is its low density (see Figure 5a). The overall pore sizes of low-density macroporous sponges seem to be large, even though these sponges have relatively small surface areas. In contrast, nano-, meso-, and microporous sponges have a very large surface area, but their pore sizes are relatively small. It mainly depends on the stages of their production process. Such varying pore size profiles can be exploited for applications such as storage capacity, loading capacity,

absorption, drug delivery, and wetting properties. Large porous bio-sponges can usually be produced using the FD method. In addition, it has been observed in many experiments that the porosity of the bio-sponge decreases with increasing density [39], [40]. The sponge's intrinsic properties, such as its dense, interconnected channels, make it very useful for many applications.

Macroscopic inspection reveals differences in the morphology and topology of biopolymer sponges. The scanning electron microscope (SEM) can be used to determine the pore size and shape on the surface of sponges (see Figure 5b), Imaging techniques such as micro-CT allow for the evaluation of information regarding the internal microstructure (see Figure 5c). The highest surface area for biopolymer sponges as determined by Brunauer-Emmett-Teller (BET) is 973 m^2 g^{-1} [41]. The surface area of sponges is an important feature that plays a significant role in determining their capacity for catalysis and adsorption.

Compressive strength has been primarily used to evaluate the mechanical characteristics of biopolymer sponges. In comparison to inorganic aerogels, biopolymer aerogels often exhibit more plastically flexible and less brittle behavior while compressed. The compressive strength of lightweight bio sponges is in the range of roughly 10-100 kPa and is dependent on the type of sponge material as well as its density, pore size, and pore shape. The stress strain curve of sponges is generally divided into three characteristic regions, the elastic region, the plateau region, and the density region (see Figure 5d). The specific compression modulus is calculated from the linear elastic region. Elastic stretching of the cell walls occurs in this region until cell breakdown begins. The plateau region is the buckling of pore cells under stress where the cell failure begins. Finally, there is the densification zone, where stress increases strongly, which is attributed to the complete deformation due to cell collapse and contact with opposing cell walls causing

densification. In addition to these properties, biopolymer sponges also have a low toxicity level, excellent biodegradability, and renewability. All of these aspects provide an extra impetus to the increasing focus on research into biopolymer sponges.

3.3 Functionalization

The properties of biopolymer sponges discussed above make them valuable for a wide range of applications. The main obstacles presented by the application of these materials are brought about by the inherent features of biopolymer sponges, which include their brittleness, high solubility, high moisture absorption, and structural integrity. The physical and chemical properties of bio-sponges can be enhanced by a variety of functionalization techniques. This is facilitated by the presence of an abundant number of active functional groups in the biopolymers. As a result of the improved characteristics of these materials, the scope of potential applications can be expanded when surface functionalization is included into biopolymer sponges.

3.3.1 Crosslinking

There are many restrictions that limit the practical usage of bio-sponges despite their unique qualities and vast range of applications. The colossal concern with bio-sponges is that they do not have enough mechanical properties and are not stable in a variety of water environments [42]. The crosslinking technique has shown to be the most successful method for overcoming these limitations. Bio-sponges may be crosslinked using either chemical crosslinking or physical crosslinking. Different methods, such as UV irradiation, gamma radiation, and hydrothermal treatment, can be used to make physical crosslinks. Chemical crosslinking uses both natural and synthetic crosslinkers, such as calcium chloride, glutaraldehyde, PEG, genipin, etc. [43]. During the crosslinking

process, molecules are interconnected, the molecular weight is increased, and, in general, higher mechanical properties and improved stability are generated. By creating a covalent or ionic bond, biopolymeric the structural stability and compressive strength of spongey materials are enhanced. Crosslinking in alginate sponges is achieved through the use of divalent ions. Techniques like plasma crosslinking and enzymatic crosslinking are also exploited in the process of bio-sponge crosslinking. Moreover, crosslinking affects the chemical and physical properties of biopolymers, which facilitates the application of these materials in environmental fields.

3.3.2 Hydrophobization

The hydrophilicity of biopolymers restricts both their long-term stability and their usefulness in situations with high levels of humidity and aqueous media. Hydrophobization is a strategy that may potentially be used to overcome this obstacle. There are many different methods for hydrophobizing biopolymers. It is possible to apply hydrophobic post-modifications to dry biopolymer sponges in two different ways, either by applying a polymer coating on the surface of the sponge, or by modifying the internal porous surface. The method in which these modifications are applied, however, is primarily determined by the final application that the sponges will be used for. Alkyl siloxanes are responsible for hydrophobizing the vast majority of biopolymer sponges by hydrogen bonding, dipole-dipole interactions, or covalent interactions. Methyltrimethoxysilane, octyltrichlorosilane, trichloro(methyl)silane, 1,1,1,3,3,3-hexamethyldisilazane, etc., are examples of silylation agents used for chemical vapor deposition and simple soaking methods. The cold plasma coating method is a promising solvent-free alternative for the hydrophobization of sponges, in which dry sponges are subjected to cold plasma created by glow discharging a gaseous hydrophobic polymer

under a moderate vacuum. The mechanical strength, heat insulation, and water resistance are improved by these functionalizations. It may represent a good option for inexpensive sponges used for separating oils in water system.

3.3.3 Nanoparticle Templating

The abundance of functional groups serve as an appropriate support or template for the nanomaterials that are immobilized within the microstructure of biopolymer sponges. The immobilization of nanoparticles within the microstructure of sponges can be accomplished in a variety of ways.

1) The nanocomposite formed by mixing nanoparticles with biopolymers can be utilized to create sponges.

2) The green synthesis of nanoparticles employing a mixture of biopolymers and metallic precursors under conditions such as sodium borohydride, plasma, microwave, and room temperature. These nanoparticle dispersions are then converted into sponges.

3) The nanoparticles are incorporated into the pre-shaped sponge via dip coating and spraying, or chemical vapor deposition.

3.3.4 Other Functionalizations

Other functionalizations that can be achieved through methods such as the grafting of functional groups into biopolymers, result in an improvement in both the physical and chemical integrity of the sponges. Bio-sponges that have amino groups grafted onto their surfaces have the potential to improve the dye and heavy metal ion separation and CO_2 capture [44]. Chitosan sponges already have a large number of amino groups in their

structure. However, other types of biopolymer sponges are amine-functionalized by using 3-aminopropyltriethoxysilane (APTES), diethanolamine (DEA), dendrimer-based polyamidoamine (PAMAM), and branching polyethyleneimine (PEI). Other common functionalization techniques for modifying biopolymer sponges for use in biomedical applications include esterification, etherification, selective oxidation, and graft copolymerizations [45].

3.4 Applications

The vast majority of research on biopolymer sponges is still carried out in academic settings, and proof-of-principle has typically only been demonstrated on a limited scale for the majority of biopolymer sponges. In spite of these significant obstacles, biopolymer sponges can be manipulated to exhibit novel combinations of properties that can be tailored to a wide range of applications, and there is a good chance that some of these materials will be successful on a commercial scale.

3.4.1 Environmental Applications

It is necessary to research the possibilities of applying biopolymer sponges in a wide range of environmental contexts (acoustic and thermal insulation, absorption, adsorption, catalysis, active packaging). Screening, choosing, and testing biopolymer sponges should be performed with the intention of using them for applications such as the clean-up of chemical spills, the removal of air and water pollutants, and the detection of contaminants, as well as for thermal and acoustic insulation. Sponge utilization in a vast array of applications, including those relating to the aerospace sector, thermal super insulations, acoustic devices, and so on, has received significant attention from researchers.

Adsorption is the easiest and most economically viable way to remove water pollution. Materials produced from petroleum products are both dangerous and expensive. Natural polymer-based adsorbent sponges reduce the danger of secondary contamination while also being renewable, biodegradable, and biocompatible [46]. Powdered adsorbents have the potential to produce further pollution, which will necessitate the completion of an extra cleaning phase. On the other hand, extremely porous and incredibly lightweight biopolymer sponges have the ability to withstand this excessive contamination [47]. In addition, the wide variety of surface-functionalized biopolymer sponges makes it easier to create binding sites for aqueous pollutants such as heavy metals, cationic and anionic dyes, and other similar substances. When it comes to the catalytic breakdown of organic pollutants, bio-sponges supported by metal nanoparticles offer an extraordinary level of reactivity and a high degree of selectivity. The hierarchical structure of these sponges makes it feasible for reactants to diffuse more easily through pores and channels. In addition, immobilized metal nanoparticles improve the catalytic efficacy of the sponges. Due to the simple methods of their manufacturing, low density, large pore volume and porosity, and exceptional adsorption capacity, bio-sponges that are both hydrophobic and oleophilic have the potential to be the most effective oil absorbents.

3.4.2 Biomedical Applications

The features of biopolymer sponges such as non-toxicity, biodegradability, biocompatibility, and inexpensiveness make them well-suited for biomedical applications. Investigations are being conducted into their potential use in a wide variety of fields, including tissue engineering, drug delivery, healing of internal and external wounds, cancer prevention, diagnosis, and therapy. In the field of tissue engineering, the use of bio-sponges as scaffolds is made possible due to their biocompatibility and

nontoxicity, biodegradability with a controlled breakdown rate, sufficient porosity, and structural integrity. Tissue engineering applications such as biological signaling, cell adhesion, cell proliferation, cell differentiation, cell response degradation, and re-modelling are also promoted.

Biopolymers are frequently used in the production of wound healing materials due to their inherent biocompatibility, low levels of toxicity, and pharmaceutic biological activity. Wound dressing membranes are formed through the dispersion and encapsulation of essential oils, nanoparticles for greater cell adhesion and proliferation, and improved antibacterial and antifungal qualities.

3.4.3 Electrical and Energy Applications

There have been recent developments in the synthesis of sponge nanostructures, with a particular emphasis on their use in the development of high-performance devices for energy conversion and storage. As a result of the superior structural properties that they possesses, sponges are an excellent material for the production of batteries, solar cells, fuel cells, and supercapacitors. The extraordinary properties of sponges, such as their enormous surface area and open porous structure, have a considerable impact on the performance of devices that convert and store energy, and they drive the creation of more sustainable electrochemical devices.

3.5 Materials

Among biopolymers, natural gums are one of the most significant examples of sustainable materials. Due to their ease of extraction, biocompatibility, biodegradability, and nontoxicity, they are the subject of a substantial amount of research [48]. Natural gums can be divided into groups based on the material they are extract from, which may be

trees, seeds, roots, or even microbial fermentation, as shown in Figure 6 [49]–[51]. Non-toxic gums with hydrocolloid properties are widely used in the food industry as thickeners, preservatives, stabilizers, and gelling agents. Likewise, extensive research has been conducted on the use of gums in non-food applications, including pharmaceuticals, coatings, paints, adhesives, membranes, energy harvesting, and oil spills. However, the extraction process of many of the most readily available biopolymers is carried out using complex reactors, harsh solvents, and hazardous chemicals. At the same time, the technique for extracting tree gum biopolymers is quite simple and no hazardous chemicals are used at any stage of the process.

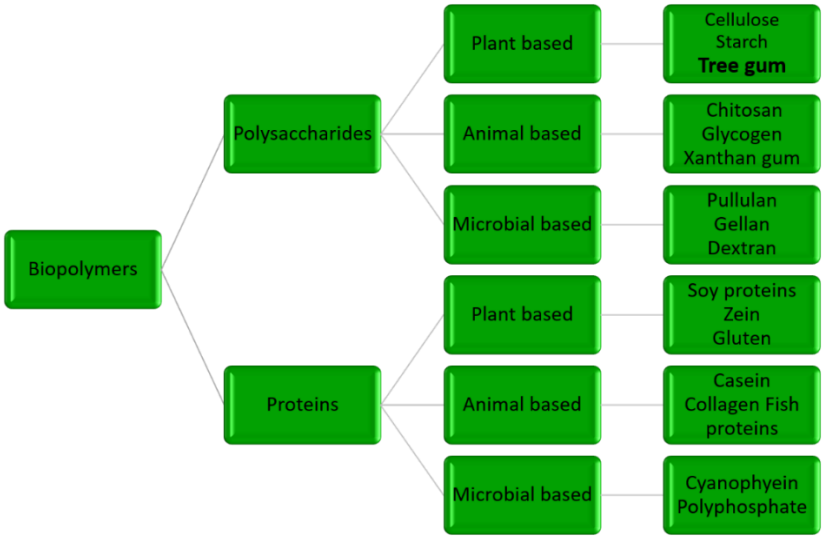

Figure 6: Classifications of biopolymers

3.5.1 Tree Gums

Tree gums are amorphous masses that have the appearance of tears and are extruded from trees and shrubs as a result of tapping or other unexpected causes. They are subjected to a process known as gummosis, which involves drying out in the sun in order to generate a substance that is dense and shiny. The most significant tree gums include gum arabic, gum tragacanth, gum karaya, gum gatti, and gum kondagogu. The use of gum as a source

of nutrition is even mentioned in the Bible. The legendary "*manna from heaven*" that sustained the Israelites as they fled Egypt was most likely an exudate of gum comparable to gum arabic or gum acacia. The tree gums are complex heterogeneous polysaccharides that have exceedingly intricate structures and very high molecular weights. Consequently, gums feature a unique combination of functions and properties that will never be replicated by competing synthetic polymers, rendering their complete replacement unattainable. Moreover, these biopolymers are biodegradable and therefore environmentally friendly. Tropical parts of the world are home to the majority of the world's tree gum producing countries, including Mexico, Sudan, Nigeria, India, Thailand, and Malissa (see Figure 7). The rural areas of these countries see an improvement in their economies as a result of research of the added value of these gums. The cultivation of trees is another beneficial aspect of agroforestry.

Their non-food-related uses in pharmaceuticals, cosmetics, textiles, and lithography, and minor forest products can also be traced back in history. Due to their molecular and supramolecular structure, and intrinsic hydrocolloidal and hydrophilic properties, tree gums and their deacetylated derivative gums have been identified as suitable bioplatforms for future research. The natural availability of tree gums, along with known gelation systems, is subject to chemical and biochemical modifications, establishing a strong foundation for future environmentally friendly practices. The research of such materials also offers the hope of eliminating traditional

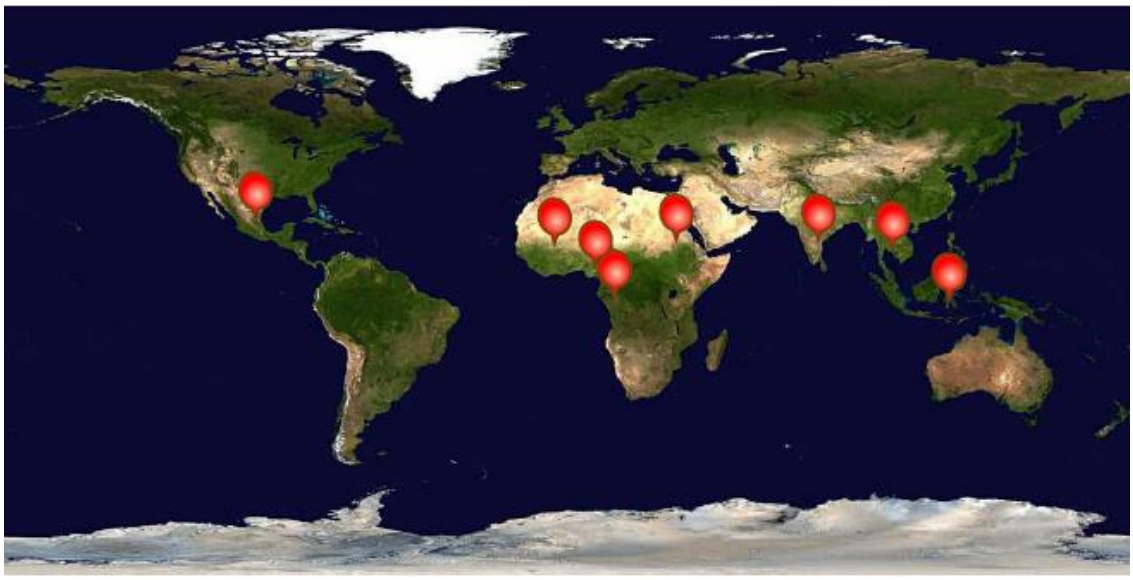

Figure 7. The major tree gums cultivated countries

plastics and completely replacing basic solutions with eco-friendly materials. Gum kondagogu, which has a high fiber content among tree gums, is commercially available today, but its three-dimensional form has yet to be fully unveiled. Such research can undoubtedly result in environmentally friendly structures.

3.5.1.1 Gum Kondagogu

Gum kondagogu(GK), also known by its scientific name *Cochlospermum gossypium*, is an exudate from plants belonging to the family *Bixaceae*. The forests and hilly terrains of tropical regions in the Americas, Africa, and India are the primary habitats for this species. Many economically deprived tribes have found a way to advance economically thanks to the harvesting of GK from plantations and forests. GK is extracted through a natural or artificial stimulant process and preferably collected after drying. According to the classification, the collected gums are divided into three main grades (see Figure 8), which are mainly based on the color (light grey to heavy tan), foreign organic matter (0.5 to 3%), and moisture content. They have been declared to be fit for human consumption by the Food and Agriculture Organization (FAO), Rome, and are included in the list of

food additives (E 416). Only 30–40% of the total output is of Grade I quality, which is mostly utilized in the food and pharmaceutical industries. Simultaneously, Grade II and III quality GKs are employed for additional purposes, but a considerable portion of them end up as biowaste. People have been exploring these biowastes for the last 15 years in order to turn them into value-added goods and various non-food applications. For my research, we procured GK from Girijan Cooperative Corporation in Hyderabad, an Andhra Pradesh government organization, in India. Throughout the entirety of our research, we referred to it as GK.

Figure 8. Classification of tree gum kondagogu granules

GK is a polysaccharide with a complex, partly acetylated, and branching structure. The main structure of the gum is made of galactose (1.2-20%), rhamnose (16.1-22.5%), galacturonic acid units (24-29%), and some of the side chains (30-45%) contain glucuronic acid [52]. The weight-average molecular weight (Mw) of native gum and deacetylated gum was determined to be 8.5×10^{6} and 2.5×10^{7} g mol^{-1}, respectively. About 15.2 ± 1.18 % of GK is water, less than 7.3% is ash, and less than 3% is insoluble solids or bark. The pH range of the GK solution is between 4.9 and 5.0. The molecules of GK contain a variety of sugar structures, which are shown in Figure 9.

The intrinsic viscosity of native GK was measured to be 32.68 dl g^{-1}, while the viscosity of deacetylated GK was measured to be 59.34 dl g^{-1}. Differential scanning calorimetry (DSC) was used to determine that the gum has a glass transition temperature of 34.5 °C. The XRD pattern of the native gum reveals that it has an amorphous structure in its whole. The amount of carbon, hydrogen, nitrogen, and sulfur found in the gum were found to be 34.97, 5.58, 0.229, and 0.128 (w/w%), respectively. The FT-IR spectrum reveals that the following functional groups are the most important in GK: 3431 cm^{-1} (–OH), 1731 cm^{-1} (CH3CO–), 1632 cm^{-1} (–COO–), 1429 cm^{-1} (–COO–), and 1249 cm^{-1} (–COO–) (–CH3CO).

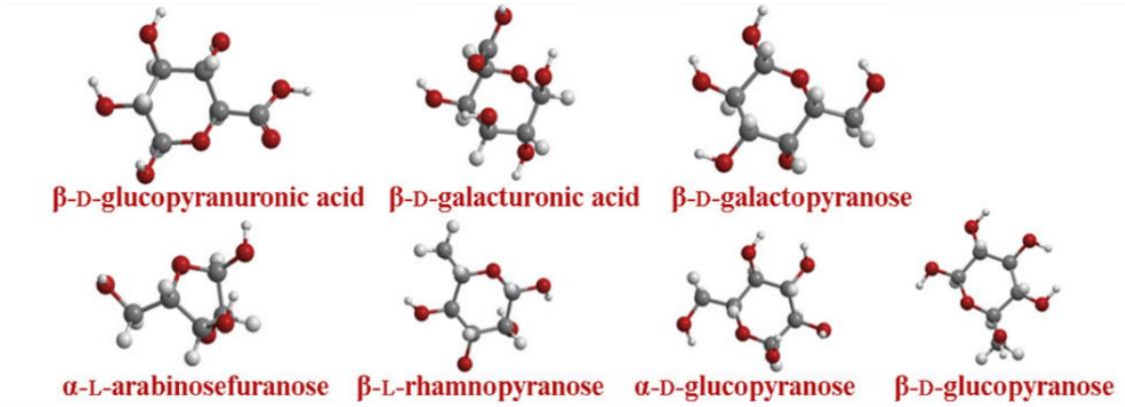

Figure 9. Sugar constituents of GK

Food applications have historically utilized these gums for emulsion, stability, thickening, and texturing functions. In recent years, however, they have been utilized for numerous non-food applications, including the greener synthesis of nanoparticles, fabrication of electrospun fibers, adsorbents, bio-catalysis, biosensors, biomedical, food packaging, and energy harvesting. It has been reported, for instance, that GK may increase the ex vivo bioadhesion time [53], resulting in greater drug release [54]. Moreover, it has served as a template for the reduction and stabilization of silver, palladium, iron, and gold nanoparticles [55]–[58]. It has been revealed that modified gum can be utilized for food

packaging films [59], and that electrospun fibers with an average diameter of 210 ± 30 nm can be manufactured [60].

Despite the benefits described above, three-dimensional structural objects are brittle and easily broken when subjected to cyclic compression due to their weak network connectivity and random porous architecture, which severely limits their practical usage. However, creating extremely elastic biomass sponges that prevent deformation and successfully resist structural breakdown is both challenging and interesting. Consequently, there is a need to have an integrated interconnected or crosslinked network to improve structural stability and benefits.

3.5.2 Sodium Alginate

Alginates are a group of naturally occurring polysaccharides extracted from different species of brown seaweed (*Laminaria hperborean, Macrocystis pyrifera* and *Ascophyllum nodosu)* and bacterial alginates (*Pseudomonas* and *Azotobacter).* Alginate was first discovered by E.C.C. Stanford in 1881. For the extraction process, the calcium/sodium/potassium salt of alginic acid alginate is followed by alkali treatment with sodium carbonate to form sodium alginate. The hydrocolloid nature of sodium alginate is particularly used in food, pharmaceuticals, textiles, and cosmetics industries. More recently, the use of alginate has been explored extensively in tissue engineering due to its biocompatibility and used in the regeneration of skin tissue, cartilage, bone, pancreas, liver, muscles, and nerves, in addition to being used in the controlled release of drugs.

Sodium alginate is a linear copolymer consists of two linked anionic monomers, β-d-mannuronic acid (M) and α-l-guluronic acid (G) residues. The polymer structure is composed of homopolymeric regions of G blocks and M blocks (see Figure 10),

interspersed with regions of heteropolymeric MG blocks. When monovalent ions (e.g., sodium in sodium alginate) are exchanged for divalent ions (especially calcium), the crosslinking reaction proceeds almost immediately, changing from a low viscosity solution to a gel structure. The G residues of the alginate chain become folded and stacked under the bond interaction, which causes the structure transformation of adjacent alginate chains from random coils to ordered ribbon-like structure. This entanglement of alginate chains finally contributes to the hydrogel with a three-dimensional gel structure. Many research papers state that the mechanical strength of the microcapsule can be raised by increasing the G and the length of the G blocks in the alginate.

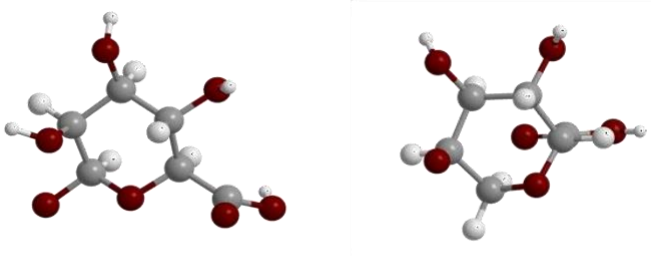

Figure 10. Chemical structure of alginate monomers

In addition, numerous free hydroxyl and carboxyl groups are distributed in the alginate backbone, making them highly active and highly adaptable to chemical reactions. The adaptive properties of alginate, such as solubility, hydrophobicity, and biological characteristics, may be modified for its potential applications. It can be formulated as films, hydrogels, beads, and sponges. It is used in packaging, biosensor, adsorbents, filters, catalysis, electrical and biomedical operations. Conjugations with reinforcing materials enhance its mechanical properties. In addition, crosslinking, and surface modifications such functionalization increase its range of use.

3.6. Conjugation

The hierarchical structure of biopolymers is often provided with undesirable features such as brittleness and hydrophilicity, limiting their efficacy. Through the creation of an integrated polymeric network known as conjugation, biopolymers with inherent and lower capabilities are changed into more structurally robust hybrid materials. Conjugation occurs when two biomolecules are coupled together or when other biomaterials or phases of matter are incorporated into biopolymer substances. This method combines two different hydrocolloids, and the physical and rheological properties of the mixed solutions are strongly altered. This is due to the compatibility/incompatibility between the two macromolecules, which depends on their molecular weight, chemical composition, adaptation, and hydration properties. This approach allows the advantages of each component to be applied in a variety of combinations, whereby enhancing the inherent properties. Physical (intermolecular interaction/molecular entanglement) and chemical (hydrogen bonding, electrostatic interaction, ionic bonding) incorporations can improve the properties of gum conjugates, resulting in enhanced structural stability, increased compressibility, reduced fragility, increased adsorption performance, and better thermal properties.

In recent years, various investigations into the utilization of gum conjugates have been performed in biomedical, packing, and environmental applications. The recently reported gum conjugate compositions and applications are summarized in Table 1.

Table 1. Gum conjugate compositions and applications

Materials	Applications	Ref.
Gum arabic (GA)/PVA	Electrospun fiber	[60]

GK/PVA	Electrospun fiber	[60]
Gum karaya/PVA	Electrospun fiber	[60]
Gum tragacanth/poly-(L-lactic acid)	Tissue engineering	[61]
Gellan gum/PVA	Tissue engineering	[62]
Gum acacia/PVA	Tissue engineering	[63]
Carboxymethyl tamarind gum/citric acid	Tissue engineering	[64]
Guar gum/PVA	Tissue engineering	[65]
Chitosan/gum arabic	Tissue engineering	[66]
Karaya gum/starch	Drug delivery	[67]
Polyacrylamide/gum karaya	Drug delivery	[68]
Karaya-chitosan	Drug delivery	[69]
Chitosan/pectin/gum arabic	Drug delivery	[70]
Alginate-gum arabic	Drug delivery	[71]
Gellan gum/konjac glucomannan	Packaging	[72]
Gellan gum/agar	Packaging	[73]
Gellan gum/xanthan gum	Packaging	[74]
Xanthan gum/gelatin	Packaging	[75]

Guar gum/sodium caseinate	Packaging	[76]
Gum Arabic/chitosan	Packaging	[77]
Gum Arabic/wild almond protein	Packaging	[78]
Gum Arabic/PVA/chitosan	Packaging	[79]
Tara gum/PVA	Packaging	[80]
Tara gum/chitosan	Packaging	[81]
Xanthan/pullulan/locust bean	Packaging	[82]
Xanthan gum/starch	Packaging	[83]
Xanthan gum/locust bean gum	Packaging	[84]
Guar gum/chitosan	Packaging	[85]
Gum tragacanth/hydroxymethyl cellulose/beeswax	Adsorbent	[86]
Karaya gum/poly(2-(dimethylamino) ethyl methacrylate)	Adsorbent	[87]
Gum karaya/poly(acrylic acid) (PAA)	Adsorbent	[88]
Karaya gum/2-methacryloyloxyethyl) Trimethylammonium chloride (METAC)	Adsorbent	[89]
Gum karaya/poly(acrylic acid-acrylamide) (P(AA-co-AAM))	Adsorbent	[90]
Gum arabic and acrylamide	Adsorbent	[91]
Agar/gum arabic	Adsorbent	[92]

To-date, only a limited number of studies that focus on the alginate/gum conjugations have been published in academic journals. However, the fact that these biopolymers have a similar molecular structure, reactive functional groups, gelation behavior, water

solubility, biocompatibility, and biodegradability make them selective and more appropriate for conjugation. It has been found that high-density alginate-gellan gum conjugates can be used very well for 3D plotting of complex tissue engineering scaffolds [93]. Studies have shown that each conjugate of alginate with gum succinate, sterculia gum, gellan gum, and locust bean gum has great potential for various drug delivery applications [94]–[97]. Recent research has demonstrated that the conjugation of alginate with agar and gellan gum can produce a super adsorbent for methylene blue in polluted water [98], [99].

3.7. Objectives

Based on the literature research, a number of objectives were formulated, and this thesis examines them in detail:

1. To study the interaction between tree gum kondagogu and sodium alginate

2. To develop a low-density, highly porous sustainable sponge based on tree gum kondagogu and sodium alginate

3. To functionalize sponges through:

3.1 Silylation

3.2 Ionic crosslinking

3.3 Fabrication of a nanocomposite sponge

4. To develop biodegradable sponges for optimized environmental applications.

4. Results and Discussions

During my Ph.D. studies, I have published one book chapter and eight articles (and additional two articles are ready for communication/review) in impact journals concerning the use of tree gum-based sponges for the treatment of environmental remediation, from which four were chosen to be presented below.

4.1 Biomacromolecule Assembly based on Gum Kondagogu-Sodium Alginate Composites and their Expediency in Flexible Packaging Films

Abstract: Bio-based macromolecules of gum kondagogu/sodium alginate (GK/SA) were fabricated using glycerol as a plasticizer and their optimum blending ratio was identified based on their physical and chemical, structural, mechanical, barrier, and morphological properties. Attenuated total reflection-Fourier transform infrared spectroscopy (ATR-FTIR) analysis showed that both biomacromolecules are well organized due to the hydrogen bond interaction between molecular chains involving the hydroxyl, carbonyl, and acetyl groups. Structural identification was performed by recording X-ray diffraction (XRD) spectra. Field emission scanning electron microscopy (FESEM) was used to identify the distinction between the surface of the films of biopolymers, and their conjugates, where the addition of SA increased the surface homogeneity and smoothness. The water contact angle of the blend films reached up to 81°, although the value for pure biomacromolecule films was very low. The blend films also exhibited high tensile strength (up to 24 MPa) compared to the pure biopolymer films. The investigation of film-forming ability, mechanical strength, permeability, transparency, and biodegradability of the developed GK/SA bio-macromolecular association may be applied in the form of green and sustainable food packaging films.

Citation : R.K. Ramakrishnan, M. Cernik, V.V.T. Padil, S. Wacławek, Biomacromolecule assembly based on gum kondagogu-sodium alginate composites and their expediency in flexible packaging films, Int. J. Biol. Macromol. 177 (2021) 526–534.

International Journal of Biological Macromolecules 177 (2021) 526–534

Contents lists available at ScienceDirect

International Journal of Biological Macromolecules

journal homepage: http://www.elsevier.com/locate/ijbiomac

Biomacromolecule assembly based on gum kondagogu-sodium alginate composites and their expediency in flexible packaging films

Rohith K. Ramakrishnan, Stanisław Wacławek, Miroslav Černík, Vinod V.T. Padil *

Institute for Nanomaterials, Advanced Technologies and Innovation (C×I), Technical University of Liberec (TUL), Studentská 1402/2, Liberec 1 461 17, Czech Republic

ARTICLE INFO

Article history:
Received 5 December 2020
Received in revised form 20 February 2021
Accepted 20 February 2021
Available online 23 February 2021

Keywords:
Biodegradation
Gum kondagogu/alginate composite film
Food packaging

ABSTRACT

The assembly of bio-based macromolecules of gum kondagogu/sodium alginate (KO/SA) was fabricated using glycerol as a plasticiser and their optimum blending ratio was identified based on their physical and chemical, structural, mechanical, barrier, and morphological properties. The attenuated total reflection-Fourier transform infrared spectroscopy (ATR-FTIR) analysis show that both biomacromolecules are well organised due to the hydrogen bond interaction between molecular chains involving the hydroxyl, carbonyl, and acetyl groups. Structural identification was performed by recording X-ray diffraction (XRD) spectra. Field emission scanning electron microscopy (FESEM) was used to identify the distinction between the surface of the films of biopolymers, and their conjugates, where the addition of SA increased the surface homogeneity and smoothness. The water contact angle of the blend films reached up to 81°, although the value for pure biomacromolecule films was very low. The blend films also exhibited high tensile strength (up to 24 MPa) compared to the pure biopolymer films. Investigation of film-forming ability, mechanical strength, permeability, transparency, and biodegradability of the developed KO/SA bio-macromolecular association may be established as green and sustainable food packaging films.

1. Introduction

Non-biodegradable plastic films create serious environmental issues, and severely affect ecosystems due to their persistence in environmental pollution [1,2]. There is a growing requirement for the development of new green and sustainable packaging materials to fulfil the increasing consumer demands and to meet environmental concerns. In this scenario, a large number of scientific research groups all over the world have become interested in the fabrication of packaging films using biodegradable and renewable materials. Recently, biological macromolecules such as polysaccharides, and proteins have been applied to a wide range of packaging film applications due to their availability, good oxygen and water vapor permeability, biocompatibility, and biodegradability [3–5]. The natural polysaccharides obtained from renewable sources provide greater opportunities to reduce the polymeric materials obtained from petroleum and to achieve a sustainable ecosystem. These are fabricated in various forms such as hydrogels, nanofibers, membranes, etc., which are used for edible (thickeners, stabilisers, gelling agents, and emulsifiers) and non-edible (pharmaceutical, catalysis, and water treatment) applications [6–9]. Although various natural polysaccharides have been evaluated and introduced as film-forming materials over the past few decades for food packaging purposes, many of the polysaccharide-based packaging applications are limited by their brittleness, high hydrophilic nature, and low mechanical properties [10]. As an alternative option, bioconjugates may be prepared from natural polysaccharides, which provide a versatile platform for the inclusion of the preferred combinations of properties for the designed applications.

Binary conjugates may be prepared from a wide variety of materials of natural origin, such as microorganisms, plants, etc., as well as from materials prepared by modification or blending of natural structures and synthetic polymeric materials [11,12]. Conjugates made from natural polymers with proper selection over biopolymer types and their combinations enable the production of films possessing a well-defined network architecture, suitable mechanical strength, negligible batch-to-batch variability, and prolonged stability, and they are also able to compete with synthetic polymers in terms of their long service life [13,14]. The physical and biochemical properties of binary conjugates largely depend on the methods used for their blending as well as their crosslinking density [15].

Among naturally derived polymers, polysaccharides such as cellulose, carrageenan, chitosan, starch, tara gum, xanthan gum, tragacanth gum, gum arabic, gelatine, agar, and alginate have been used as biodegradable materials for food packaging [16–23]. Gum kondagogu (*Cochlospermum gossypium*) is a polysaccharide obtained from the exudate of a tree growing naturally in the forests of India [24]. Due to the non-toxicity, biocompatibility, and feasibility of this gum, it has a great potential for use in

* Corresponding author.
E-mail address: vinod.padil@tul.cz (V.V.T. Padil).

https://doi.org/10.1016/j.ijbiomac.2021.02.156
0141-8130/

various applications [25]. Alginate is a naturally occurring poly-anionic polysaccharide derived from brown marine algae (Phaeophyceae) [26]. Alginate is made up of a linear block copolymer of 1, 4-linked-d-mannuronic and-l-guluronic residues in varying proportions [27]. As a low-cost, abundantly available, biocompatible, and environmentally friendly biopolymer, it has been used in numerous applications in the food and biotechnology industries such as a non-toxic food additive, thickening and gelling agent, and as a colloidal stabiliser [28]. The chemical structures of KO and SA are given in Fig. 1.

The similarity in their basic structure contributes to their better interaction, which in effect affords good film-forming properties. Synergistic interactions between binary components are attractive commercially because they offer the potential to improve and control the physical and chemical properties of products in various applications. It is a good strategy to improve the film matrix characteristics in order to obtain high-performance packaging materials [29]. The binary and ternary sustainable composites fabricated from gellan gum, 2-hydroxyethyl cellulose, and lignin combination were found to be flexible and transparent [30]. The shelf life of the material may also be enhanced by exploiting the interaction between the biopolymers and by the incorporation of other materials [31].

This work describes the development of a flexible packaging film based on the combination of biomacromolecules such as KO and SA using glycerol as a plasticiser and characterises the functional possessions for identifying the optimum ratio of their film-forming properties. This is the first-ever report on the film casting of KO with SA using an aqueous medium. The strength and texture of the composite films are dependent on the ratio of polymer concentration. The KO has hard and brittle films, whereas their combination with sodium alginate offers flexibility, elasticity, and good surface texture. Brittleness is an inherent property of natural polymers, while the use of a plasticiser improves flexibility by decreasing intermolecular forces along the polymer chains [32]. The physical, morphological and mechanical properties of the films were studied and the ratio between the gum and sodium alginate for the film formation was optimised from tensile strength, water contact angle, water permeability, transparency, and surface texture analysis.

2. Materials and methods

2.1. Materials

Gum kondagogu (KO) was purchased from the Girijan cooperative society, Andra Pradesh, India, and sodium alginate (SA) was purchased from Sigma Aldrich Co., USA. Glycerol was obtained from Merck Life Sciences Pvt. Ltd., Mumbai, India. Deionised water was used in all of the experiments.

2.2. Preparation of composite biomacromolecules films

The films were prepared by the casting method. The compositions were prepared using glycerol and 1.5% (*w*/w) aqueous solutions of KO and SA in a magnetic stirrer at 1500 rpm for 2 h at room temperature as per the ratios presented in the supplementary information (Table S1). The solutions were degassed with a vacuum pump to remove air bubbles before casting. The films cast in plates were dried at 40 °C for 48 h. They were then carefully peeled off from the plates and kept in a vacuum desiccator for at least 48 h before characterisation. A schematic representation of the fabrication of a composite KO/SA film is shown in Fig. 2.

3. Characterisation

3.1. ATR-FTIR spectroscopy

The Fourier transform infrared spectra of the films were recorded in an FTIR (Perkin Elmer, UK) spectrometer in the attenuated total reflectance (ATR) mode over a 4000–400 cm^{-1} spectral range.

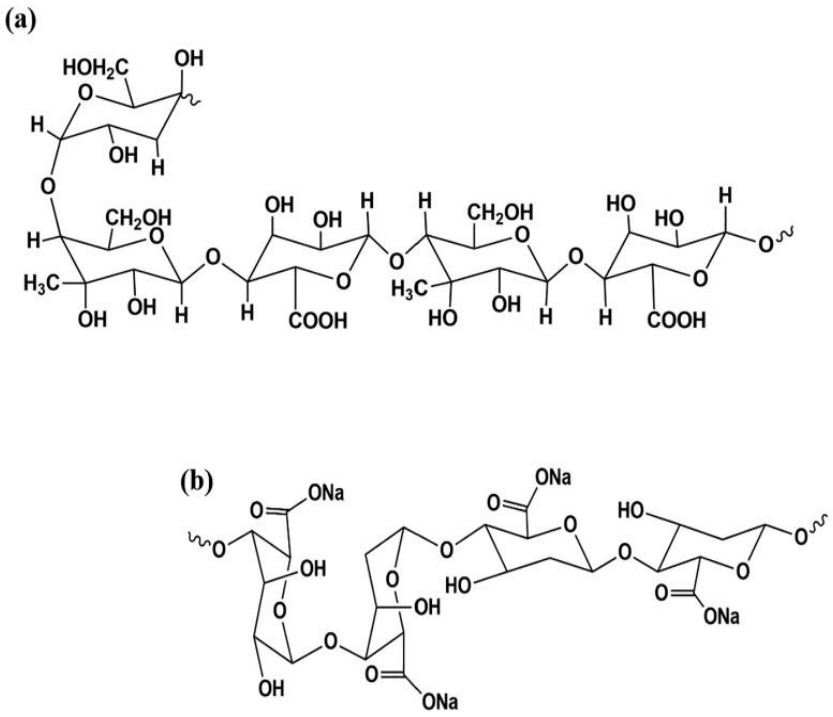

Fig. 1. Chemical structure of (a) gum kondagogu (KO) and (b) sodium alginate (SA) biomacromolecules.

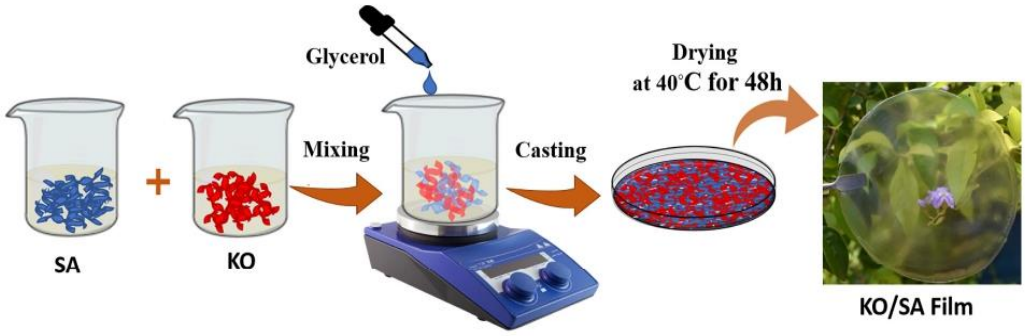

Fig. 2. Scheme for the fabrication of a composite KO/SA bio-macromolecule film.

3.2. X-ray diffraction

X-ray diffraction (XRD) of the films was performed to study the crystallinity using an X-ray diffractometer (PANALYTICAL, Aeris Research, Netherlands). Samples with a rectangular shape (1 × 1 cm) were placed on a glass slide, and the spectra were recorded using Cu Kα radiation (wavelength of 0.1541 nm) at 40 kV and 15 mA. The diffraction pattern was obtained at diffraction angles of 2Θ = 5–60° with a step size of 0.04^0/s at room temperature.

3.3. Optical properties

The transparency of the films was measured in a 200–800 nm wavelength range with a measurement resolution of 1 nm in a Perkin Elmer Lambda 365 UV/Vis spectrophotometer (Perkin-Elmer, USA) with a film holder. Three repetitions per sample were conducted for all of the samples.

3.4. Moisture absorption

The films, previously dried at 100 °C in an air oven, were placed inside an environmental chamber maintained at 75% relative humidity (RH) and 23 ± 2 °C. Each sample was taken out of the chamber at regular time intervals and weighed with a precision of ±0.0001 g. The moisture content of the films was calculated from the weight of the samples at equilibrium (We), which occurred after approximately 8 h of absorption of moisture, and the initial (dry) weight (W_1) as follows:

$$\text{Moisture content}\ (\%) = \frac{W_e - W_1}{W_1} \times 100 \quad (1)$$

To ensure the reproducibility of the results, four specimens of each sample were tested.

3.5. Water contact angle

Water contact angles of the samples were measured using a Ramehart contact angle goniometer by dispensing deionised water from a syringe. A droplet (5 μL) of deionised water was deposited on the surface of the samples and the contact angle was measured. An average of ten measurements was taken for each sample.

3.6. Water vapor permeability (WVP)

The WVP of films was determined gravimetrically at 25 °C under 50% RH conditions for 8 h using water vapor transmission measuring cups in accordance with the ASTME-96-95 standard method. The WVP (g/m^2 s Pa) of the film was then calculated using the following Eq. (2):

$$WVP = \frac{\Delta W \times L}{A \times \Delta P \times \Delta t} \quad (2)$$

where, ΔW is the weight gain (g) of the cups during time Δt (s), A is the area of exposed film (0.0049 m^2), L is the mean thickness of the film (m), and ΔP is the partial water vapor pressure difference (Pa) across the film. At least three samples were taken from each film to obtain the WVP value [33].

3.7. Mechanical properties

Tensile strength (TS) and elongation at break (EB) were measured by a universal testing machine. TS and EB of the films were measured according to the ASTM standard method [34] in Instron (Hounsfield, Model H5KS, UK). The samples were cut into rectangle strips of 1 cm × 7 cm and the test was conducted at a crosshead speed of 5 mm min^{-1}. Data were the average of five samples.

3.8. Morphology of the films

Field-emission scanning electron microscopy (FESEM) characterisation of the films was performed at ZEISS, SIGMA, Germany at an accelerating voltage of 10 kV and a working distance of 10 mm. The samples were stuck onto the sample holder with a carbon pad and sputter-coated with gold.

3.9. Biodegradation study

The biodegradability of the optimised film was investigated by determining the biochemical oxygen demand (BOD) using the ISO 14851: 1999 standard. Aniline and polyethylene were used as positive and negative controls, respectively and the tests were performed in a closed Micro-Oxymax respirometer for 28 days. The tests were performed in bottles containing approximately 2 g of the sample, 95 mL of an inorganic medium, and 5 mL of an inoculum. The inoculum used was supernatant of the settled sludge from a wastewater treatment plant in the city of Liberec with 3.9 g/L dry matter and approximately 100,000 CFU/mL. The percentage of biodegradation was then calculated from the weight difference (initial weight and weight of the sample at the end of the test).

4. Results and discussion

4.1. ATR-FTIR analysis

ATR-FTIR spectra for the KO, SA (K10S0, K0S10) films and the blends (K2S8, K4S6, K6S4, and K8S2) are shown in Fig. 3. The major functional groups present in the ATR-FTIR spectrum of both the KO and SA were at 3660–3000 cm^{-1} (–OH stretch), 2935 cm^{-1} (-CH_2 stretching), and at

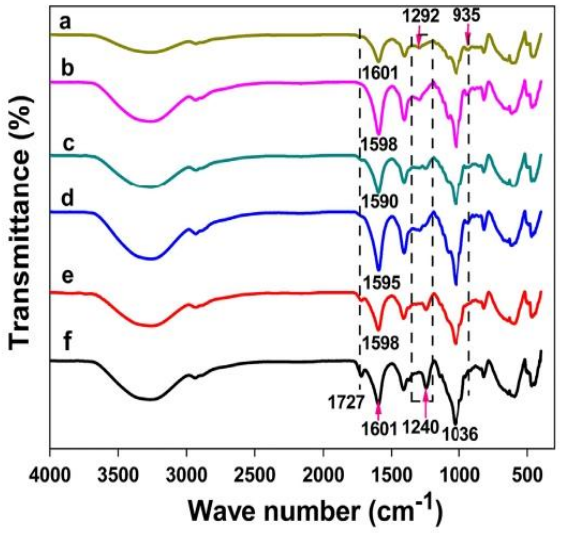

Fig. 3. ATR-FTIR spectra of binary KO/SA films (a) K0S10, (b) K2S8, (c) K4S6, (d) K6S4, (e), K8S2, and (f) K10S0.

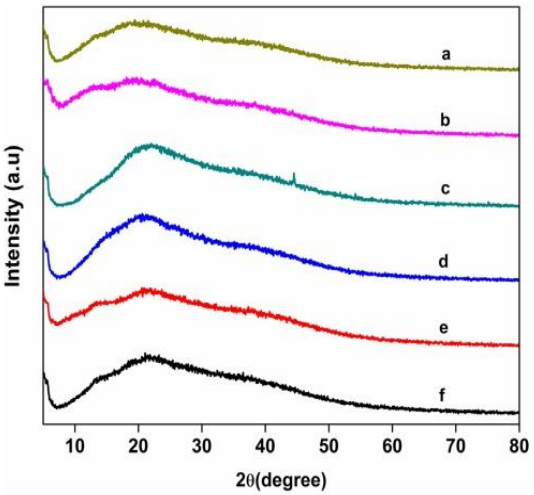

Fig. 4. X-ray diffractograms of binary KO/SA films (a) K10S0, (b) K8S2, (c) K6S4, (d) K4S6, (e) K2S8, and (f) K0S10.

1601 and 1410 cm^{-1} (carboxylate groups). The other bands of KO at 1727 cm^{-1} and 1240 cm^{-1} are due to the acetyl -C=O vibrations. The peaks at 1150 and 1036 cm^{-1} may be attributed to C—O stretching of C—O— C and primary alcohol (C-O-H), respectively. SA showed the mannuronic acid functional group at wavenumber 820 cm^{-1} and the uronic acid functional group at wavenumber 935 cm^{-1}. The -CO and -CO-C vibrations of groups in the mannuronic and glucuronic units are marked at 1094 and 1024 cm^{-1}, respectively. In addition to these peaks, skeletal vibration of the alginate occurred at 1292 cm^{-1}.

In the composite films, the intensity of peaks at 1727, 1240, and 1150 cm^{-1} characteristic of KO gradually decreased in the order K10S0, K8S2, K6S4, K4S6, and K2S8, and disappeared in K0S10. As the ratio of KO decreased, the peaks corresponding to KO also decreased. Similarly, the peaks at 1297 cm^{-1}, 1094 cm^{-1}, and 935 cm^{-1} showed a decreasing trend in intensity as the ratio of SA reduced in the binary conjugate, and these were absent in K10S0. The carboxyl group vibrational frequency of KO and SA was observed at around 1601 cm^{-1} and 1410 cm^{-1}, as seen in K10S0 and K0S10. While in the binary films, these bands were shifted to a lower wavenumber range (1598–1590 cm^{-1}) and 1404 cm^{-1}, respectively as a result of hydrogen bonding interaction. A slight shift in the O—H stretching frequency from 3306 cm^{-1} to lower wavenumbers in the binary films also confirms the existence of hydrogen bonding interaction between the polymers [35]. This implies that there is a strong interaction between KO and SA through the hydrogen bonding involving the hydroxyl, carbonyl, and acetyl groups. This reduces the availability of free hydrophilic groups in the binary films, which in turn affects the water or moisture absorption as a function of the degree of interaction. Furthermore, the interaction will obviously afford mechanical strength, which is one of the essential criteria to be satisfied by packaging films.

4.2. X-ray diffraction (XRD) analysis

XRD patterns of the samples are given in Fig. 4. The alginate diffraction pattern consisted of two peaks at approximately $2\theta = 13.6^0$ and 21.9^0, which are observed in K0S10 [36]. In the binary films, these peaks became less intense with the reducing content of SA. This phenomenon probably results from hydrogen bonding interactions between the two biopolymers and their excellent miscibility. No characteristic peaks in the spectrum of K10S0 were observed, indicating that the gum is completely amorphous [24].

4.3. Optical properties

To evaluate the transparency, the transmittance of the films was measured in the wavelength range of 200–800 nm (Fig. 5). The lowest transmittance was exhibited by K10S0 and it improved gradually after the addition of SA. Specifically, at 600 nm, the transmittance shown by K10S0, K8S2, K6S4, K4S6, K2S8, and K0S10 was 48%, 63%, 64%, 68%, 71%, and 74%, respectively. The transmittance of films in food packaging is of importance for various applications. Light-sensitive food materials undergo oxidation if visible light is transmitted through the package; therefore films with less transmittance are desirable for such applications. Other applications require transparent packaging films. From the transmittance results obtained, the transparency of the binary film may be altered by varying the SA proportion for a given application [36]. The films fabricated in this work showed strong UV-light absorption properties, as indicated by the significantly low transmittance of UV light [37].

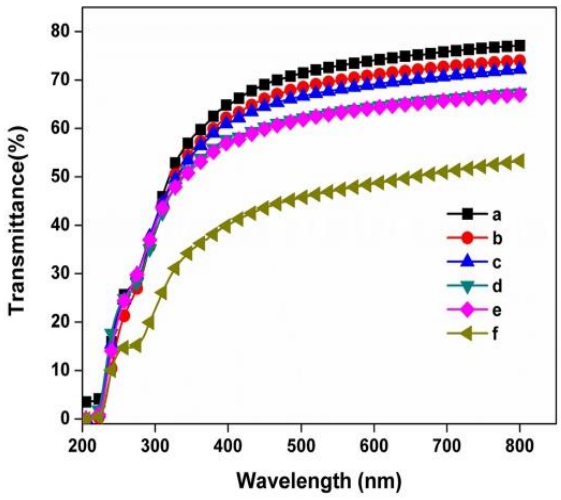

Fig. 5. UV transmittance spectra of native and binary films (a) K0S10, (b) K2S8, (c) K4S6, (d) K6S4, (e) K8S2, and (f) K10S0.

4.4. Mechanical properties

Packaging material should be capable of withstanding stress and should maintain structural integrity during shipping, handling, and storage. Mechanical properties, such as tensile strength and elongation at break of the polymer blends, are known to be influenced by the interaction or compatibility between the polymer components. The tensile strength and elongation at break for native gums are low due to the inter-chain interaction. However, it was noticed here that a blended film composition had higher tensile strength and elongation at break after the addition of SA, up to a composition having 60% SA, whereafter it decreased.

The tensile strength of the KO film (K10S0) was 9 MPa, which increased in the binary films to 13, 15, and 24 MPa for K8S2, K6S4, and K4S6, respectively (Table S2; supplementary information). The addition of SA up to 60% increased the tensile strength. Further addition of SA reduced the tensile strength, as shown in sample K2S8 with a tensile strength of 22 MPa and K0S10 with 20 MPa. Therefore, it is assumed that there is an interaction between the KO and SA and this interaction reaches a maximum at a particular composition. After this composition, free functionalities appear. For blends, the interactions between KO and SA are due to the hydrogen bonding between the plentiful hydroxyl, carbonyl, and acetyl groups present in the polymers, as seen in the ATR-FTIR results, leading to an increase in TS. The presence of SA seemed to prevent the inter-chain interaction KO (self-aggregation), and subsequently the TS values increased. According to the results, K4S6 and K2S8 systems are good enough to improve the mechanical properties of binary KO/SA films. K4S6 exhibited the highest tensile strength due to it having the highest degree of hydrogen bonding interaction between the polymers. The tensile results indicated that different polysaccharide ratios may be used to improve the mechanical properties depending on the degree of interaction between the molecules of the components. Superior mechanical properties are exhibited by compatible polymer blends, whereas incompatible polymer blends result in inferior mechanical properties [36]. The tensile strength values of the film are comparable to those of other biopolymer blend films, such as konjac glucomannan–xanthan gum and tragacanth–locust bean gum films [38,39]. The carrageenan/glucomannan combination increased the compatibility of the composite film, which improved the mechanical properties such as tensile strength and elongation at break [40].

4.5. Water contact angle (WCA)

Water contact angle measurements were taken to explore the influence of blending on the wettability of the KO/SA films performed. The images and water contact angles in degrees are presented with standard deviation in Fig. 6a. Pure KO and SA have a contact angle of 57° and 33°, respectively (as seen in K10S0 and K0S10, respectively), which shows the very high hydrophilicity of the films. However, in the blend films, the contact angle increased since the hydrophilicity decreased. The addition of SA into the KO system resulted in an increase in the water contact angle to a maximum of 81 ± 2.5° (for K4S6). The decrease in hydrophilicity of the biopolymer after blending may be due to the decreased number of hydrophilic groups, such as free –OH, carbonyl, etc., of the KO and SA on the surface of the films to interact with the water molecules. A possible scheme for the interaction of hydrophilic groups is given in Fig. 6b. The improvement in the hydrophobic nature of the composite films due to the interaction of polymer components is already reported in the literature. The interconnection between the components reduces the accessibility of the polar hydroxyl groups to interact with water molecules and, therefore, the films become more hydrophobic, as reported for carrageenan/xanthan gum/gellan gum hydrogel films, which reflected a significant increase in the water contact angle [41]. A similar observation was later reported by the same group for binary and ternary sustainable composite films of gellan gum, hydroxyethyl cellulose, lignin, and whey protein isolate/psyllium seed gum composites [30,42,43]. The value of the contact angle increased with the addition of SA as follows: 57 ± 1.2°, 61 ± 1.4°, 62 ± 2.2°, and 81 ± 2.5° for K10S0, K8S2, K6S4, and K4S6, respectively. However, for K2S8, the WCA was 68 ± 4.1° and for K0S10 it was 33 ± 3.3°. The addition of SA beyond 60% led to the presence of additional carboxyl groups, which are hydrophilic and reduced the WCA. In addition to the surface functional groups, the wettability and hence the contact angle of solid surfaces are also determined by the surface morphology [44]. Generally, with increasing surface roughness, the contact angle decreases for hydrophilic materials and increases for hydrophobic materials; although, no rigid quantitative correlation has been experimental verified [44]. In the present case, in terms of surface morphology, the addition of SA to KO made the surface more homogeneous up to 60% addition of SA. Accordingly, the values of the contact angle increased from 57 ± 1.2° to 81 ± 2.5° from K10S0 to K4S6. For K2S8, there was a slight increase in the surface roughness and a subsequent decrease in the contact angle to 68 ± 4.1°. This is in agreement with the general observation that for hydrophilic materials, with decreasing surface roughness, the contact angle increases [41,44].

The hydrophilic-hydrophobic character may be modified by varying the ratio of SA in the binary films. A similar trend was also observed in terms of the mechanical properties, where the addition of more than 60% SA decreased the tensile strength due to the free functional groups, which do not take part in the bonding with other polymer chains in the binary film. Therefore, the mechanical and wettability properties indicate the superiority of K4S6 over the other compositions for packaging film fabrication.

4.6. Water vapor permeability (WVP)

The water vapor barrier properties were determined by measuring the permeability of water vapor through the films. The WVP of the films depends on many factors, such as the integrity of the film, the hydrophilic-hydrophobic ratio, the crystalline-amorphous ratio, and the polymeric chain mobility [36,45]. Table S2 (supplementary information) shows the results of the WVP study for the binary KO/SA films. The conjugating reactions affect the moisture diffusion coefficient in the films, indicating the structural changes in the polymeric matrix, which is in accordance with the WCA values of the films. The pure biomacromolecule films (K10S0 and K0S10) exhibited higher WVP values (6.03×10^{-9} and 5.44×10^{-9} g^{-2}Pa s). In the binary films, the WVP decreased to K4S6, whereafter they increased. The WVP for K8S2, K6S4, and K4S6 were 5.76×10^{-9}, 4.85×10^{-9} and 4.39×10^{-9} $g^{-2}Pa^{-1}s^{-1}$, respectively. The WCP for K2S8 was slightly less than that for K4S6 since there was only a slight difference in their WCAs. The difference in the WVP values between these films may be attributed to the formation of hydrogen bonding between the KO and SA, promoting a denser crosslinked network with a reduced free volume in the composite KO/SA films.

4.7. Moisture absorption ability

As illustrated in Fig. 7, K0S10 exhibits higher moisture absorption than bio-macromolecular films due to greater exposure of hydroxyl groups, which enhance binding to more water molecules. It is clear from the values that the blended film had a lower moisture absorption ability than the corresponding pure SA film. Generally, the primary structure, long-range structure, and condensed states of the polymers affect the moisture absorbability of the film [39]. Therefore, taking the structural changes into account, the low water absorbability of the blends may be due to the less exposed OH groups owning to hydrogen bonding and decreasing interaction with the water.

Regarding the films prepared with gum, it was noticed that the addition of only a small ratio of gum to the composite film lead to a sharp decrease in the moisture uptake. KO "blocks" hydrophilic sites of SA by hydrogen bonds, leaving fewer OH groups to interact with water molecules, resulting in lower moisture absorption values. By adding higher

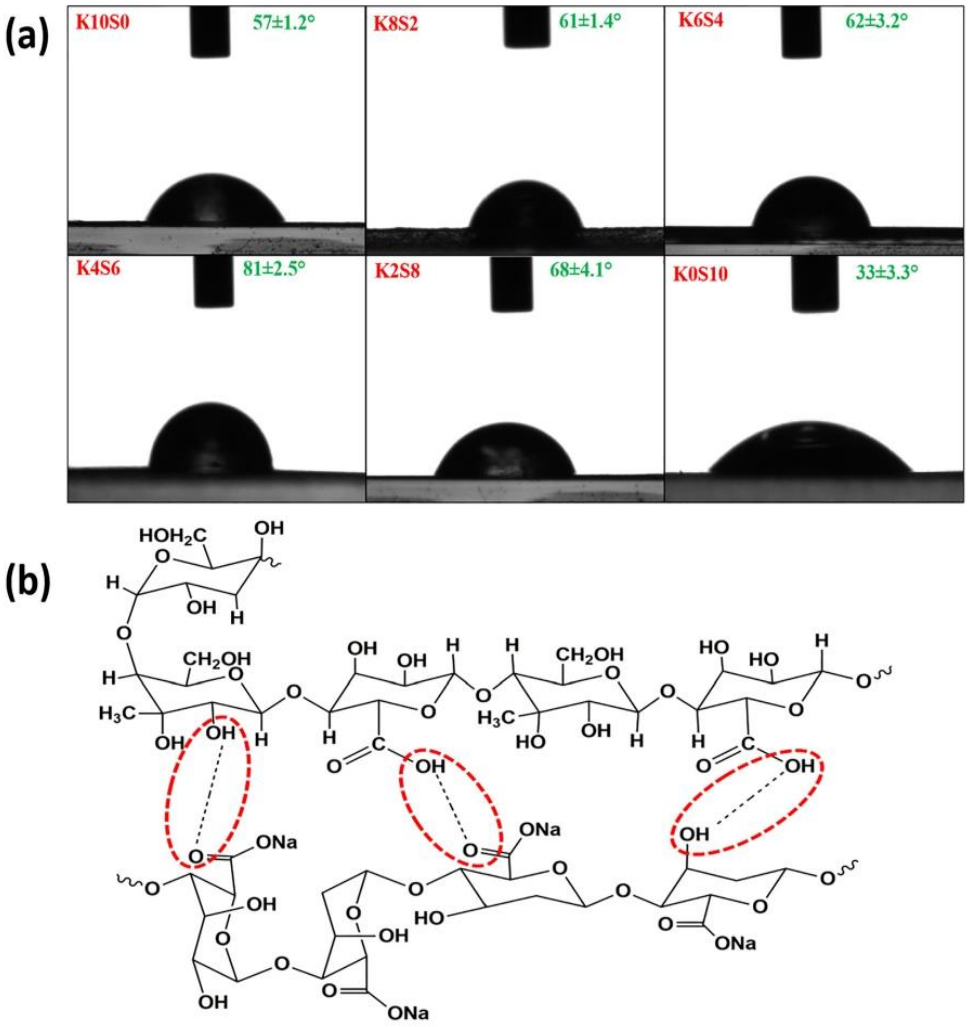

Fig. 6. Water contact angle images of all of the KO/SA films (a), representation of a plausible scheme for the interaction between KO and SA (b).

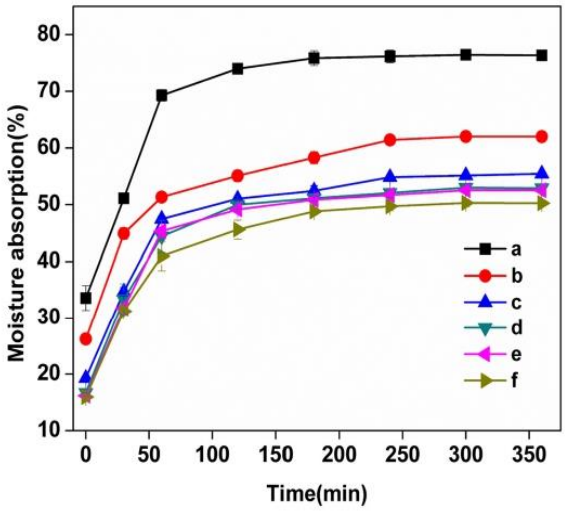

Fig. 7. Moisture absorption of the composite KO/SA films (a) K0S10, (b) K2S8, (c) K4S6, (d) K6S4, (e) K8S2, and (f) K10S0.

KO contents, a straight decrease of moisture absorption was observed, which was attributed to the formation of an interpenetrating network of the two bio-macromolecules with hydrogen bonding.

4.8. Film morphology

Field emission scanning electron microscopy (FESEM) analysis performed to characterise the microstructure and homogeneity of the pure and composite biomacromolecules films is presented in Fig. 8. The K0S10 film was found to be very smooth with a compact surface structure, while K10S0 appeared to possess rough surfaces. The interchain interaction of KO leads to self-aggregation forming a continuous and dense network and rough surface as seen in Fig. 8. The addition of SA to KO prevents this interchain interaction, which in effect results in smoothening of the surface texture. This may be observed in the increasing homogeneity of the surface of the films with increasing amounts of SA, which improve the flexibility and tensile strength of the films. The smooth and compact surfaces of the films suggest high miscibility and high compatibility between the biomacromolecules. These results show a reasonable interconnection between the biomacromolecules, and an increase in mechanical strength with the addition of SA. The results also indicate that the K6S4 composition is optimum in terms of mechanical

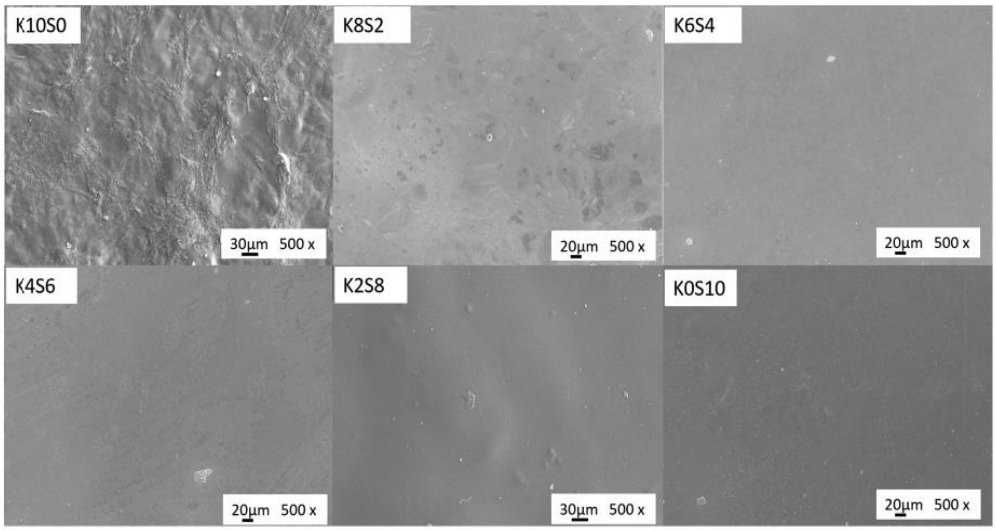

Fig. 8. FESEM images of the KO/SA biomacromolecules films.

strength, wettability, water vapor permeability, moisture absorption, flexibility, and surface texture.

4.9. Biodegradation

The ability for packaging materials to undergo biodegradation when disposed of is of great importance due to sustainable development. The susceptibility of the optimised ratio of the K4S6 composite film to biodegradation was examined using a closed respirometer and the course of the biodegradation by continuous assessment of the total biochemical oxygen demand (BOD) for 28 days is shown in Fig. 9. The BOD involves the oxygen consumed for the oxidation of the biodegradable KO/SA composite film material. The rate of degradation decreased after 2 days (15 mg O_2/L) and was followed by a quick degradation step, eventually attaining a plateau of oxygen consumption after 20 days. The oxygen consumption reached approximately 300 mg O_2/L and the sample was degraded by 92% (calculated from the initial and final weight differences of the sample) on the 28th day. The degradation profile is very similar to that of a carrot bioplastic degraded by seawater organisms [46]. The biodegradation rate obtained in the present study is significantly higher than those observed for polyurethane/polyisocyanurate foams [47] and PLA samples [48,49].

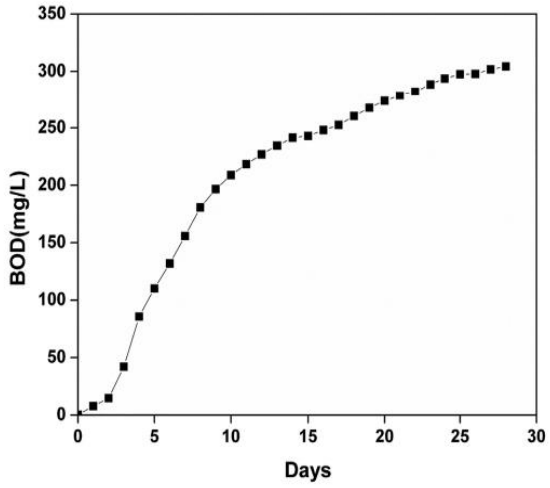

Fig. 9. Biological oxygen demand (BOD) of the K4S6 composite film over 28 days.

5. Conclusions

The synergistic interaction between KO and SA biomacromolecules was utilised for the first time to obtain packaging films with improved properties. This study provides useful information on the structural properties of composite KO/SA films. The mechanical and barrier properties of the KO/SA films changed with varying ratios of these biomacromolecules due to varying degrees of interaction. The good miscibility between KO and SA for film production was explained by FTIR, XRD, SEM, water contact angle, moisture absorption, and water vapor permeability. Furthermore, the composite films exhibited good UV absorption properties. The composite film with 40% KO and 60% SA was found to be the optimum composition from the desired physical and chemical as well as surface properties. The findings of the present study highlight that suitable KO/SA biomacromolecules blends may be promising for the production of films with the desired quality for food packaging applications.

CRediT authorship contribution statement

Conceptualization, **Rohith K.R. and V.V.T. Padil**; methodology, **Rohith K.R.** and **V.V.T. Padil**; validation, **S. Wacławek**; investigation, **Rohith K.R**.; writing–original draft preparation, **Rohith K.R**.; writing-review and editing, **V.V.T. Padil & M. Černík**.; supervision, **V.V.T. Padil**.; project administration,: **V.V.T. Padil**.; funding acquisition, **M. Černík**. All authors have read and agreed to the published version of the manuscript.

Declaration of competing interest

The authors declare no conflict of interest.

Acknowledgments

The authors would like to acknowledge the assistance provided by the Research Infrastructure NanoEnviCz, supported by The Ministry of Education, Youth and Sports of the Czech Republic in the framework of Project No. LM2018124. This work was supported by the project

"Tree Gum Polymers and their Modified Bioplastics for Food Packaging Application" granted by the Bavarian-Czech-Academic-Agency (BTHA) (registration numbers LTAB19007 and BTHA-JC-2019-26) and The Ministry of Education, Youth and Sports in the Czech Republic under the "Inter Excellence Action Programme" within the framework of the project "Bio-based Porous 2D Membranes and 3D Sponges Based on Functionalized Tree Gum Polysaccharides and their Environmental Application" (registration number LTAUSA19091) – TUL internal No.: 18309/136. This work was also supported by The Ministry of Education, Youth and Sports of the Czech Republic and the European Union—European Structural and Investment Funds in the framework of the Operational Program Research, Development and Education—Project Hybrid Materials for Hierarchical Structures (HyHi, Reg. No. CZ.02.1.01/0.0/0.0/16_019/0000843).

Appendix A. Supplementary data

Supplementary data to this article can be found online at https://doi.org/10.1016/j.ijbiomac.2021.02.156.

References

[1] B. Priya, V. Kumar, D. Pathania, A. Singh, Synthesis, characterization and antibacterial activity of biodegradable starch/PVA composite films reinforced with cellulosic fiber, Carbohydr. Polym. 109 (2014) 171–179, https://doi.org/10.1016/j.carbpol.2014.03.044.
[2] K. Mansur, A. De Campos, M. Corso, B. Ribeiro, J. Manoel, Corn and cassava starch with carboxymethyl cellulose films and its mechanical and hydrophobic properties, Carbohydr. Polym. 223 (2019), 115055, https://doi.org/10.1016/j.carbpol.2019.115055.
[3] S. Benavides, R. Villalobos-carvajal, J.E. Reyes, Physical, mechanical and antibacterial properties of alginate film: effect of the crosslinking degree and oregano essential oil concentration, J. Food Eng. 110 (2012) 232–239, https://doi.org/10.1016/j.jfoodeng.2011.05.023.
[4] J. Liu, H. Wang, P. Wang, M. Guo, S.S. Jiang, X. Li, S.S. Jiang, Films based on k -carrageenan incorporated with curcumin for freshness monitoring, Food Hydrocoll. 83 (2018) 134–142, https://doi.org/10.1016/j.foodhyd.2018.05.012.
[5] S.A.A. Mohamed, M. El-sakhawy, Abdel-monem, M. El-sakhawy, Polysaccharides, protein and lipid -based natural edible films in food packaging: a review, Carbohydr. Polym. 238 (2020)https://doi.org/10.1016/j.carbpol.2020.116178.
[6] J. Puskuri, V. Katukam, R.B. Sashidhar, Immunological evaluation of gum kondagogu (Cochlospermum gossypium): a tree gum with potential applications in food and pharma industry, Bioact. Carbohydrates Diet. Fibre. 11 (2017) 48–52, https://doi.org/10.1016/j.bcdf.2017.07.003.
[7] S. Park, D. Choi, H. Jeong, J. Heo, J. Hong, Drug loading and release behavior depending on the induced porosity of chitosan/cellulose multilayer nanofilms, Mol. Pharm. 14 (2017) 3322–3330, https://doi.org/10.1021/acs.molpharmaceut.7b00371.
[8] N.A. Ismail, K. Anuar, M. Amin, M.H. Razali, Novel gellan gum incorporated TiO_2 nanotubes film for skin tissue engineering, Mater. Lett. 228 (2018) 116–120, https://doi.org/10.1016/j.matlet.2018.05.140.
[9] F. Jiang, Y.-L. Hsieh, Amphiphilic superabsorbent cellulose nanofibril aerogels, J. Mater. Chem. A (2014) 6337–6342, https://doi.org/10.1039/c4ta00743c.
[10] F. Liu, W. Chang, M. Chen, F. Xu, J. Ma, F. Zhong, Film-forming properties of guar gum, tara gum and locust bean gum, Food Hydrocoll. 98 (2020)https://doi.org/10.1016/j.foodhyd.2019.03.028.
[11] V.V.T. Padil, S. Wacławek, M. Černík, R.S. Varma, Tree gum-based renewable materials: sustainable applications in nanotechnology, biomedical and environmental fields, Biotechnol. Adv. 36 (2018) 1984–2016, https://doi.org/10.1016/j.biotechadv.2018.08.008.
[12] S. Abbasiliasi, T.J. Shun, T.A. Tengku Ibrahim, N. Ismail, A.B. Ariff, N.K. Mokhtar, S. Mustafa, Use of sodium alginate in the preparation of gelatin-based hard capsule shells and their evaluation: in vitro, RSC Adv. 9 (2019) 16147–16157, https://doi.org/10.1039/c9ra01791g.
[13] S. Bandyopadhyay, N. Saha, P. Sáha, Bacterial cellulose and guar gum based modified PVP-CMC hydrogel films: characterized for packaging fresh berries, Food Packag. Shelf Life 22 (2019)https://doi.org/10.1016/j.fpsl.2019.100402.
[14] G.W. Oh, S.Y. Nam, S.J. Heo, D.H. Kang, W.K. Jung, Characterization of ionic cross-linked composite foams with different blend ratios of alginate/pectin on the synergistic effects for wound dressing application, Int. J. Biol. Macromol. 156 (2020) 1565–1573, https://doi.org/10.1016/j.ijbiomac.2019.11.206.
[15] K.R. Aadil, A. Nathani, C.S. Sharma, N. Lenka, Investigation of poly (vinyl) alcohol-gellan gum based nano fiber as scaffolds for tissue engineering applications, J. Drug Deliv. Sci. Technol. 54 (2019), 101276, https://doi.org/10.1016/j.jddst.2019.101276.
[16] V.V.T. Padil, C. Senan, S. Waclawek, M. Černík, S. Agarwal, R.S. Varma, Bioplastic fibers from gum arabic for greener food wrapping applications, ACS Sustain. Chem. Eng. 7 (2019) 5900–5911, https://doi.org/10.1021/acssuschemeng.8b05896.
[17] J. Guo, L. Ge, X. Li, C. Mu, D. Li, Periodate oxidation of xanthan gum and its crosslinking effects on gelatin-based edible fi lms, Food Hydrocoll. 39 (2014) 243–250, https://doi.org/10.1016/j.foodhyd.2014.01.026.
[18] M. Sapper, P. Wilcaso, M.P. Santamarina, A. Chiralt, Antifungal and functional properties of starch-gellan fi lms containing thyme (Thymus zygis) essential oil, Food Control 92 (2018) 505–515, https://doi.org/10.1016/j.foodcont.2018.05.004.
[19] N. Zhang, J. Xu, X. Gao, X. Fu, D. Zheng, Factors affecting water resistance of alginate/gellan blend films on paper cups for hot drinks, Carbohydr. Polym. 156 (2017) 435–442, https://doi.org/10.1016/j.carbpol.2016.08.101.
[20] F. Tatar, M. Tugçe, M. Dervisoglu, D. Cekmecelioglu, T. Kahyaoglu, Evaluation of hemicellulose as a coating material with gum arabic for food microencapsulation, Food Res. Int. 57 (2014) 168–175, https://doi.org/10.1016/j.foodres.2014.01.022.
[21] A.A. Oun, J. Rhim, Carrageenan-based hydrogels and films: effect of ZnO and CuO nanoparticles on the physical, mechanical, and antimicrobial properties, Food Hydrocoll. 67 (2017) 45–53, https://doi.org/10.1016/j.foodhyd.2016.12.040.
[22] D. Khodaei, K. Oltrogge, Z. Hamidi-esfahani, Preparation and characterization of blended edible films manufactured using gelatin, tragacanth gum and, Persian gum, LWT Food Sci. Technol. 117 (2020)https://doi.org/10.1016/j.lwt.2019.108617.
[23] A. Amalraj, J.T. Haponiuk, S. Thomas, S. Gopi, Preparation, characterization and antimicrobial activity of polyvinyl alcohol/gum arabic/chitosan composite films incorporated with black pepper essential oil and ginger essential oil, Int. J. Biol. Macromol. 151 (2020) 366–375, https://doi.org/10.1016/j.ijbiomac.2020.02.176.
[24] V.T.P. Vinod, R.B. Sashidhar, K.I. Suresh, B. Rama Rao, U.V.R. Vijaya Saradhi, T. Prabhakar Rao, Morphological, physico-chemical and structural characterization of gum kondagogu (Cochlospermum gossypium): a tree gum from India, Food Hydrocoll. 22 (2008) 899–915, https://doi.org/10.1016/j.foodhyd.2007.05.006.
[25] S. Kalaignana Selvi, J. Mahesh Kumar, R.B. Sashidhar, Anti-proliferative activity of gum kondagogu (Cochlospermum gossypium)-gold nanoparticle constructs on B16F10 melanoma cells: an in vitro model, Bioact. Carbohydrates Diet. Fibre. 11 (2017) 38–47, https://doi.org/10.1016/j.bcdf.2017.07.002.
[26] Y. Pang, F. Xi, J. Luo, G. Liu, T. Guo, C. Zhang, An alginate film-based degradable triboelectric nanogenerator, RSC Adv. 8 (2018) 6719–6726, https://doi.org/10.1039/c7ra13294h.
[27] F. Ugur Nigiz, Graphene oxide-sodium alginate membrane for seawater desalination through pervaporation, Desalination. 485 (2020)https://doi.org/10.1016/j.desal.2020.114465.
[28] Q. Wu, Q. Wang, J. Fu, R. Ren, Polysaccharides derived from natural sources regulate triglyceride and cholesterol metabolism: a review of the mechanisms, Food Funct. 10 (2019) 2330–2339, https://doi.org/10.1039/c8fo02375a.
[29] E. Tavassoli-Kafrani, H. Shekarchizadeh, M. Masoudpour-behabadi, Development of edible films and coatings from alginates and carrageenans, Carbohydr. Polym. 137 (2016) 360–374, https://doi.org/10.1016/j.carbpol.2015.10.074.
[30] B. Rukmanikrishnan, S. Ramalingam, S. Kumar, J.J. Lee, J.J. Lee, S.K. Rajasekharan, J.J. Lee, J.J. Lee, Binary and ternary sustainable composites of gellan gum, hydroxyethyl cellulose and lignin for food packaging applications: biocompatibility, antioxidant activity, UV and water barrier properties, Int. J. Biol. Macromol. 153 (2020) 55–62, https://doi.org/10.1016/j.ijbiomac.2020.03.016.
[31] B. Saberi, S. Chockchaisawasdee, J.B. Golding, C.J. Scarlett, C.E. Stathopoulos, Characterization of pea starch-guar gum biocomposite edible films enriched by natural antimicrobial agents for active food packaging, Food Bioprod. Process. 105 (2017) 51–63, https://doi.org/10.1016/j.fbp.2017.06.003.
[32] T. Karbowiak, H. Hervet, L. Léger, D. Champion, F. Debeaufort, A. Voilley, Effect of plasticizers (water and glycerol) on the diffusion of a small molecule in iota-carrageenan biopolymer films for edible coating application, Biomacromolecules 7 (2006) 2011–2019, https://doi.org/10.1021/bm060179r.
[33] C. Li, W. Zhu, H. Xue, Z. Chen, Y. Chen, X. Wang, Physical and structural properties of peanut protein isolate-gum Arabic fi lms prepared by various glycation time, Food Hydrocoll. 43 (2015) 322–328, https://doi.org/10.1016/j.foodhyd.2014.06.003.
[34] ASTM D882, Standard Test Method for Tensile Properties of Thin Plastic Sheeting, vol. 87, 2013 3–5, https://doi.org/10.1520/D0882-10.2.
[35] B. Rukmanikrishnan, F. Rigana, M. Ismail, R. Kumar, S. Soo, J. Lee, Blends of gellan gum/xanthan gum/zinc oxide based nanocomposites for packaging application: rheological and antimicrobial properties, Int. J. Biol. Macromol. 148 (2020) 1182–1189, https://doi.org/10.1016/j.ijbiomac.2019.11.155.
[36] L. Yang, J. Yang, X. Qin, J. Kan, F. Zeng, J. Zhong, Ternary composite films with simultaneously enhanced strength and ductility: effects of sodium alginate-gelatin weight ratio and graphene oxide content, Int. J. Biol. Macromol. 156 (2020) 494–503, https://doi.org/10.1016/j.ijbiomac.2020.04.057.
[37] S. Shankar, L.F. Wang, J.W. Rhim, Preparations and characterization of alginate/silver composite films: effect of types of silver particles, Carbohydr. Polym. 146 (2016) 208–216, https://doi.org/10.1016/j.carbpol.2016.03.026.
[38] W. Jin, R. Song, W. Xu, Y. Wang, J. Li, B. Ramin, Y. Li, B. Li, Analysis of deacetylated konjac glucomannan and xanthan gum phase separation by fi lm forming, Food Hydrocoll. 48 (2015) 320–326, https://doi.org/10.1016/j.foodhyd.2015.02.007.
[39] F. Sadat, R. Kadkhodaee, B. Emadzadeh, Preparation and characterization of tragacanth – locust bean gum edible blend films, Carbohydr. Polym. 139 (2016) 20–27, https://doi.org/10.1016/j.carbpol.2015.11.069.
[40] A. Ramu, M. Shanmugam, P. Ilansuriyan, R. Anandhakumar, Composite film for edible oil packaging from carrageenan derivative and konjac glucomannan: application and quality evaluation, Polym. Test. 78 (2019)https://doi.org/10.1016/j.polymertesting.2019.105936.
[41] R. Balasubramanian, S.S. Kim, J. Lee, Novel synergistic transparent k-carrageenan/xanthan gum/gellan gum hydrogel film: mechanical, thermal and water barrier properties, Int. J. Biol. Macromol. 118 (2018) 561–568, https://doi.org/10.1016/j.ijbiomac.2018.06.110.
[42] B. Rukmanikrishnan, C. Jo, S. Choi, S. Ramalingam, J. Lee, Flexible ternary combination of gellan gum, sodium carboxymethyl cellulose, and silicon dioxide nanocomposites fabricated by quaternary ammonium silane : rheological, thermal, and

antimicrobial properties, ACS Omega 5 (2020) 28767–28775, https://doi.org/10.1021/acsomega.0c04087.
[43] X. Zhang, Y. Zhao, Y. Li, L. Zhu, Z. Fang, Q. Shi, Physicochemical, mechanical and structural properties of composite edible films based on whey protein isolate/psyllium seed gum, Int. J. Biol. Macromol. 153 (2020) 892–901, https://doi.org/10.1016/j.ijbiomac.2020.03.018.
[44] T.T. Chau, W.J. Bruckard, P.T.L. Koh, A.V. Nguyen, A review of factors that affect contact angle and implications for flotation practice, Adv. Colloid Interf. Sci. 150 (2009) 106–115, https://doi.org/10.1016/j.cis.2009.07.003.
[45] S. Seyedi, A. Koocheki, M. Mohebbi, Y. Zahedi, Lepidium perfoliatum seed gum: a new source of carbohydrate to make a biodegradable film, Carbohydr. Polym. 101 (2014) 349–358, https://doi.org/10.1016/j.carbpol.2013.09.072.
[46] G. Perotto, L. Ceseracciu, R. Simonutti, U.C. Paul, S. Guzman-Puyol, T.N. Tran, I.S. Bayer, A. Athanassiou, Bioplastics from vegetable waste: via an eco-friendly water-based process, Green Chem. 20 (2018) 894–902, https://doi.org/10.1039/c7gc03368k.
[47] M. Borowicz, J. Paciorek-Sadowska, J. Lubczak, B. Czupryński, Biodegradable, flame-retardant, and bio-based rigid polyurethane/polyisocyanurate foams for thermal insulation application, Polymers (Basel) 11 (2019)https://doi.org/10.3390/polym11111816.
[48] M. Borowicz, J. Paciorek-Sadowska, M. Isbrandt, Ł. Grzybowski, B. Czupryński, Glycerolysis of poly(lactic acid) as away to extend the "life cycle" of this material, Polymers (Basel) 11 (2019)https://doi.org/10.3390/polym11121963.
[49] R. Scaffaro, A. Maio, F. Sutera, E. ortunato Gulino, M. Morreale, Degradation and recycling of films based on biodegradable polymers: a short review, Polymers (Basel) 11 (2019)https://doi.org/10.3390/polym11040651.

4.2. Hierarchically Porous Bio-Based Sustainable Conjugate Sponge for Highly Selective Oil/Organic Solvent Absorption

Abstract: This paper describes a novel conjugate biodegradable sponge based on tree gum kondagogu with excellent selective oil/organic solvent absorption ability. The conjugate sponge is made hydrophobic (water contact angle 133°) by post-process vapor phase silylation, and has a porosity of ≈94% with very low density (18.4 mg cm−3). The sponge can selectively absorb up to 19–43 times its weight of oils and organic solvents. Meanwhile, good reusability is also observed in at least 10 cycles. The biodegradation behavior is studied from biological oxygen demand (BOD) analysis, where the non-silylated and silylated sponges degraded over 28 days by 92% and 76%, respectively, in wastewater sludge. The novel conjugate bio-based and biodegradable sponge used in this study is a promising sustainable material for clearing oil spills and for water treatment.

Citation: R.K. Ramakrishnan, V.V.T. Padil, M. Škodová, S. Wacławek, M. Černík, S. Agarwal, Hierarchically Porous Bio-Based Sustainable Conjugate Sponge for Highly Selective Oil/Organic Solvent Absorption, Adv. Funct. Mater. 2100640 (2021) 1–9.

RESEARCH ARTICLE

ADVANCED FUNCTIONAL MATERIALS
www.afm-journal.de

Hierarchically Porous Bio-Based Sustainable Conjugate Sponge for Highly Selective Oil/Organic Solvent Absorption

Rohith K. Ramakrishnan, Vinod V. T. Padil, Marcela Škodová, Stanisław Wacławek, Miroslav Černík,* and Seema Agarwal**

This paper describes a novel conjugate biodegradable sponge based on the tree gum kondagogu with excellent selective oil/organic solvent absorption ability. The conjugate sponge is made hydrophobic (water contact angle 133°) by post-process vapor phase silylation, has porosity of ≈94% with very low density (18.4 mg cm^{-3}). The sponge can absorb selectively up to 19–43 times its weight of oils and organic solvents. Meanwhile, good reusability is also observed in up to at least 10 cycles. The biodegradation behavior is studied from BOD (biological oxygen demand) analysis, where the non-silylated and silylated sponges degraded over 28 days by 92% and 76%, respectively, in waste-water sludge. The novel conjugate bio-based and biodegradable sponge used in this study is a promising sustainable material for clearing oil spills and for water treatment.

1. Introduction

Severe environmental and ecological problems created due to oil pollution are a global concern.[1] Although biodegradation, burning, mechanical collection, and chemical treatment are some of the most common methods employed for cleaning oil pollutants from water, the collection of oil with porous absorbent materials is highly efficient, convenient, and without the risk of secondary pollution.[2,3] For practical and industrial usage, the sorbent should show 1) high selectivity for oil in comparison to water, 2) oil absorption capacity, 3) fast oil uptake, 4) reusability, and 5) mechanical strength for reuse, as well as environmental friendliness and low cost.[4]

Open-cell porous materials, also known as sponges, can be the ideal oil absorbents due to their simple fabrication methods, low density, large pore volume, porosity, and superabsorbent capacity.[5–7] However, commercially used polypropylene has limited sorption capability (less than 10 g g^{-1}) and non-biodegradability.[8] Traditional inorganic sponges, such as silica sponges, are too brittle, and carbon-based sponges,[9] graphene oxide (GO) sponges,[10] magnetic PDA (polydopamine)-coated MF (melamine-formaldehyde) sponges,[11] 3D-SiO_2 electrospun nanofibers-PMF (poly(melamine-formaldehyde)/LDH (layered double hydroxide) sponges,[12] and MS@PIDO (melamine sponge @poly(imide dioxime)/Alg (alginate) hybrid sponges[13] require expensive equipment, processing under harsh conditions, and sophisticated technologies, which restricts their practical applications.[14,15] In contrast, natural organic sorbents and polysaccharides, including alginate,[16] sawdust,[17] corn straw,[18] and wood chips,[19] are sustainable alternatives for the removal of oil from water. Other advantages include recyclability, recoverability of oils and chemicals, their relatively easy disposal, and degradability. However, the presence of hydroxyl groups in natural polysaccharides makes them amphiphilic, which in turn leads to poor selectivity for the adsorption of oil and hydrophobic compounds.[20–22] Hence, there is a need to study new and modified sponge materials with promising properties.

Tree exudate gums are naturally occurring polysaccharide biopolymers, which are endowed with excellent gel-forming ability, although in a pristine form, they are not suitable for oil absorption from an aqueous environment due to their higher hydrophilicity and brittleness.[23] In fact, they absorb water to make a hydrogel. Consequently, feasible approaches to enhancing their hydrophobicity, for example, by surface functionalization with hydrophobic molecules such as organosilicon compounds, are in high demand.[24,25]

Here we report the preparation and use of sustainable hydrophilic biopolymers gum kondagogu (GK) and sodium alginate (SA) for the fabrication of a reusable, hydrophobic, flexible, and ultralightweight (18 mg cm^{-3}) conjugate sponge for the selective and efficient separation of oil and organic solvents from aqueous

R. K. Ramakrishnan, Dr. V. V. T. Padil, M. Škodová, Dr. S. Wacławek, Prof. M. Černík
Institute for Nanomaterials
Advanced Technologies and Innovation (CXI)
Technical University of Liberec (TUL)
Studentská 1402/2, Liberec 461 17, Czech Republic
E-mail: vinod.padil@tul.cz; miroslav.cernik@tul.cz
Prof. S. Agarwal
Macromolecular Chemistry II, Bavarian Polymer Institute
University of Bayreuth
Universitätsstraße 30, Bayreuth 95447, Germany
E-mail: agarwal@uni-bayreuth.de
The ORCID identification number(s) for the author(s) of this article can be found under https://doi.org/10.1002/adfm.202100640.

DOI: 10.1002/adfm.202100640

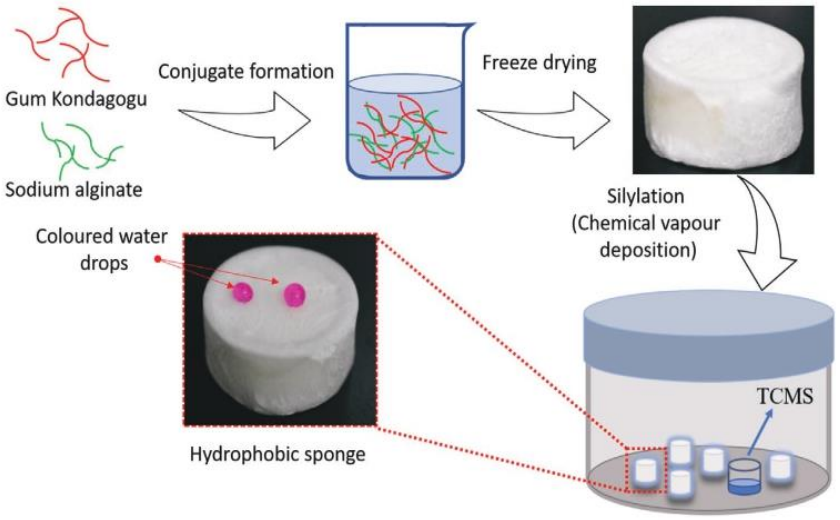

Figure 1. The fabrication of a conjugate GK/SA sponge and the silylation process by the chemical vapor deposition of TCMS on its surface is shown here.

solution mixture. Gum kondagogu, a cheap and sustainable polysaccharide, alone does not make a mechanically stable sponge due to its brittle nature. The non-toxic gum kondagogu, exudated from *Cochlospermum gossypium*, containing uronic acid, glucuronic acid, galacturonic acid, and low amounts of proteins, etc., has plentiful functional groups such as hydroxyl, acetyl, carbonyl, and carboxylic, which expedite network formation with other biopolymers. It can form a conjugate with sodium alginate, which is another polysaccharide comprised of two repeating, mannuronic acid and guluronic acid monosaccharide units, showing excellent liquid-gel behavior in an aqueous environment. The similarities in the basic structural units of these polysaccharides lead to the formation of a sponge with excellent mechanical properties. The method of conjugate sponge preparation as the first step is elaborated. Furthermore, silylation from the vapor phase may be performed to change the surface wetting behavior of sponges to make them suitable for selective absorption of oil, that is, hydrophilicity to hydrophobicity and oleophilic transition. The optimized silylation process provided homogenous modification of the conjugate sponge. Hydrophobically modified sponges show selectivity for the absorption of several organic solvents and oils of different viscosities from water mixture in a short period of time for several different cycles. The bio-based polysaccharide-based biodegradable conjugate sponges with high oil/organic solvent-water absorption selectivity and after-use biodegradation provide a sustainable solution to environmental protection against oil spills and pollution.

2. Results and Discussion

2.1. GK/SA Sponge Preparation Procedure

The optimal proportions of GK and SA for obtaining a stable sponge were examined by the preparation of 11 samples with a decreasing ratio of GK to SA. From pure GK, the produced sponge has no stable structure (Figure S1, Supporting Information). In a GK/SA mixture, due to the interaction between GK and SA, the structural integrity is formed, and the stability is proportional to SA addition. Similarly, the bulk density of the sponges was found to increase with an increasing proportion of SA (Figure S2, Supporting Information). Between 10% and 50%, there is only a slight increment in density (from 17.0 to 18.4 mg cm^{-3}), but after that, the density rises steeply (to more than 30 mg cm^{-3} for pure SA). Therefore, we used a GK to SA ratio of 1:1 for further studies, considering the lowest density with sufficient structural integrity. The synthesis of the GK/SA sponge and the silylation process is illustrated in **Figure 1**.

2.2. Morphology

The digital photograph of an optimized GK/SA sponge (**Figure 2**A) and a sponge on Foxtail grass is shown in Figure 2B. The ultra-light weighing character results from the GK/SA sponges morphology examined by scanning electron microscopy (SEM) (Figure 2C,E). This highly porous and open channel oriented structure is formed during freeze-drying by the space left after ice sublimation.[26] The cells are highly regular compared to the irregular topology of alginate sponge reported in the past,[27] probably due to the GK-SA conjugate formation. According to Tang et al.,[28] oriented open cells enhance the mechanical robustness of the pore structure. The formed porous structure is well-preserved and is not affected by the trichloromethylsilane (TCMS) hydrophobic modification (Figure 2D,F), which overcomes the previously observed limitation of the aqueous silylation process.[29]

The successful silylation of the GK/SA sponge was confirmed by the sharp Si peak on the recorded energy dispersive X-ray spectroscopy spectrum compared to the no-peak for the unmodified sponge (Figure S3, Supporting Information). The elemental distribution also indicates a high degree of Si homogeneity without aggregates of silane within the sponge. The advantage of the chemical vapor deposition (CVD) method with an extremely volatile TCMS is that a homogeneous Si-based hydrophobic surface is formed without significant change in the pore structure. The density increase was minor (21 ± 0.5 mg cm^{-3}).

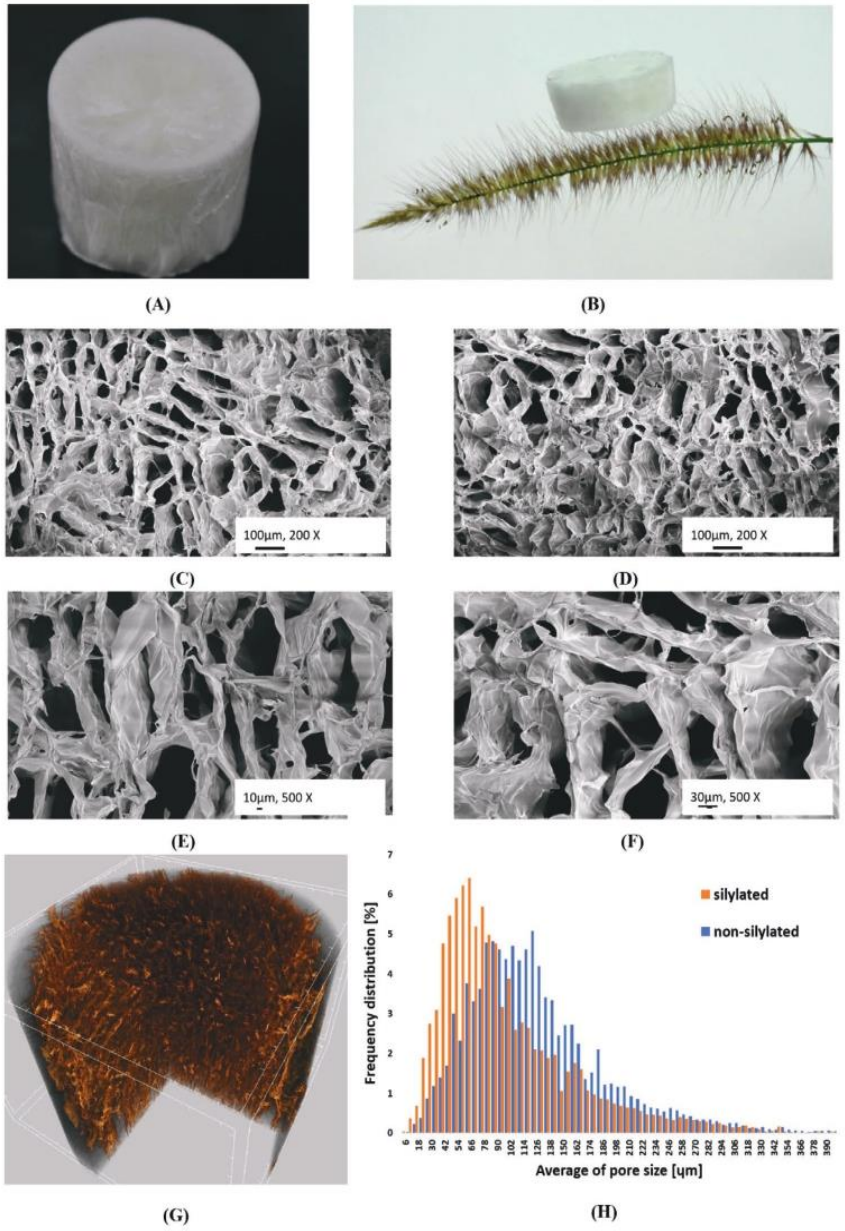

Figure 2. Digital photograph of the GK/SA sponge (A) kept on Foxtail grass showing the ultra-lightweight nature of the sponge (B), FE-SEM micrographs of GK/SA sponge (C,E), and silylated sponge (D,F). 3D micro-CT images of silylated sponge (G), the pore size distribution of non-silylated and silylated GK/SA sponges (H).

2.3. Porosity

Low bulk sponge density and high porosity are critical features that significantly influence the absorption capacity of the sponge. The microCT image of non-silylated (shown in Figure S4, Supporting Information) and silylated (Figure 2G) materials confirmed the very porous structure (in a measured range of 3 to 570 µm). The silylated sponge retains the open pore structure with only a very slight change in the porosity to 93% (with an omissible closed porosity of 10^{-4}%), whereas the non-silylated material has an open porosity of 94% and a closed one again of 10^{-4}%. A determining bulk density of more than 18.4 ± 0.6, mg cm^{-3} implies the presence of additional smaller pores, which were not determined by microCT. These microscopic and nanosized pores were formed during the swelling of the GK/SA polymer mixture and remain after silylation. When the GK and SA were added to water, the inter and intra molecular H bonding and ionic interactions bound them together,

which led to the formation of a structure where water exists in the µm as well as nm-sized channels/cages created by the biopolymer network. During lyophilization, water molecules were sublimed, leaving behind a porous sponge network possessing micro and nanopores.

During the silylation process, micropores are covered by silanes, and therefore their size is slightly reduced from a mean pore size of 122 to 100 µm (Figure 2H).

2.4. Attenuated Total Reflection-Fourier Transform Infrared Analysis

Fourier transform infrared (FTIR) spectroscopy provides information about the molecular structure and is useful for the characterization of biopolymers (Figure S5, Supporting Information). The detailed FTIR peak correlations with the biopolymer structure are provided in the Supporting Information. The abundant hydroxyl groups on the GK/SA sponge matrix created the hydrophilic character of the sponge. Subsequently, these groups may be used in the silylation that leads to surface hydrophobicity by reaction with TCMS (Figure S7, Supporting Information).

Compared to the spectrum of the unmodified sample, the silylated sponge showed a specific absorbance at 779 and 1273 cm^{-1}, assignable to the Si—CH_3 stretching and bending vibrations, respectively.[30,31] This alludes to the presence of methyl silane moieties and successful modification of sponge (Figure S6, Supporting Information). The Si—OH vibrations were assigned to the band at ≈940 cm^{-1}. Furthermore, the peak at approximately 1637 cm^{-1} that appeared in the silylated sample is due to the O—H bending vibrations arising from the adsorbed moisture content. Therefore, the new peaks in the spectrum imply successful silylation on the surface of the modified GK/SA sponge.

2.5. Water Contact Angle and Wettability

The original GK/SA sponge exhibited highly hydrophilic characteristics and a strong affinity for water. After silylation, the sponge surface became hydrophobic (and oleophilic), as confirmed by contact angle measurements with water.

Although the original sponge immediately absorbed water droplets and no measurable value was recorded (**Figure 3**A), the silylated sponge showed a high contact angle of 133° (Figure 3B) since the hydrophobic silicone coating formed on the surface repels water droplets.

The unmodified GK/SA sponge is amphiphilic, absorbs both the water and oil droplets immediately without any selectivity (Figure 3C). In contrast, the modified sample was very selective in terms of the absorption of oil. It showed instant wetting by the oil droplet, whereas water could not penetrate the surface (Figure 3D).

When non-silylated and silylated GK/SA sponges were placed on the water surface, the silylated sample stayed on the surface, while the non-silylated sample absorbed water and sank immediately (Figure 3E). Moreover, the hydrophilic GK/SA sponge disintegrated because of the penetration of water and collapsing the sponge structure. The silylated GK/SA sponge immersed in water showed no structural changes (Figure 3F).

2.6. Mechanical Properties

The mechanical properties of the non-silylated and silylated GK/SA sponges were evaluated by compression measurements. The typical stress–strain curves of the samples are shown in Figure S8, Supporting Information. The compressive stress at 20% strain of the non-silylated GK/SA sponge (6.5 kPa) was more than twice that of the alginate sponge reported earlier.[32] The notable improvement in stiffness may be closely related to the strong interaction between SA and GK through hydrogen bonding. After silylation, the compressive stress was significantly reduced due to the interrupted interaction between GK/SA. The reduction of compressive stress after silylation is assigned to two factors; one is the repulsive interactions existing between the polysiloxane methyl groups.[33] The other reason is the decrease in the degree of hydrogen bonding within the conjugate network after silylation, which leads to reduced conjugate bridge density within the material. However, the modified GK/SA sponge presented here possesses significantly more promising mechanical properties compared to other biomass-derived sponges.[34]

2.7. Oil and Solvent Absorption

The 3D inter-connected open pores and the goal-directed hydrophobically modified surface of the GK/SA sponge make it a promising and sustainable bio-based porous system for the removal of oils and organic solvents from water. **Figure 4**A,B shows its strong sorption capability for both low density (diesel oil) and high density (chloroform) solvents from water (also see Movie S1 and Movie S2, Supporting Information). When the GK/SA sponge came into contact with a diesel slick (stained with Oil Red EGN dye) floating on the water surface, it absorbed the diesel entirely within seconds without losing its form. After sorption, the sponge floated on the surface, indicating its potential use for the easy removal of oil spillages and chemical leakages. Similarly, the GK/SA sponge quickly absorbed chloroform and organic solvents denser than water (Figure 4B and Movie S2, Supporting Information). Detailed results for chloroform, ethanol, diesel, toluene, waste oil, hexane, coconut oil, and petroleum ether are shown in Table S1, Supporting Information.

The silylated bio-based GK/SA sponge showed a very high affinity for organic compounds with an absorption capacity of ≈43 times its initial weight. This high absorption capacity is comparable to carbon sponges and conjugate sponges made from the cellulose-based waste newspaper (29–51 g g^{-1})[35] and cellulose nanocrystal/poly(vinyl alcohol) sponges (32.7 g g^{-1}).[36]

The removal of oil by the sponges is mainly governed by adsorption on the surface and absorption into the bulk by capillary diffusion. The microchannels on the sponges formed during lyophilization greatly facilitate the transport of oils through the interior of the material, resulting in excellent oil absorption performance, which is illustrated in **Figure 5**.

2.8. Crude Oil Absorption Study

Crude oil spillage is one of the most common types of water contamination. Figure S9, Supporting Information, shows the absorption test using a mixture in which 2 mL of crude oil

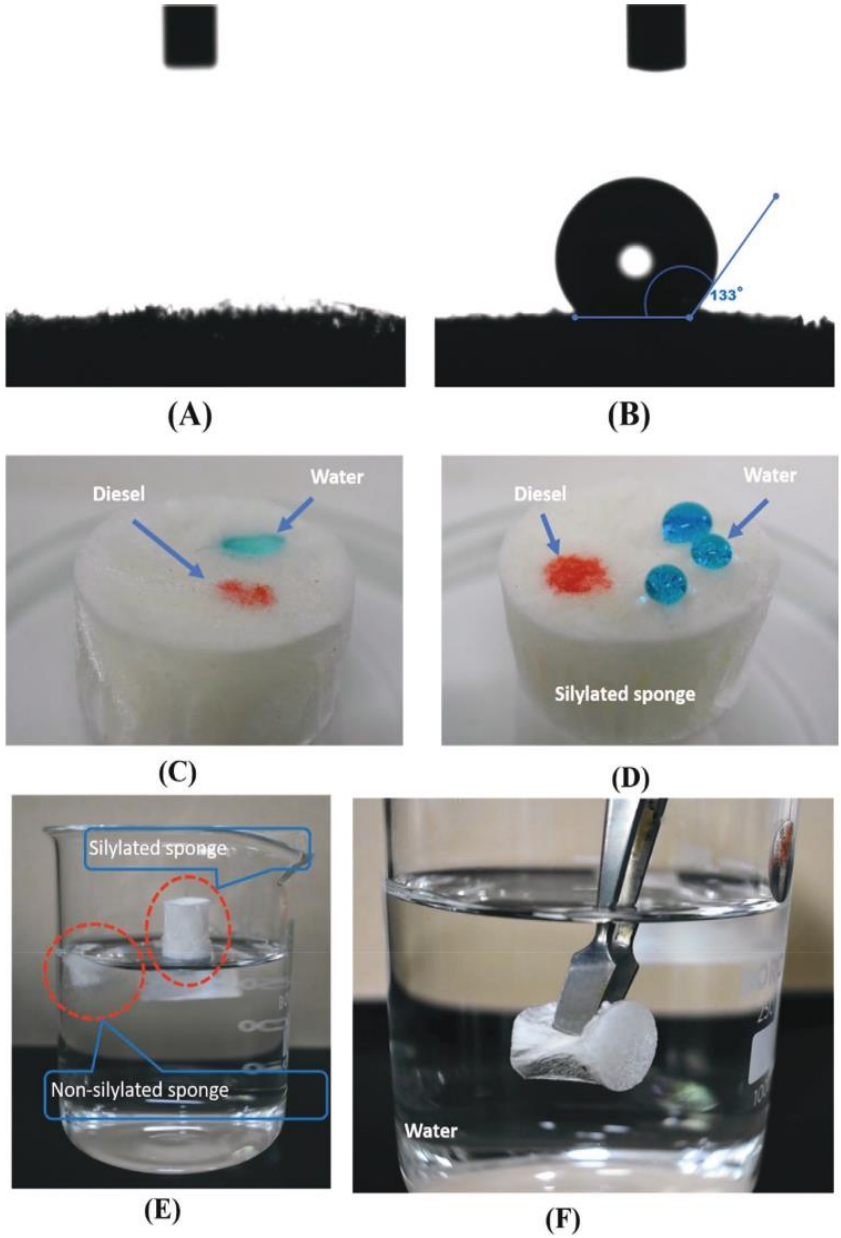

Figure 3. Images taken during measurement of contact angle for A) GK/SA sponge, and B) TCMS modified GK/SA sponge, C,D) Optical images of water and diesel oil droplet absorption on GK/SA sponge and TCMS modified sponge respectively, E) floating on the water surface, and F) a sample of the modified GK/SA sponge immersed in water.

was mixed with 10 mL of water. After approximately 1 min, the oil was completely absorbed (99.9%) by the GK/SA sponge (Movie S3, Supporting Information). Therefore, the kinetics of pure crude oil absorption was studied in more detail. The determined absorption is fast. In total, 23.8, 27.8, and 28.5 g g^{-1} of crude oil were absorbed within 0.5, 1, and 2 min, respectively, which indicates the high affinity of the present sponges for the specific absorption of crude oil. The maximum absorption capacity of 28.5 g g^{-1} achieved at 3 min is nearly double that of state-of-the-art polypropylene fibrous mats,[8] higher than that of cellulose sponges made from waste paper (20 g g^{-1}),[37] superhydrophobic sawdust (17.5 g g^{-1}),[17] and is comparable with graphene-carbon nanotube sponges (30 g g^{-1}).[38]

2.9. Reusability

The reusability of the hydrophobic GK/SA sponge is advantageous for its practical application as a sustainable oil/organic

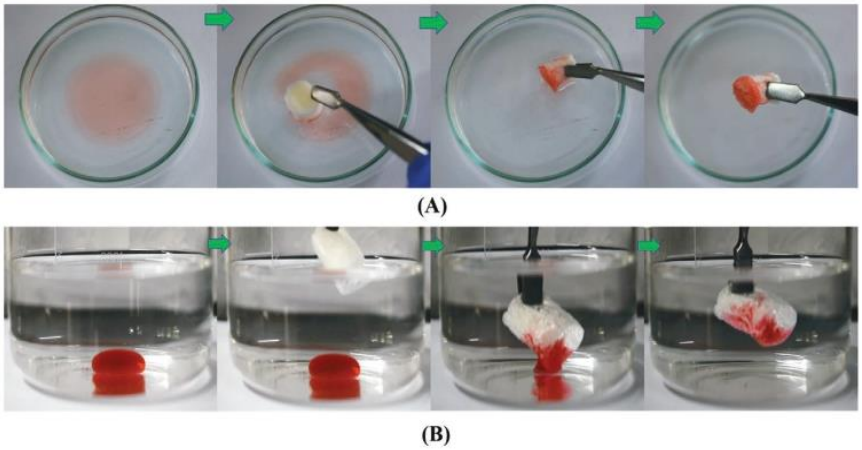

Figure 4. The fast and selective absorption process of diesel (A) and chloroform (B) from water by the silylated GK/SA sponge (both diesel and chloroform are stained by the Oil Red EGN dye).

solvent absorbent. Therefore, the material was tested for repeated absorption of crude oil and diesel, as examples of high and lower viscous liquids, respectively.

Crude oil was used six times for repeated absorption and manual squeezing (Figure S11A, Supporting Information). The sample showed high absorption capacity (28.5 g g^{-1}) and absorbed 1.813 g of crude oil in the first cycle. The squeezing removed only 1.548 g of the absorbed oil (squeezed ratio of 85%), and therefore 0.265 g of the oil remained absorbed. During this first squeezing, the porous structure of the sponge substantially collapsed, which was observed previously,[39] and therefore, its capacity for the second absorption was reduced. In

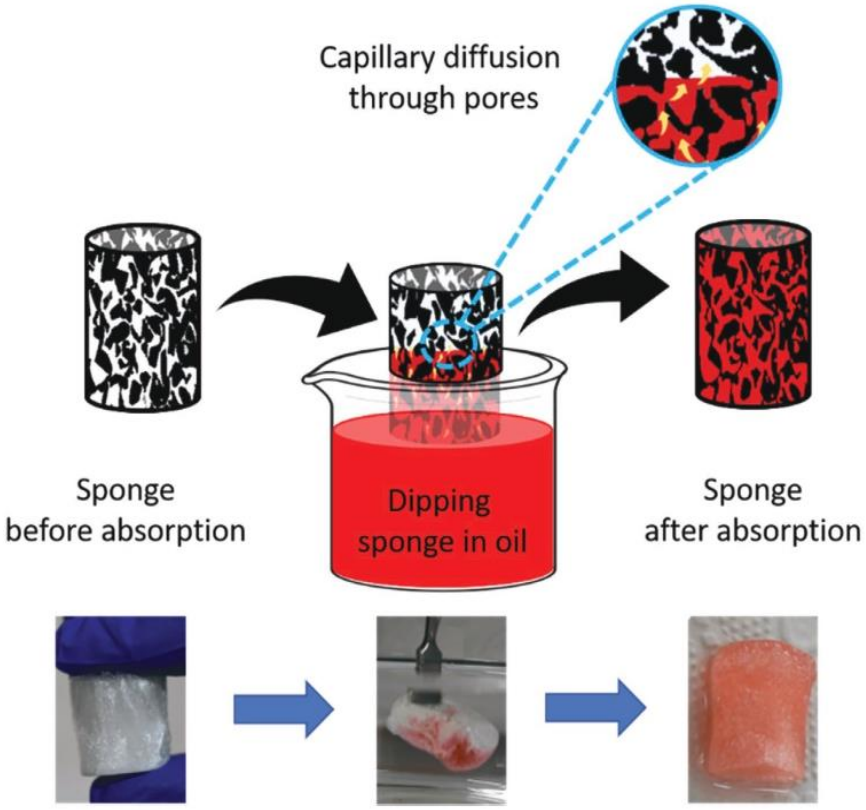

Figure 5. Absorption of oils by the silylated GK/SA sponge driven by capillary diffusion through the interconnected pores.

the second cycle, only 1.061 g of oil was absorbed, which gave the newly absorbed amount of 16.7 g g^{-1}, which was 20.85 g g^{-1}, including the remaining oil. The same amount (1.026 g) was squeezed back, and the squeezed ratio reached 97%. Hence, the sponge structure and its capacity were not significantly influenced by the second squeezing. Similarly, in the subsequent cycles, the absorbed amounts were slightly below 1 g (0.847–0.975 g), the adsorbed concentration was ≈15 g g^{-1}, and the squeezing ratios were roughly around 100% (98–104%). It was reported earlier that the squeezing force should not be too high to sustain the structure of the sponges.[35]

Similarly, Figure S11B, Supporting Information, shows the absorption/squeezing process for diesel up to ten cycles. Only a slight decrease in an absorbed amount from 26 to 21 g g^{-1} was determined after 10 absorptions/squeezing cycles, indicating excellent reusability performance of the GK/SA sponge as an absorbent for diesel (Figure S10, Supporting Information). Most of the bio-based sponges intended as superabsorbents lose mechanical resiliency and oil-absorption capacity after multiple absorption cycles.[40] However, the biomass-derived GK/SA sponges presented in this study maintain their mechanical integrity during ten cycles of absorption/squeezing, with diesel recovery of ≈100%. The reusability of sponges in oil/organic solvent absorption is directly related to its compressive stress. The material possessing high compressive stress and flexibility easily comes back to its original dimension upon removing the applied force. While performing reusability studies of the sponges by successive absorption-squeezing cycles, the oil/organic solvent absorbed in the material can easily come out of it and almost 100% porosity is available for the next cycles of absorption. Thus, high compressive strength makes the material available for a large number of cycles of absorption without compromising its structural integrity.[41]

The difference in the sponge performance for the absorption of crude oil and diesel in the absorption-squeezing cycles is due to their difference in viscosity. Crude oil has a higher viscosity than diesel. Due to the fact that a high squeezing force cannot be applied to the sponge without significantly altering its structure, it is difficult for the crude oil to extrude through the micro-channels of the sponge. Consequently, a higher amount of crude oil remains in the sample after squeezing compared to the low viscose diesel. Even after gentle squeezing of the crude oil-saturated sponge, its porosity is reduced, in contrast to squeezing of the diesel-saturated sponge.

2.10. Biodegradation of the Sponge

The curves of biochemical oxygen demand (BOD) analysis for the GK/SA sponge and silylated GK/SA sponge are shown in Figure S12, Supporting Information. In this process, the biopolymers are broken into smaller compounds by aerobic microbial organisms through metabolic or enzymatic processes and finally converted to carbon dioxide. The results indicating that during the whole of the measured period, BOD for GK/SA was higher than in the case of the silylated sponge. The final value of 304.3 ± 16.7 mg O_2/L after 28 days is approximately 50% higher than the value of 208.6 ± 34.5 mg O_2/L for the silylated sponge. The greater degradation rate of the non-silylated sponge compared to the silylated sponge implies that the microorganisms present in the sludge may act faster on the non-silylated sponge. However, this may be influenced by the acclimatization time, the time required to produce enzymes, and the extent of biodegradation. In the early degradation stage, the carbohydrates are broken down by microorganisms into the corresponding monomers, which are glucose molecules. These monomers may either be converted to carbon dioxide and water or various other oxygenated species. The aerobes consume oxygen to oxidize substrates such as sugar in order to obtain energy. Oxygen demand is proportional to the degradation rate. The hydrophobic network of silane formed on the surface of the silylated GK/SA sponge decelerates the action of microorganisms on the material, thereby reducing the rate of degradation. Overall, the results suggest that the GK/SA sponge biodegraded more rapidly (92%) than the silylated sponge (76%) over 28 days. The conjugate sponge has higher stability against biodegradation due to a strong interaction between the polymer chains. Gum arabic bioplastic materials reported in the literature degraded completely within 15 days, whereas the GK/SA sponge took twice as long to degrade to the same extent.[42] The degradation of the GK/SA samples reported in this study is comparable to that of fiber-reinforced starch and cellulose materials.[43] The bio-based biodegradable adsorbent materials are assumed to have greater importance in industry as a green choice for reducing the amounts of waste generated as well as the cost of production. Biodegradable sponge materials of renewable resource origin could contribute to sustainable development by eliminating the possibility of secondary pollution arising due to the disposal of the sponge after the desired function. At the same time, it makes the recycling process more easily achievable.

3. Conclusion

In this study, a highly porous, lightweight conjugate sponge was fabricated based on renewable and biodegradable resources, polysaccharide GK and SA. Surface modification of the material was accomplished via a feasible chemical vapor deposition method using TCMS, which endowed the sponge with hydrophobic (water contact angle 133°) and oleophilic properties, without altering its microporous structure or porosity. The modified GK/SA sponge was highly selective for oil and organic solvents in comparison to water and performed extremely well, showing a high absorption capacity for a wide range of oils and organic solvents (up to 43 g g^{-1}) compared with the absorption capacities reported for many other biomass-derived sponges. At the same time, it shows good mechanical integrity and excellent reusability up to 10 cycles with a diesel absorption retention of 91% compared to the first cycle. The material undergoes biodegradation, which is a green option for reducing waste volumes after use.

4. Experimental Section

All experimental details regarding the materials and their characterization are provided in the Supporting Information.

Fabrication of Conjugate Sponge: Firstly, 1.5% (w/v) aqueous solutions of GK and SA were prepared and thoroughly mixed at various GK/SA (w/w) ratios (10:0, 9:1, 8:2, 7:3, 6:4, 5:5, 4:6, 3:7, 2:8, 1:9, and 0:10), and stirred at room temperature (≈1500 rpm, 22 °C) for 2 h. The resulting GK/SA solutions were poured into a mold, frozen at −80 °C overnight, and lyophilized for 72 h.[44] The conjugates with different concentrations of GK and SA; 0.5, 1.0, 1.5, and 2.0% (w/v) were tried. A stable structure using 0.5% and 1.0% concentrations were not obtained, while a brittle and high-density structure has resulted in 2.0%. Considering the suitable structural stability, density and flexibility, the concentration was fixed at 1.5%(w/v).

Hydrophobic Coating on The Conjugate Sponge: CVD of TCMS on the GK/SA sponge was performed by placing them both into a glass bottle in an oven at 50 °C for 30 min.[19] Subsequently, the formed silylated GK/SA sponge was placed in a vacuum oven to remove the excess TCMS from the surface of the sample.

Supporting Information

Supporting Information is available from the Wiley Online Library or from the author.

Acknowledgements

The authors would like to acknowledge the assistance provided by the Research Infrastructure NanoEnviCz, supported by the Ministry of Education, Youth and Sports of the Czech Republic in the framework of Project No. LM2018124. This work was also supported by the project "Tree Gum Polymers and their Modified Bioplastics for Food Packaging Application" granted by Bavarian-Czech-Academic-Agency (BTHA) (registration numbers LTAB19007 and BTHA-JC-2019-26) and the Ministry of Education, Youth and Sports in the Czech Republic under the "Inter Excellence – Action program" within the framework of the project "Bio-based Porous 2D Membranes and 3D Sponges Based on Functionalized Tree Gum Polysaccharides and their Environmental Application" (registration number LTAUSA19091) – TUL internal No.: 18309/136. Scientific discussions with Prof. Andreas Greiner during the progress of the work are kindly acknowledged.

Open access funding enabled and organized by Projekt DEAL.

Conflict of Interest

The authors declare no conflict of interest.

Data Availability Statement

The data that supports the findings of this study are available in the supplementary material of this article.

Keywords

conjugate sponge, freeze-drying, gum kondagogu/sodium alginate, oil absorption, silylation

Received: January 20, 2021
Revised: February 3, 2021
Published online:

[1] W.-J. Yang, A. Chun Yin Yuen, A. Li, B. Lin, T. Bo Yuan Chen, W. Yang, H.-D. Lu, G. H. Yeoh, *Cellulose* **2019**, *26*, 6449.
[2] M. B. Wu, S. Huang, C. Liu, J. Wu, S. Agarwal, A. Greiner, Z. K. Xu, *J. Mater. Chem. A* **2020**, *8*, 11354.
[3] S. Wang, X. Peng, L. Zhong, J. Tan, S. Jing, X. Cao, W. Chen, C. Liu, R. Sun, *J. Mater. Chem. A* **2015**, *3*, 8772.
[4] H. Sai, R. Fu, L. Xing, J. Xiang, Z. Li, F. Li, T. Zhang, *ACS Appl. Mater. Interfaces* **2015**, *7*, 7373.
[5] S. Jiang, S. Agarwal, A. Greiner, *Angew. Chem., Int. Ed.* **2017**, *56*, 15520.
[6] G. Duan, S. Jiang, V. Jérôme, J. H. Wendorff, A. Fathi, J. Uhm, V. Altstädt, M. Herling, J. Breu, R. Freitag, S. Agarwal, A. Greiner, *Adv. Funct. Mater.* **2015**, *25*, 2850.
[7] S. Zhao, W. J. Malfait, N. Guerrero-Alburquerque, M. M. Koebel, G. Nyström, *Angew. Chem., Int. Ed.* **2018**, *57*, 7580.
[8] Q. F. Wei, R. R. Mather, A. F. Fotheringham, R. D. Yang, *Mar. Pollut. Bull.* **2003**, *46*, 780.
[9] M. B. Wu, S. Huang, T. Y. Liu, J. Wu, S. Agarwal, A. Greiner, Z. K. Xu, *Adv. Funct. Mater.* **2020**, *31*, 2006806.
[10] F. Liu, T. S. Seo, *Adv. Funct. Mater.* **2010**, *20*, 1930.
[11] Y. Liu, X. Wang, S. Feng, *Adv. Funct. Mater.* **2019**, *29*, 1.
[12] W. Lv, Q. Mei, J. Xiao, M. Du, Q. Zheng, *Adv. Funct. Mater.* **2017**, *27*, 1.
[13] D. Wang, J. Song, S. Lin, J. Wen, C. Ma, Y. Yuan, M. Lei, X. Wang, N. Wang, H. Wu, *Adv. Funct. Mater.* **2019**, *29*, 1.
[14] H.-Y. Mi, X. Jing, H. X. Huang, X. F. Peng, L. S. Turng, *Ind. Eng. Chem. Res.* **2018**, *57*, 1745.
[15] S. Gupta, N. H. Tai, *J. Mater. Chem. A* **2016**, *4*, 1550.
[16] R. R. Escudero, M. Robitzer, F. Di Renzo, F. Quignard, *Carbohydr. Polym.* **2009**, *75*, 52.
[17] D. Zang, F. Liu, M. Zhang, Z. Gao, C. Wang, *Chem. Eng. Res. Des.* **2015**, *102*, 34.
[18] Y. Li, X. Liu, W. Cai, Y. Cao, Y. Sun, F. Tan, *Korean J. Chem. Eng.* **2018**, *35*, 1119.
[19] Z. Zhu, S. Fu, L. A. Lucia, *ACS Sustainable Chem. Eng.* **2019**, *7*, 16428.
[20] S. Zhou, P. Liu, M. Wang, H. Zhao, J. Yang, F. Xu, *ACS Sustainable Chem. Eng.* **2016**, *4*, 6409.
[21] A. Tripathi, G. N. Parsons, O. J. Rojas, S. A. Khan, *ACS Omega* **2017**, *2*, 4297.
[22] L. Y. Long, Y. X. Weng, Y. Z. Wang, *Polymers* **2018**, *8*, 1.
[23] L. Wang, M. Sánchez-Soto, T. Abt, *Ind. Crops Prod.* **2016**, *91*, 15.
[24] J. S. Acevedo, C. Boris, I. K. Thelma, E. S. Quezada, *Pet. Sci.* **2017**, *14*, 84.
[25] J. Shi, L. Lu, W. Guo, J. Zhang, Y. Cao, *Carbohydr. Polym.* **2013**, *98*, 282.
[26] L. Wang, D. A. Schiraldi, M. Sanchez-Soto, *Ind. Eng. Chem. Res.* **2014**, *53*, 7680.
[27] H. B. Chen, Y. Z. Wang, M. Sánchez-Soto, D. A. Schiraldi, *Polymer* **2012**, *53*, 5825.
[28] P. Lv, X. Tang, R. Zheng, X. Ma, K. Yu, W. Wei, *Nanoscale Res. Lett.* **2017**, 12.
[29] G. Chantereau, N. Brown, M. A. Dourges, C. S. R. Freire, A. J. D. Silvestre, G. Sebe, V. Coma, *Carbohydr. Polym.* **2019**, *220*, 71.
[30] A. G. Cunha, C. Freire, A. Silvestre, C. P. Neto, A. Gandini, M. N. Belgacem, D. Chaussy, D. Beneventi, *J. Colloid Interface Sci.* **2010**, *344*, 588.
[31] J. Yang, H. Li, T. Lan, L. Peng, R. Cui, H. Yang, *Carbohydr. Polym.* **2017**, *178*, 228.
[32] Y. Cheng, L. Lu, W. Zhang, J. Shi, Y. Cao, *Carbohydr. Polym.* **2012**, *88*, 1093.
[33] F. Zou, L. Peng, W. Fu, J. Zhang, Z. Li, *RSC Adv.* **2015**, *5*, 76346.
[34] S. Zhao, O. Emery, A. Wohlhauser, M. M. Koebel, C. Adlhart, W. J. Malfait, *Mater. Des.* **2018**, *160*, 294.
[35] S. Han, Q. Sun, H. Zheng, J. Li, C. Jin, *Carbohydr. Polym.* **2016**, *136*, 95.
[36] X. Gong, Y. Wang, H. Zeng, M. Betti, L. Chen, *ACS Sustainable Chem. Eng.* **2019**, *7*, 11118.

[37] S. T. Nguyen, J. Feng, N. T. Le, A. T. T. Le, N. Hoang, V. B. C. Tan, H. M. Duong, *Ind. Eng. Chem. Res.* **2013**, *52*, 18386.
[38] S. Kabiri, D. N. H. Tran, T. Altalhi, D. Losic, *Carbon* **2014**, *80*, 523.
[39] A. Tripathi, G. N. Parsons, S. A. Khan, O. J. Rojas, *Sci. Rep.* **2018**, *8*, 1.
[40] J. Jiang, Q. Zhang, X. Zhan, F. Chen, *ACS Sustainable Chem. Eng.* **2017**, *5*, 10307.
[41] C. Li, D. Jiang, H. Liang, B. Huo, C. Liu, W. Yang, J. Liu, *Adv. Funct. Mater.* **2018**, *28*, 1.
[42] V. V. T. Padil, C. Senan, S. Waclawek, M. Černík, S. Agarwal, R. S. Varma, *ACS Sustainable Chem. Eng.* **2019**, *7*, 5900.
[43] J. C. Bénézet, A. Stanojlovic-Davidovic, A. Bergeret, L. Ferry, A. Crespy, *Ind. Crops Prod.* **2012**, *37*, 435.
[44] S. Suenaga, M. Osada, *Int. J. Biol. Macromol.* **2019**, *126*, 1145.

4.3. Sustainable, Biodegradable, and Recyclable Bio-Sponge for Rapid and Practical Bioremediation of Dye from Water

Abstract: For the first time, a simple synthesis of an ionically cross-linked tree gum-based sponge with structural stability was investigated for effective cationic dye adsorption. Hierarchical three-dimensional structures were formed between gum kondagogu (GK) and sodium alginate (SA) primarily through hydrogen bonding, and were enhanced further by Ca^{2+} ionic crosslinking. Fourier transform infrared spectroscopy, TGA, SEM, and micro-CT were used to characterize the sponge. The adsorption capacity of the sponge for the cationic dye, methylene blue (MB), was studied as a function of pH, dosage, reaction time, and initial dye concentrations. The MB adsorption of the sponge in the present work (1250 mg/g) shows a higher adsorption capacity than many other natural sponges. The maximum adsorption was recorded at pH 9, and recyclability without significant loss of efficiency for five adsorption cycles was also obtained. Furthermore, pseudo-second order kinetics and the Langmuir adsorption isotherm fit the experimental results well. This biodegradable adsorbent is a promising material for cost-effective wastewater treatment via waste-to-resource conversion.

Citation: R.K. Ramakrishnan, V.V.T. Padil, S. Wacławek, M. Černík, D. Tiwari, Sustainable, Biodegradable, and Recyclable Bio-Sponge for Rapid and Practical Bioremediation of Dye from Water, J. Environ. Chem. Eng. (2022) 108285

Journal of Environmental Chemical Engineering 10 (2022) 108285

Contents lists available at ScienceDirect

Journal of Environmental Chemical Engineering

journal homepage: www.elsevier.com/locate/jece

Sustainable, biodegradable, and recyclable bio-sponge for rapid and practical bioremediation of dye from water

Rohith K. Ramakrishnan [a], Vinod V.T. Padil [a,*], Stanisław Wacławek [a], Miroslav Černík [a], Diwakar Tiwari [b]

[a] Institute for Nanomaterials, Advanced Technologies and Innovation (CXI), Technical University of Liberec (TUL), Studentská 1402/2, Liberec 1 461 17, Czech Republic
[b] Department of Chemistry, Mizoram University (A Central University), Aizawl 796004, Mizoram, India

ARTICLE INFO

Editor: Xin Yang

Keywords:
Sustainable sponge
Tree gum
Dye adsorption: Recyclability
Biodegradation

ABSTRACT

For the first time, a simple synthesis of an ionically cross-linked tree gum-based sponge with structural stability was investigated for effective cationic dye adsorption. Hierarchical three-dimensional structures were formed between gum kondagogu (K) and sodium alginate (S) primarily through hydrogen bonding, and enhanced further by Ca^{2+} ionic crosslinking. Fourier transform infrared spectroscopy, TGA, SEM, and micro-CT were used to characterize the sponge. The adsorption capacity of the sponge for the cationic dye, methylene blue (MB), was studied as a function of pH, dosage, reaction time, and initial dye concentrations. The MB adsorption of the sponge in the present work (1250 mg g^{-1}) shows a higher adsorption capacity than many other natural sponges. The maximum adsorption was recorded at pH 9, and recyclability without significant loss of efficiency for five adsorption cycles was also obtained. Furthermore, pseudo-second order kinetics and the Langmuir adsorption isotherm fit the experimental results well. This biodegradable adsorbent is a promising material for cost-effective wastewater treatment via waste-to-resource conversion.

1. Introduction

Modern industries such as textile, paper, leather, food, and cosmetic goods industries produce vast amounts of effluents in the form of synthetic dyes and other organic contaminants [1]. These excessive dye effluents in the aquatic environment prevent the entry of light into the water in a way that inhibits photosynthesis [2]. Therefore, this contaminant water must be treated in various ways, such as flocculation-coagulation, precipitation, photocatalytic degradation, adsorption, and ion exchange [3–8] . Of these, adsorption is the easiest and most economically feasible method. However, many of the adsorbents used are made from petroleum products, making them expensive and toxic. On the contrary, adsorbents made from natural polymers are renewable, biodegradable, biocompatible, and reduce the risk of secondary contamination [9].

Methylene blue (MB) is a heterocyclic aromatic chemical compound that is utilized as a redox indicator as well as for a variety of other industrial uses [10]. Continuous use of MB contaminates water at concentrations even lower than one ppm may cause various side effects, including permanent damage to the skin and eyes of humans and other organisms [11]. The natural materials used as MB dye adsorbents include clay [12], sawdust [13], chitosan [14,15], alginate [16], cellulose nanofibrils [17], agar [18], tragacanth [19,20], carrageenan [21], xanthan [22,23], and gum karaya [24]. However, further research on sustainable adsorbent materials is necessary because many recently reported bioadsorbents show low removal efficiency. Wu et al., for example, observed MB removal using membrane produced from the chitosan/cellulose nanofibrils composite [25], which had a maximum adsorption capacity of 14.71 mg g^{-1}. Njuguna et al. produced xanthan gum hydrogel with adsorption capacity of 435 mg g^{-1} for the elimination of MB [26] and Zhang et al. investigated the adsorption capacity of cork dust based porous carbon (887.7 mg g^{-1}) [27]. Furthermore, the maximum adsorption capabilities of several biomasses such as nanofibrilled cellulose, sludge-derived biochar, alginate/carrageenan, and sugarcane bagasse have been found to be 107 mg g^{-1}, 160.78 mg g^{-1}, 132 mg g^{-1}, and 207.16 mg g^{-1}, respectively [28–31]. Therefore, development of a biobased adsorbent with high adsorption capacity using an inexpensive and abundant material is required.

Recently, biopolymer sponges have been introduced as a new class of highly porous and ultra-lightweight materials, in contrast to

* Corresponding author.
E-mail address: vinod.padil@tul.cz (V.V.T. Padil).

https://doi.org/10.1016/j.jece.2022.108285
Received 19 March 2022; Received in revised form 14 June 2022; Accepted 15 July 2022
Available online 19 July 2022

conventional non-degradable sponges that cause secondary pollution [32]. Furthermore, there is a wide variety of types of surface chemistry accessible for biopolymers that may be used to make the sponges. Modifiable macrostructure and porosity characteristics are achieved mainly through a freeze-drying process [33]. The higher number of functional groups present in biopolymer structures facilitate their modification and integration. In addition, such functional groups exist as binding sites for waterborne contaminants such as heavy metals, and cationic and anionic dyes [34]. Biopolymer sponge structures with excellent surface area, flexibility, and compressibility increase the practical usability of sustainable and renewable materials.

Gum kondagogu is a gum extruded from the bark of *Cochlospermum gossypium* found in tropical countries. This gum comprises uronic acid, glucuronic acid, galacturonic acid, and fewer proteins, with functional groups such as hydroxyl, acetyl, carbonyl, and carboxylic groups. These functional groups expedite network formation with other biopolymers [35,36]. Despite its special advantages, this gum is not used alone in the formation of 3D shapes because of its lack of structural stability. Therefore, it is necessary to use an interconnected or crosslinked network that enhances structural integrity and other related advantages. The conjugation of such biopolymers with sodium alginate, another polysaccharide derived from brown algae comprised of two repeating, mannuronic acid and guluronic acid monosaccharide units, provides a stable 3D structure [37]. Similarities in the excellent liquid-gel behavior and basic structural units of these polysaccharides lead to the formation of a conjugate with excellent mechanical properties [38].

Here, we report a facile and eco-friendly method to prepare a conjugate sponge based on tree gum kondagogu (K) and sodium alginate (S) through ionic crosslinking (by Ca^{2+} ions) followed by freeze-drying. These self-assembled low-density (22.6 mg cm^{-3}) sponges exhibit an excellent adsorption capacity (1250 mg g^{-1}) and five-times recyclability without significant loss in adsorption performance for the cationic dye in an aqueous medium. The adsorption mechanism and adsorption-desorption kinetics were investigated. Degradation tests were also performed to verify whether the material is sustainable. The findings indicate that biowaste has a promising potential for effectively removing of these hazardous, carcinogenic coloring contaminants. The main objective of this study was to apply and use an inexpensive, and readily available adsorbent with a good adsorption capacity for the treatment of organic pollutants via waste-to-resource value conversion.

2. Experimental section

2.1. Materials

Gum kondagogu (K) was provided by the Girijan cooperative society, Andra Pradesh, India. Sodium alginate (S), calcium chloride ($CaCl_2$, ≥93.0%), and sodium hydroxide (NaOH, ≥98%) were supplied by Sigma Aldrich Co., USA. Methylene blue (MB) was purchased from Lach-Ner, Neratovice, Czech Republic. Hydrochloric acid (HCl, 37%) was obtained from Penta chemicals limited, Czech Republic. All the chemicals in this work were used without further purification. The water used in all the experiments was purified and deionized by a Milli-Q plus water purification system (Millipore Corporate, Billerica, MA).

2.2. Sponge preparation

The sponges were prepared based on one of our previous works, with small modifications [39]. Briefly, 1.5 w/w% solutions of gum kondagogu and sodium alginate were mixed (1:1 wt/wt%) and lyophilized (KS sponge). The pre-shaped sponges were crosslinked by immersion in 5 wt/wt% of a calcium chloride solution for 30 min. The crosslinked sponges (CKS sponges) were then washed three times with distilled water to remove the redundant salt from their surfaces and lyophilized for further testing [40].

2.3. Characterization of the sponges

The bulk density of the sponges was determined by weighing the sample and measuring its volume using a vernier caliper. To analyze the functional groups of the sponges, an ATR-FTIR spectrometer (Nicolet iZ10, Thermo Scientific, Waltham, MA, USA) with a fixed 45° angle and horizontal ATR accessory with diamond crystal was employed. The morphology of the sponges was analyzed using field-emission scanning electron microscopy (FE-SEM) on a ZEISS Sigma device (Germany) at a 10 kV accelerating voltage. To assess the composite microstructure and porosity, X-ray computed tomography (micro-CT, Skyscan 1272, Bruker) was utilized. The scanning parameters were as follows: 50 kV source, 200 μA current, 3 μm image pixel size, 672 ms exposure period, and 0.2° rotation step. A Q500 thermogravimetric analyzer (TA Instruments, USA) was used to determine thermal stability and composition. The experiment was conducted in a nitrogen atmosphere at a flow rate of 60 mL min^{-1}, and the sample was heated from 30° to 600°C at a heating rate of 10 °C min^{-1}.

2.4. Adsorption test

Adsorption ability was evaluated by immersing 2 mg of the sponge in 10 mL of MB (1:5 mg mL^{-1} sponge to dye w/v ratio) with concentrations ranging from 25 to 400 mg L^{-1}. The solution container was then placed in a shaker at 200 rpm at an ambient temperature for 2 h. At fixed time intervals, the concentration of the dye solution was measured at 664 nm using a UV–vis spectrophotometer (Hach DR 3900). The amount of MB adsorbed on the sponge at each time interval was calculated using Eq. 1:

$$q_e = \frac{C_0 - C_e \times V}{m} \quad (1)$$

where qe indicates the quantity of the dye adsorbed, C_0 is the initial dye concentration (mg L^{-1}), C_e is the equilibrium dye concentration (mg L^{-1}), V is the solution volume (L), and m is the mass (g) of the sponge.

The percentage of MB removal was calculated using Eq. 2:

$$Percentage \quad removal \quad = \frac{C_0 - C_e}{C_0} \times 100 \quad \% \quad (2)$$

Furthermore, MB adsorption was carried out with various sponge to MB solution ratios (1:5–10:5) using a MB concentration of 100 mg L^{-1} and different pH values ranging from 4 to 10 (previously adjusted with either HCl or NaOH, at 0.1 N).

2.5. Desorption of methylene blue

Desorption of MB was investigated on the sponge with pre-adsorbed dye (120 mg g^{-1}) in 10 mL of 0 mM, 10 mM, and 100 mM solutions of hydrochloric acid. At fixed time intervals, the concentration of the salt solution was measured at 664 nm using a UV–vis spectrophotometer, and the experiment was stopped once there were no longer any significant changes in absorbance for three consecutive readings. The percentage of dye desorption was calculated by Eq. 3:

$$Dye \quad desorption = \frac{C_e \times V}{m \times q_e} \times 100\% \quad (3)$$

where C_e is the equilibrium dye concentration, V is the volume (L) of the HCl solution, m is the mass (g) of the sponge, and q_e is the equilibrium dye amount on the sponge after 40 min in the 100 mg L^{-1} MB solution.

2.6. Biodegradation

The non-crosslinked and ionic crosslinked sponges were tested for biodegradation under aerobic conditions in an aqueous medium. The oxygen demand for the ultimate aerobic biodegradability was measured in a Micro-Oxymax respirometer (Columbus Instruments International,

USA). The supernatant of the settled sludge from the municipal wastewater treatment plant in Liberec was used as an inoculum. Approximately 2 g of the tested material was added to 95 mL of the biological medium (based on ISO 14851:1999) and 5 mL of activated sludge. The mixture was subsequently dosed into a 250 mL respiration cell. The testing period was 28 days [41].

3. Results and discussion

3.1. Bulk density and water solubility

The KS sponge was fabricated through freeze-drying, followed by ionic crosslinking by Ca^{2+} ions as shown in Scheme 1. The hydrogen bonding interaction between the biopolymers and further ionic crosslinking made a stable three-dimensional (3D) structure. The bulk density of the KS sponge (18.8 mg cm^{-3}) was changed after crosslinking (22.6 mg cm^{-3}), which is still lower than that of the porous alginate structure (34.6 mg.cm^{-3}) reported previously [42].

3.2. ATR-FTIR spectroscopy

Fig. 1**a** shows the FT-IR spectra of the KS and CKS sponges. The peaks observed at 1028, 1253, 1723, 2928, and 3353 cm^{-1} in the KS sponge correspond to C-O-C, –C–O, C═O, C–H, and O–H vibrations, respectively, while the peaks at 818 and 890 cm^{-1} are characteristic of polysaccharide structures. In the CKS sponge, the O-H absorbance peak shifted from 3340 to 3329 cm^{-1}. Similarly, the peaks at 1599 and 1410 cm^{-1} shifted to 1593 and 1415 cm^{-1}, respectively, showing the involvement of the COO- group in the crosslinking process [40]. Furthermore, the intensity of the characteristic peaks was observed to decrease in the crosslinked sample compared to that of the pristine sample.

As previously stated, freeze-dried KS sponges have the ability to maintain their macroscopic integrity via conjugate hydrogen bonding [39]. Cylindrical samples of both the KS and CKS sponges were submersed into deionized water. The KS sponge disintegrated after a few seconds of mild shaking by hand (Fig. S1a). The hydrogen link was replaced by a conjugate-water hydrogen connection and the network structure was completely destroyed. On the other hand, the CKS sponge sample maintained its network structure even after vigorous shaking (Fig. S1b), demonstrating strong ionic interactions after crosslinking, as demonstrated by the FTIR analysis.

3.3. Thermo-gravimetric analysis

The thermogram in Fig. 1**b** was used to investigate the thermal stability of the pristine and crosslinked sponges. The derivative thermogravimetric curve (inserted) clearly shows a vertical shift in temperature. Polysaccharides have a strong affinity to water, and the water molecules may be bound to the sponge by the hydrophilic groups and, therefore, the curves below 200 °C correspond to moisture loss. These functional groups are involved in the ionic crosslinking and adsorb less moisture than the pristine sponge. Sponge degradation occurs at a temperature around 200–330 °C, and the KS sponge possesses a sharp peak at 268 °C, corresponding to maximum degradation. The degradation peak is broader for the CKS sponge, and the appearance of the shoulder indicates degradation at a relatively high temperature (293 °C) compared to the KS sponge (268 °C). Beyond 200 °C, the KS sponge degraded rapidly up to 62% until 600 °C, whereas degradation of the CKS sponge was slower in the same range, with 35% remaining even after 600 °C. This observation results from the increased thermal stability of the CKS sponge imparted by the crosslinking.

3.4. Shape recovery

The shape recovery of the CKS sponge was examined prior to its application as an adsorbent (Fig. 1**c and** Movie S1), from which its exceptional water stability was observed. The capillary forces imparted by the sponge's mesopores aid in ultra-rapid water absorption [43], and to its maximum loading in less than 10 s. In addition, the sponge formed a stable 3D structure with no visible volume change or structural disintegration after soaking in water. The cyclic absorption capacity of the sponges was evaluated to determine their reusability and desorption by squeezing out the water (Fig. S2). The absorption capacity decreased slightly, which is consistent with shape recovery. More precisely, the absorption capacity of the sponges decreased from 40% to 37% in the first cycle and it was consistent even after the tenth cycle of water adsorption. This result again proves that the conjugation of the gum with alginate improves the network structure via hydrogen bonds and further enhancement in the ionic coordination during crosslinking.

Supplementary material related to this article can be found online at doi:10.1016/j.jece.2022.108285.

3.5. Microstructure analysis

Scanning electron microscopy (SEM) was used to analyze the surface morphology of the sponges. The SEM images in Fig. 2 show that the KS and CKS sponges have a significantly smoother surface with porous and interlinked networks. These interconnected channels form a 3D network frame passing through a narrow border. Furthermore, the SEM images revealed that crosslinking slightly reduced the pore size but did not significantly alter the overall structure of the KS sponge. The KS sponge possesses a pore diameter in the range of 20–200 μm, whereas in the case of the CKS sponge it was decreased to 20–180 μm due to the compactness of the conjugate after ionic crosslinking (Fig. S3). Many tiny holes and channels present in the sponge offered more adsorption spaces and sites. The SEM image of the sponge shows layered structures with macropores, which may have been created by direct sublimation of ice crystals during the freeze-drying process [24]. The presence of calcium is clearly visible in the elemental analysis and elemental mapping of the CKS sponge, as illustrated in Fig. S4. Micro-CT was applied to further illustrate the porosity and pore distribution of the CKS sponge

Scheme 1. Schematic illustration of the fabrication of the ionically crosslinked gum kondagogu-sodium alginate conjugate sponge (CKS sponge).

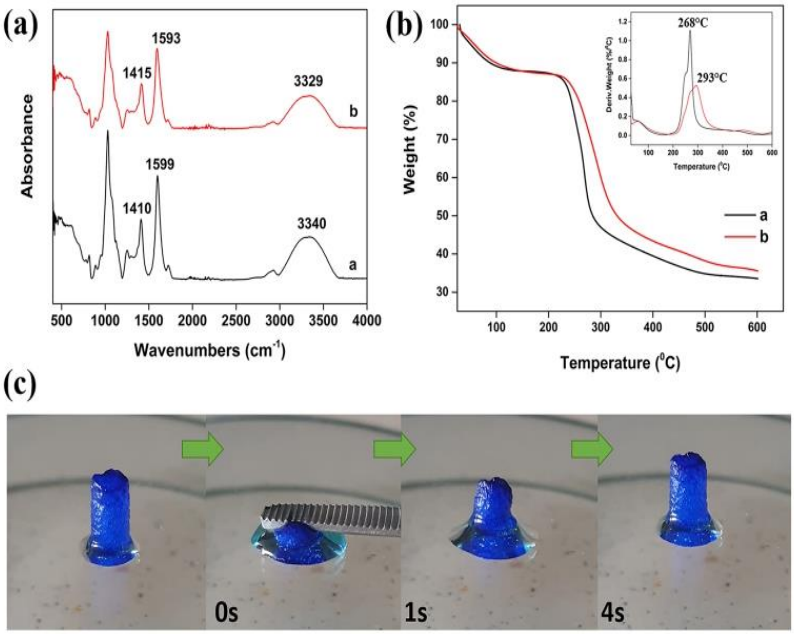

Fig. 1. a) FTIR spectra and b) Thermograms of the KS and CKS sponges (the derivative thermogravimetric curve is inserted). c) Shape recovery of the CKS sponge in water, where the sponge is colored using methylene blue.

[44]. In addition to the 3D morphology (Fig. 2**e**), a vertical section of the CKS sponge is shown in Fig. 2**f**. The cross-section view illustrates the porous structure distribution and pore homogeneity. It was found that the CKS sponge porosity was 92.5% (avoidable closed hole 10^{-4}%). Such a highly porous material with abundant functional groups provides a large number of adsorption sites for the removal of contaminants from water.

The structure and self-assembly characteristics of the CKS sponge are improved by the bioconjugation, allowing them to manage and regulate the internal structure to a greater extent [39]. Compared to polysaccharide sponges like alginate (39 mg cm^{-3}) and gum arabic sponges (85 mg cm^{-3}), the CKS sponge has a low bulk density [45,46]. In addition, water stability may be improved by conjugation and ionic crosslinking, which in effect enhances the reusability of the sponge. Altogether, the CKS sponge uses its water resiliency and numerous surface functional groups to separate a large number of water pollutants.

3.6. Dye adsorption

3.6.1. Adsorption behavior toward MB

Fig. 3**a** depicts the influence of pH on MB adsorption by the CKS sponge under constant process conditions (100 mg L^{-1}, 1:5 mg mL^{-1} sponge/dye w/v ratio). Both the degree of ionization of the dye molecules and the surface charge of the adsorbents are affected by the pH of the solution. The adsorption process is influenced by the charging of functional groups on the active sites in the adsorbent surface [47]. As the pH rises, the cationic dye adsorption rises due to an increase in the negative surface charge of adsorbents. This is explained by the electrostatic interaction of cationic MB molecules with the negatively charged sponge surface. At a low pH, the competition between the hydrogen ions and cationic ions in MB to connect to the adsorbent sites results in decreased dye removal [48].

The removal of MB at a concentration of 100 mg L^{-1} was investigated further using different sponge dosages (Fig. 3**b**). There is a steep rise in the percentage of MB removed, from 30.8% to 92.0% as the sponge/MB ratio increased from 1:5–10:5 mg mL^{-1}. This is related to an increase in the active sites of the adsorbent surface [43]. With an increasing sponge to dye ratio, the equilibrium MB adsorption in the CKS sponge fell from 388.3 to 46.0 mg g^{-1}.

3.6.2. Adsorption kinetic study

The adsorption of the MB dye onto the CKS sponge (pH 9, 1:5 mg mL^{-1} sponge/MB w/v ratio) occurred at all initial MB concentrations from 25 to 400 mg L^{-1} (Fig. 4**a**). The MB adsorption rate increased with the increasing initial dye concentrations. This rapid adsorption capacity is attributed to the hierarchical macro-and mesoporous structure of the sponges. However, the percentage of MB removed from aqueous dye solutions decreased with increasing initial concentrations, i.e., from 82% to 58% at the lower 25 mg L^{-1} to the higher 400 mg L^{-1} concentrations, respectively (Fig. 4**b**).

The adsorption kinetics of MB on the CKS sponge were evaluated with both pseudo-first-order and pseudo-second-order models, expressed as Eqs. 4 and 5:

$$\log(q_e - q_t) = \log q_e - \frac{k_1}{2.303} t \tag{4}$$

$$\frac{t}{q_t} = \frac{t}{q_e} + \frac{1}{k_2 q_e^2} \tag{5}$$

where q_t and q_e are the amount of MB adsorbed at time t and at equilibrium (mg g^{-1}), respectively, k_1 is the pseudo-first-order rate constant (min^{-1}), and k_2 is the pseudo-second-order rate constant (g $mg^{-1}min^{-1}$).

The adsorption data were plotted as t/q_t versus t and fitted to a linear expression giving the initial adsorption rate v_0 at $t = 0$, which may be calculated from Eq. 6.

$$v_0 = k_2 \times q_e^2 \tag{6}$$

The dye adsorption kinetics were evaluated using two kinetic models- pseudo-first-order (Fig. 4**c**) and pseudo-second order models (Fig. 4**d**). The experimental adsorption data fitted well to the pseudo-second order kinetic model, with all R^2 values being above 0.99, showing linearity in the t/q_t versus t plots. This indicates that the overall rate of MB adsorption onto the sponge is controlled by chemisorption. From the pseudo-second order kinetic model, the initial MB adsorption rate (v_0) was found to increase from 6.14, 8.57, 18.13, 27.55, and

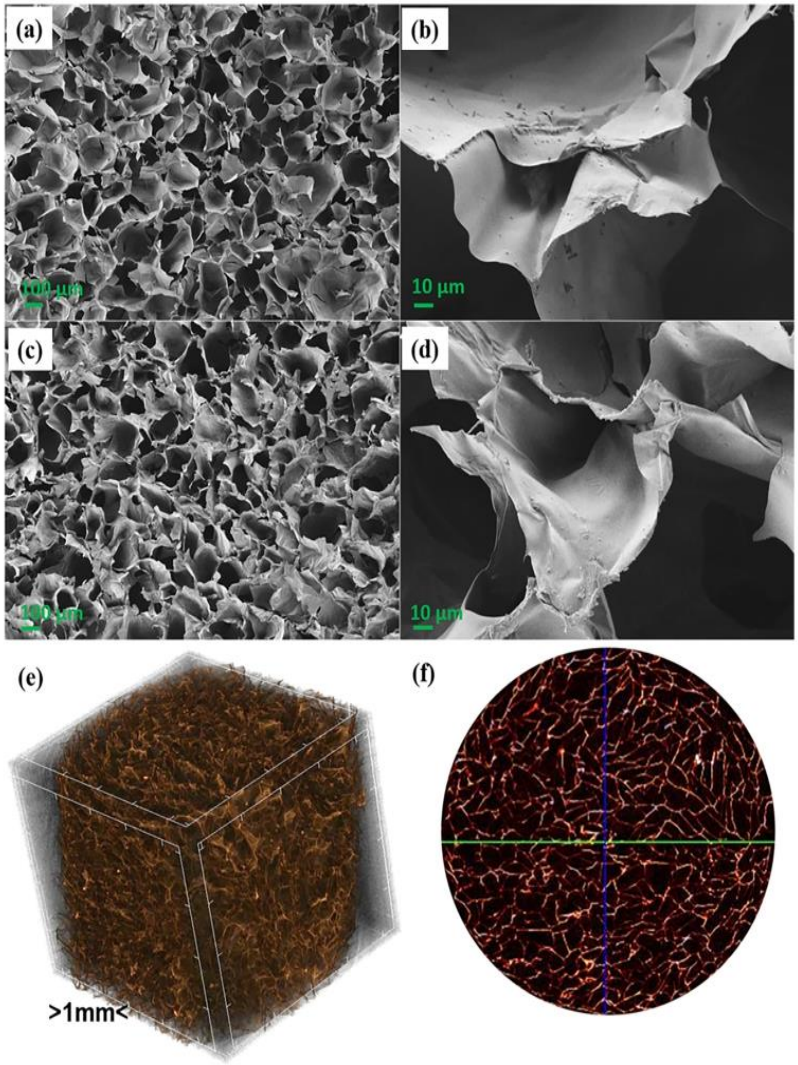

Fig. 2. SEM images at different magnifications of a, b) KS, and c, d) CKS sponges, respectively. Micro-CT images of e) 3D morphology, and f) Cross-sectional view of the CKS sponge.

149.47 mg $g^{-1}min^{-1}$ with increasing original dye concentrations from 25, 50,100, 200, and 400 mg L^{-1} respectively.

The values of different parameters for kinetic models were obtained as shown in Table 1. The q_{exp} values (101.96, 199.43, 388.20, 605.05, and 1178.65 mg g^{-1}) were much closer to the q_{cal} values (123.00, 250.00, 469.48, 740.74, and 1237.62 mg g^{-1}) of the pseudo-second-order model than the q_{cal} values (80.47, 179.07, 324.68, 538.18, and 579.55 mg g^{-1}) of the pseudo-first-order model. Based on this, the adsorption kinetics may be fitted to the pseudo-second-order model.

In order to compare the validity of the kinetic model, the normalized standard deviation Δq (%) was calculated using Eq. 7.

$$\Delta q = \sqrt{\frac{\sum \left(\left(q_{exp} - q_{cal} \right) / q_{exp} \right)^2}{N-1}} \times 100\% \quad (7)$$

where q_{exp} and q_{cal} represent the experimental and theoretical amount of dye adsorbed on the sponges, respectively, and N is the number of determination times.

Generally, the Δq (%) will be lower when the model data are closer to the experimental data. Analysis of the Δq (%) values for both models indicated that the pseudo-second-order agreed well with the experimental kinetic data due to the lower Δq (%) values (0.225) compared to the pseudo-first-order values (0.296).

3.6.3. Adsorption isotherm

To further understand the mechanism of adsorption of MB onto the CKS sponge and to determine the equilibrium data, the adsorbed quantities and residual dyes in the solution were fitted in both Langmuir and Freundlich isotherms. The linear relationships of the Langmuir and Freundlich isotherms may be expressed as Eqs. 8 and 9, respectively:

$$\frac{1}{q_e} = \left(\frac{1}{K_L Q_m} \right) \frac{1}{C_e} + \frac{1}{Q_m} \quad (8)$$

$$log \quad q_e = \frac{1}{n} log \quad C_e + log \quad K_F \quad (9)$$

where qe is the adsorbed MB at equilibrium (mg g^{-1}), q_{max} is the adsorption capacity (mg g^{-1}), K_L is the equilibrium adsorption constant (L mg^{-1}), Ce is the equilibrium MB concentration in the solution, K_F is the Freundlich constant ((mg g^{-1})(L g^{-1})n), and n is the heterogeneity factor.

The Langmuir plot of $1/q_e$ versus $1/C_e$ shows a linear regression curve with a slope of $1/Q_m$ and intercept of $1/(K_L . Q_m)$ (Fig. S5a) as well

Table 1
Pseudo-first and pseudo-second order kinetic model parameters for the adsorption of MB onto the CKS sponge.

C_0 [mg L^{-1}]	q_{exp} [mg g^{-1}]	Pseudo-first-order			Pseudo-second-order		
		q_e [mg g^{-1}]	K_1 [min^{-1}]	R^2	q_e [mg g^{-1}]	K_2 [g mg^{-1} min^{-1}]	R^2
25	101.96	80.47	3.41E-03	0.95	123.00	9.75E-05	0.99
50	199.43	179.07	2.42E-03	0.99	250.00	5.02E-05	0.99
100	388.20	324.68	2.13E-03	0.98	469.48	8.22E-05	0.99
200	605.05	538.18	1.74E-03	0.97	740.74	1.37E-04	0.99
400	1178.65	579.55	2.04E-03	0.96	1237.62	4.05E-04	0.99

Table 2
Langmuir and Freundlich model fitting parameters for the adsorption of MB on the KS sponge at 1:5 mg mL^{-1} sponge/dye w/v ratios with a dye concentration of 25–400 mg L^{-1}.

Sample	Langmuir isotherm			Freundlich isotherm		
	Q_m [mg g^{-1}]	K_L [L mg^{-1}]	R^2	K_F [L g^{-1}]	N [mg g^{-1}][L g^{-1}] n	R^2
KS sponge	1250	0.02	0.99	42.89	1.5	0.97

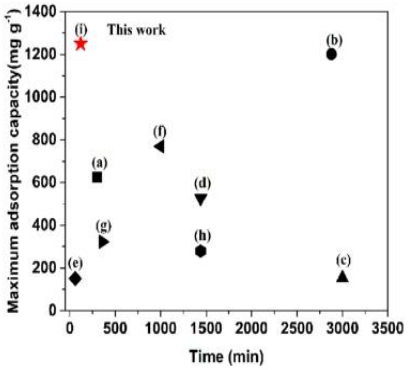

Fig. 5. Comparison of the maximum adsorption capacity of MB dye: a) Cellulose nanofibril/ graphene oxide/silica [53], b) Sodium alginate foam [50], c) Microcrystalline cellulose [54], d) Cellulose/chitosan [55], e) Graphene oxide-montmorillonite/sodium alginate [56], f) Activated carbon-alginate [51], g) Sodium alginate/gelatin/graphene oxide [52], h) Graphene oxide-chitosan [57], i) Magnetic graphene composite [58], j) Graphene [59], k) Cellulose nanofibril/rectorite composite [60], and l) CKS sponge (This work) and the details are listed in Table S1 in the Supporting Information.

desorption process indicates that the sponge may be facilely regenerated for repeated dye removal applications.

3.6.5. Mechanism of adsorption and desorption

The above results show that the adsorption of MB by the CKS sponge is affected by many factors including electrostatic interaction, hydrogen bonding, and π-π interactions between the dye molecules and sponge surface active sites. A schematic illustration of the adsorption mechanism is shown in Fig. 7. Under the combined action of these forces, the CKS sponge exhibited an excellent dye adsorption performance. The FTIR spectrum of MB adsorbed on the CKS sponge (Fig. S6) further supports the adsorption mechanism. The sharp peak at 1590 cm^{-1} is assigned to the C-C stretching of the benzene ring, and the peak at 1333 cm^{-1} is attributed to the CH_3 stretching in the MB, which is adsorbed by the sponge [61]. Since there are no apparent changes in the

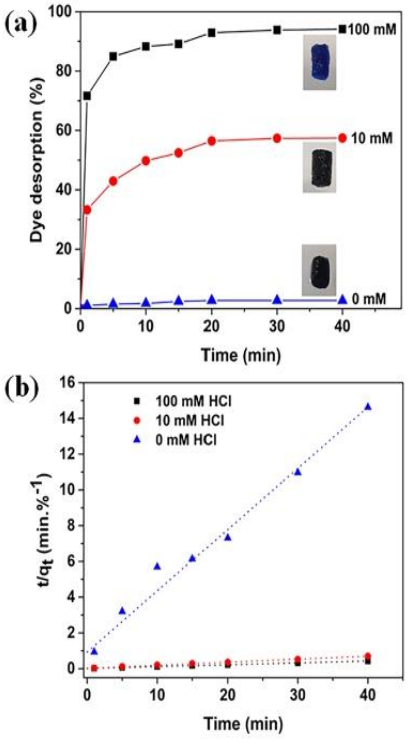

Fig. 6. Desorption of MB from the CKS sponge at a) Various HCl concentrations, the inserts are images of the sponge after desorption; b) Fitting pseudo-second-order desorption kinetics.

Table 3
Kinetic parameters of the pseudo-second-order desorption of MB from the CKS sponge.

HCl (C_0)	Pseudo-second-order			
	q_e (%)	K_2 (% $^{-1}$ min^{-1})	V_o (% min^{-1})	R^2
0 mM	3.03	0.083	0.76	0.98
10 mM	59.88	0.010	6.15	0.99
100 mM	95.23	0.016	145.10	0.99

absorption bands of other functional groups, it is suggested that the adsorption mechanism is mainly attributed to the strong π-π interaction and electrostatic charge attraction between the negatively charged CKS sponge and the cationic MB dye.

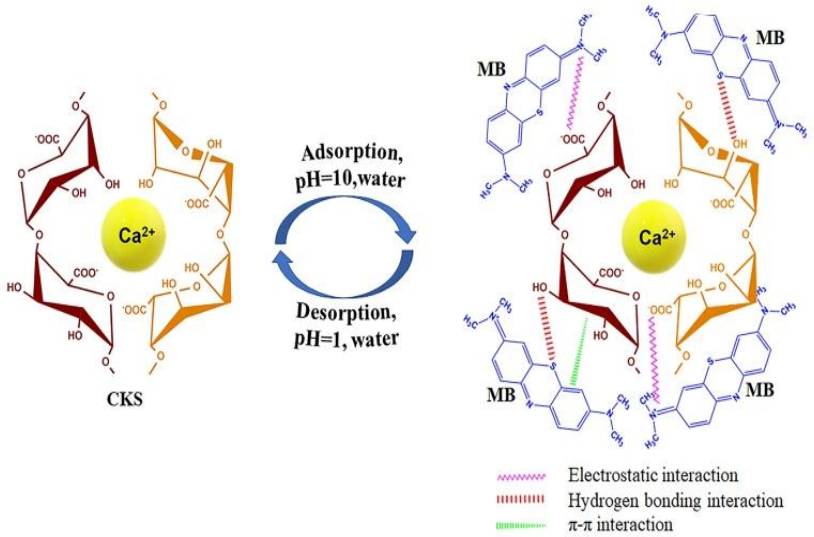

Fig. 7. Mechanism of the adsorption and desorption of MB dye on the CKS sponge.

The desorption of MB occurs via ion exchange between the protons of the acid and the dye. The H^+ ions are attracted to the -COO groups of the CKS sponge based on their p^{Ka} values of 3.4–3.7, which primarily protonate the ionized acids of the adsorbent and promote MB desorption. Overall, no structural changes occurred in the CKS sponge by the adsorption of MB dye. Following the adsorption-desorption process, the adsorbent returns to its initial form and continues the adsorption cycle, which is highly suitable for repeated use of the material.

3.6.6. Recycling

The recycling adsorption-desorption property is an important factor in determining the designed adsorbent's efficacy. The recycling test of the CKS sponge against MB dye was performed using a simple washing procedure. After each adsorption cycle, the sponge was put into 20 mL of 0.1 M HCl solution and shaken for 4 h. The desorbed sponge was washed several times with 0.1 M NaCl followed by deionized water. Then, the sponge was used repeatedly to study the regeneration property. The adsorption efficiency during each cycle was calculated. Five cycles of adsorption–desorption were completed, and the results of the study are shown in Fig. 8. As observed from the figure, minor changes were observed up to five consecutive cycles. The structural stability is retained during adsorption, and the adsorption efficiency still reaches 93% after five cycles, indicating that the sponge structure remains stable throughout the adsorption experiments and has an excellent capability of cyclic utilization and regeneration. The SEM images of the conjugate sponge after five circulations represented in Fig. S7 **a and b** show the structural integrity of the sponge after the repeated dye adsorption process. It is clear that the cell walls separate the pores in the sponge, and no adhesion is observed between the adjacent cell walls on the sponge surface. Therefore, the adsorption of the contaminant works without changing the porous structure of the sponges.

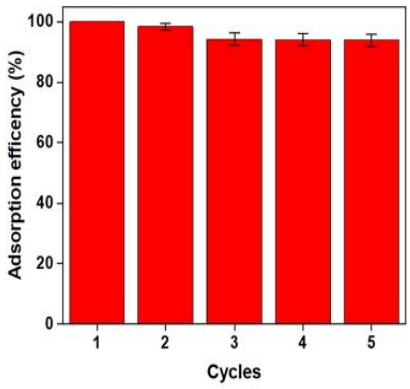

Fig. 8. Cycling adsorption of CKS sponge against MB dye (2 mg, 100 mg L^{-1}, 10 mL).

3.7. Biodegradation

The biochemical oxygen demand (BOD) analysis curves for the KS sponge and CKS sponge are shown in Fig. S8. In this process, the biopolymers are broken into smaller compounds by aerobic microbial organisms through metabolic or enzymatic processes and are finally converted to carbon dioxide. The results indicate that the BOD for the KS sponge was slightly higher during the whole measured period than in the case of the CKS sponge. The final values of 1846.7 ± 16.7 mg O_2 L^{-1} for the KS sponge, and 1578.3 ± 34.5 mg O_2 L^{-1} for the CKS sponge were achieved after 28 days. In the early stage, the ionic bonding on the CKS sponge decelerated the action of the microorganisms on the material, thereby reducing the rate of degradation. Overall, the results suggest that the CKS sponge biodegraded very similarly (90%) to the KS sponge (92%) over 28 days, although the initial degradation was slower for the CKS sponge. The biodegradability of these materials eliminates the risk of secondary contamination caused by sponge removal after activity such as adsorption. The obtained biodegradation rate in the present study is much higher than what was observed for polyurethane/polyisocyanurate foams [62] and poly(lactic acid) samples [63].

In the present investigation, a simpler fabrication of a green and sustainable sponge based on tree gum kondagogu is reported. The synthesis procedure involved no harmful solvents or chemicals, yielding, non-toxic, and biodegradable adsorbent with a three-dimensional structure that can remove cationic dyes like MB. The removal efficacy of the CKS sponge for MB dye is greater than that of many of the recently described materials. The exceptional reusability, economic feasibility, and biodegradability of this sponge make it a viable substitute for practical water remediation applications.

4. Conclusions

We successfully fabricated an ionically crosslinked conjugate sponge (CKS sponge) based on low-cost tree gum, through a simple freeze-drying method. The crosslinked sponge showed low density

(22.6 mg cm^{-3}), high porosity (92%), and high water stability. The uniform pores and interconnected channels in the sponge increase the dye adsorption capacity. All of these parameters contribute to its excellent performance as a dye adsorbent.

The maximum adsorption of the cationic dye, methylene blue, by the sponge was 1250 mg g^{-1} at pH 9. The pH level plays a vital role in the sponge adsorption process, as it alters the electrostatic interaction between the surface of the sponge and the MB dye molecules. Adsorption kinetics and isotherm data fitted well with the pseudo-second-order model and Langmuir model, respectively, which may be used to describe the adsorption process of the MB dye onto the CKS sponge. The adsorption may be simply regenerated up to five times while retaining structural stability and sorption capability. Together with its recyclability, the biodegradability of this adsorbent suggests the usage of biowaste to treat wastewater containing toxic dyes.

CRediT authorship contribution statement

Rohith K. Ramakrishnan: Writing – original draft, Conceptualization, Investigation, Methodology. **Vinod V.T. Padil**: Investigation, Supervision, Writing – review & editing. **Stanisław Wacławek**: Experimental, Validation. **Miroslav Černík**: Data curation, Project administration. **Diwakar Tiwari**: Writing – review & editing.

Declaration of Competing Interest

There is no conflict of interest connected with this artticle.

Acknowledgments

The authors would like to acknowledge the assistance provided by the Research Infrastructure NanoEnviCz (Project No. LM2018124) and the "Inter Excellence Action Programme" within the framework of the project "Bio-Based Porous 2D Membranes and 3D Sponges Based on Functionalized Tree Gum Polysaccharides and their Environmental Application" (registration number LTAUSA19091) – TUL internal No.: 18309/136, supported by the Ministry of Education, Youth and Sports of the Czech Republic.

Appendix A. Supporting information

Supplementary data associated with this article can be found in the online version at doi:10.1016/j.jece.2022.108285.

References

[1] C. Zhu, Y. Xia, Y. Zai, Y. Dai, X. Liu, J. Bian, Y. Liu, J. Liu, G. Li, Adsorption and desorption behaviors of HPEI and thermoresponsive HPEI based gels on anionic and cationic dyes, Chem. Eng. J. 369 (2019) 863–873, https://doi.org/10.1016/j.cej.2019.03.169.

[2] H. Mittal, A. Maity, S.S. Ray, Effective removal of cationic dyes from aqueous solution using gum ghatti-based biodegradable hydrogel, Int. J. Biol. Macromol. 79 (2015) 8–20, https://doi.org/10.1016/j.ijbiomac.2015.04.045.

[3] M. Lee, W. Wang, Y. Du, T. Jeon, S. Shin, Q. Wu, G. Dao, H. Hu, Applications of UV / H 2 O 2, UV / persulfate, and UV / persulfate / Cu 2 + for the elimination of reverse osmosis concentrate generated from municipal wastewater reclamation treatment plant: toxicity, transformation p, Sci. Total Environ. 762 (2021), https://doi.org/10.1016/j.scitotenv.2020.144161.

[4] M.K. Uddin, U. Baig, Synthesis of Co3O4 nanoparticles and their performance towards methyl orange dye removal: characterisation, adsorption and response surface methodology, J. Clean. Prod. 211 (2019) 1141–1153, https://doi.org//10.1016/j.jclepro.2018.11.232.

[5] M.B. Nguyen, G.H. Le, T.D. Nguyen, Q.K. Nguyen, T.T.T. Pham, T. Lee, T.A. Vu, Bimetallic Ag-Zn-BTC/GO composite as highly efficient photocatalyst in the photocatalytic degradation of reactive yellow 145 dye in water, J. Hazard. Mater. 420 (2021), 126560, https://doi.org/10.1016/j.jhazmat.2021.126560.

[6] S. Senguttuvan, P. Senthilkumar, V. Janaki, S. Kamala-Kannan, Significance of conducting polyaniline based composites for the removal of dyes and heavy metals from aqueous solution and wastewaters - a review, Chemosphere 267 (2021), 129201, https://doi.org/10.1016/j.chemosphere.2020.129201.

[7] B.K. Tripathy, M. Kumar, Sequential coagulation/flocculation and microwave-persulfate processes for landfill leachate treatment: assessment of bio-toxicity, effect of pretreatment and cost-analysis, Waste Manag. 85 (2019) 18–29, https://doi.org/10.1016/j.wasman.2018.12.014.

[8] H. Ghasemi, S. Mozaffari, S.H. Mousavi, B. Aghabarari, N. Abu-Zahra, Decolorization of wastewater by heterogeneous Fenton reaction using MnO2-Fe3O4/CuO hybrid catalysts, J. Environ. Chem. Eng. 9 (2021), 105091, https://doi.org/10.1016/j.jece.2021.105091.

[9] V. López Durán, J. Erlandsson, L. Wågberg, P.A. Larsson, Novel, cellulose-based, lightweight, wet-resilient materials with tunable porosity, density, and strength, ACS Sustain. Chem. Eng. 6 (2018) 9951–9957, https://doi.org/10.1021/acssuschemeng.8b01165.

[10] L. Huang, M. He, B. Chen, Q. Cheng, B. Hu, Facile green synthesis of magnetic porous organic polymers for rapid removal and separation of methylene blue, ACS Sustain. Chem. Eng. 5 (2017) 4050–4055, https://doi.org/10.1021/acssuschemeng.7b00031.

[11] S. Mallakpour, F. Tabesh, Effective adsorption of methylene blue dye from water solution using renewable natural hydrogel bionanocomposite based on tragacanth gum: linear-nonlinear calculations, Int. J. Biol. Macromol. 187 (2021) 319–324, https://doi.org/10.1016/j.ijbiomac.2021.07.105.

[12] L. Mouni, L. Belkhiri, J.C. Bollinger, A. Bouzaza, A. Assadi, A. Tirri, F. Dahmoune, K. Madani, H. Remini, Removal of Methylene Blue from aqueous solutions by adsorption on Kaolin: kinetic and equilibrium studies, Appl. Clay Sci. 153 (2018) 38–45, https://doi.org/10.1016/j.clay.2017.11.034.

[13] S.D. Khattri, M.K. Singh, Removal of malachite green from dye wastewater using neem sawdust by adsorption, J. Hazard. Mater. 167 (2009) 1089–1094, https://doi.org/10.1016/j.jhazmat.2009.01.101.

[14] A. Mokhtar, S. Abdelkrim, A. Djelad, A. Sardi, B. Boukoussa, M. Sassi, A. Bengueddach, Adsorption behavior of cationic and anionic dyes on magadiite-chitosan composite beads, Carbohydr. Polym. 229 (2020), 115399, https://doi.org/10.1016/j.carbpol.2019.115399.

[15] Q. Liu, H. Yu, F. Zeng, X. Li, J. Sun, C. Li, H. Lin, Z. Su, HKUST-1 modified ultrastability cellulose / chitosan composite aerogel for highly efficient removal of methylene blue, Carbohydr. Polym. 255 (2021), 117402, https://doi.org/10.1016/j.carbpol.2020.117402.

[16] W. Wang, Y. Zhao, H. Bai, T. Zhang, V. Ibarra-galvan, Methylene blue removal from water using the hydrogel beads of poly (vinyl alcohol) -sodium alginate-chitosan-montmorillonite, Carbohydr. Polym. 198 (2018) 518–528, https://doi.org/10.1016/j.carbpol.2018.06.124.

[17] J. Luo, X. Ma, X. Zhou, Y. Xu, Construction of physically crosslinked cellulose nanofibrils/alkali lignin/montmorillonoite/polyvinyl alcohol network hydrogel and its application in methylene blue removal, Cellulose 28 (2021) 5531–5543, https://doi.org/10.1007/s10570-021-03847-1.

[18] L. Chen, Y. Li, Q. Du, Z. Wang, Y. Xia, E. Yedinak, J. Lou, L. Ci, High performance agar/graphene oxide composite aerogel for methylene blue removal, Carbohydr. Polym. 155 (2017) 345–353, https://doi.org/10.1016/j.carbpol.2016.08.047.

[19] S. Sadeghi, A.Z. Moghaddam, M. Massinaei, Novel tunable composites based on bentonite and modified tragacanth gum for removal of acid dyes from aqueous solutions, RSC Adv. 5 (2015) 55731–55745, https://doi.org/10.1039/c5ra07979a.

[20] T. Etemadinia, A. Allahrasani, B. Barikbin, ZnFe2O4@SiO2@Tragacanth gum nanocomposite: synthesis and its application for the removal of methylene blue dye from aqueous solution, Polym. Bull. 76 (2019) 6089–6109, https://doi.org/10.1007/s00289-019-02681-7.

[21] G. Song, Y. Shi, A. Li, H. Wang, G. Ding, Facile preparation of three-dimensional graphene oxide/ ι -carrageenan composite aerogel and its efficient ability for selective adsorption of methylene blue, J. Mater. Sci. 56 (2021) 14866–14879, https://doi.org/10.1007/s10853-021-06211-7.

[22] E. Makhado, S. Pandey, P.N. Nomngongo, J. Ramontja, Preparation and characterization of xanthan gum-cl-poly(acrylic acid)/o-MWCNTs hydrogel nanocomposite as highly effective re-usable adsorbent for removal of methylene blue from aqueous solutions, J. Colloid Interface Sci. 513 (2018) 700–714, https://doi.org/10.1016/j.jcis.2017.11.060.

[23] E. Makhado, S. Pandey, J. Ramontja, Microwave assisted synthesis of xanthan gum-cl-poly (acrylic acid) based-reduced graphene oxide hydrogel composite for adsorption of methylene blue and methyl violet from aqueous solution, Int. J. Biol. Macromol. 119 (2018) 255–269, https://doi.org/10.1016/j.ijbiomac.2018.07.104.

[24] R.K. Ramakrishnan, V.V.T. Padil, M. Černík, S. Wacławek, R.S. Varma, Eco-friendly and economic, adsorptive removal of cationic and anionic dyes by bio-based karaya gum—chitosan sponge, Polymers 13 (2021) 1–21, https://doi.org/10.3390/polym13020251.

[25] J. Wu, Z. Dong, X. Li, P. Li, J. Wei, M. Hu, L. Geng, X. Peng, Constructing acid-resistant chitosan/cellulose nanofibrils composite membrane for the adsorption of methylene blue, J. Environ. Chem. Eng. 10 (2022), 107754, https://doi.org/10.1016/j.jece.2022.107754.

[26] D.G. Njuguna, H. Schönherr, Smart and regeneratable Xanthan gum hydrogel adsorbents for selective removal of cationic dyes, J. Environ. Chem. Eng. 10 (2022), https://doi.org/10.1016/j.jece.2022.107620.

[27] X. Zhang, I. Elsayed, R.M.O. Nayanathara, X. Song, R. Shmulsky, E.B. Hassan, Biobased hierarchically porous carbon featuring micron-sized honeycomb architecture for CO_2 capture and water remediation, J. Environ. Chem. Eng. 10 (2022), 107460, https://doi.org/10.1016/j.jece.2022.107460.

[28] S. Miri, H. Nadeem, Y. Hora, B.W.X. Chin, P.C. Andrews, W. Batchelor, Depth filtration application of nanofibrillated cellulose-mesoporous silica nanoparticle composites as double-layer membranes, J. Environ. Chem. Eng. 10 (2022), 106892, https://doi.org/10.1016/j.jece.2021.106892.

[29] I.I. Shahib, J. Ifthikar, D.T. Oyekunle, Z. Elkhlifi, A. Jawad, J. Wang, W. Lei, Z. Chen, Influences of chemical treatment on sludge derived biochar; physicochemical properties and potential sorption mechanisms of lead (II) and

methylene blue, J. Environ. Chem. Eng. 10 (2022), 107725, https://doi.org/10.1016/j.jece.2022.107725.
[30] R.A. Rather, M.A. Bhat, A.H. Shalla, Multicomponent interpenetrating metal based Alginate-Carrageenan biopolymer hydrogel beads substantiated by graphene oxide for efficient removal of methylene blue from waste water, Chem. Eng. Res. Des. 182 (2022) 604–615, https://doi.org/10.1016/j.cherd.2022.04.017.
[31] F.M. Jais, S. Ibrahim, C.Y. Chee, Z. Ismail, High removal of crystal violet dye and tetracycline by hydrochloric acid assisted hydrothermal carbonization of sugarcane bagasse prepared at high yield, Sustain. Chem. Pharm. 24 (2021), 100541, https://doi.org/10.1016/j.scp.2021.100541.
[32] S. Jiang, S. Agarwal, A. Greiner, Low-density open cellular sponges as functional materials, Angew. Chem. Int. Ed. 56 (2017) 15520–15538, https://doi.org/10.1002/anie.201700684.
[33] A.A. Pawar, H. Kim, Sustainable, hydrophobic, and reusable paper waste aerogel as an effective and versatile oil absorbent, J. Environ. Chem. Eng. 10 (2022), 107356, https://doi.org/10.1016/j.jece.2022.107356.
[34] N. Asim, M. Badiei, M.A. Alghoul, M. Mohammad, A. Fudholi, M. Akhtaruzzaman, N. Amin, K. Sopian, Biomass and industrial wastes as resource materials for aerogel preparation: opportunities, challenges, and research directions, Ind. Eng. Chem. Res. 58 (2019) 17621–17645, https://doi.org/10.1021/acs.iecr.9b02661.
[35] V.T.P. Vinod, R.B. Sashidhar, B. Sreedhar, Biosorption of nickel and total chromium from aqueous solution by gum kondagogu (Cochlospermum gossypium): a carbohydrate biopolymer, J. Hazard. Mater. 178 (2010) 851–860, https://doi.org/10.1016/j.jhazmat.2010.02.016.
[36] V.V.T. Padil, S. Wacławek, M. Černík, Green synthesis: nanoparticles and nanofibres based on tree gums for environmental applications, Ecol. Chem. Eng. S 23 (2016) 533–557, https://doi.org/10.1515/eces-2016-0038.
[37] C. Ji, S. Yang, T.E. Cheng Y., X. Hao, Y. Li, Three-dimensional network graphene oxide/sodium alginate aerogel beads with slit-shaped structure: synthesis, performance and selective adsorption mechanism for Cu(II), J. Environ. Chem. Eng. 9 (2021), 106819, https://doi.org/10.1016/j.jece.2021.106819.
[38] K. Yong, D.J. Mooney, Alginate: properties and biomedical applications, Prog. Polym. Sci. 37 (2012) 106–126, https://doi.org/10.1016/j.progpolymsci.2011.06.003.
[39] R.K. Ramakrishnan, V.V.T. Padil, M. Škodová, S. Wacławek, M. Černík, S. Agarwal, Hierarchically porous bio-based sustainable conjugate sponge for highly selective oil / organic solvent absorption, Adv. Funct. Mater. 2100640 (2021) 1–9, https://doi.org/10.1002/adfm.202100640.
[40] M.J. Costa, A.M. Marques, L.M. Pastrana, S.M. Sillankorva, M.A. Cerqueira, Physicochemical properties of alginate-based films: effect of ionic crosslinking and mannuronic and guluronic acid ratio, Food Hydrocoll. 81 (2018) 442–448, https://doi.org/10.1016/j.foodhyd.2018.03.014.
[41] V.V.T.T. Padil, C. Senan, S. Waclawek, M. Černík, S. Agarwal, R.S. Varma, Bioplastic fibers from gum arabic for greener food wrapping applications, ACS Sustain. Chem. Eng. 7 (2019) 5900–5911, https://doi.org/10.1021/acssuschemeng.8b05896.
[42] X. Shen, P. Huang, F. Li, X. Wang, T. Yuan, R. Sun, Compressive alginate sponge derived from seaweed biomass resources for methylene blue removal from wastewater, Polymers 11 (2019) 4–8, https://doi.org/10.3390/polym11060961.
[43] F. Jiang, Y. Hsieh, Super water absorbing and shape memory nanocellulose aerogels from TEMPO-oxidized cellulose nano fibrils via cyclic freezing – thawing, J. Mater. Chem. A 2 (2014) 350–359, https://doi.org/10.1039/c3ta13629a.
[44] S.T. Ho, D.W. Hutmacher, A comparison of micro CT with other techniques used in the characterization of scaffolds, Biomaterials 27 (2006) 1362–1376, https://doi.org/10.1016/j.biomaterials.2005.08.035.
[45] Y. Cheng, L. Lu, W. Zhang, J. Shi, Y. Cao, Reinforced low density alginate-based aerogels: preparation, hydrophobic modification and characterization, Carbohydr. Polym. 88 (2012) 1093–1099, https://doi.org/10.1016/j.carbpol.2012.01.075.
[46] L. Wang, M. Sánchez-soto, T. Abt, Properties of bio-based gum Arabic / clay aerogels, Ind. Crop. Prod. 91 (2016) 15–21, https://doi.org/10.1016/j.indcrop.2016.05.001.
[47] A. Bashir, A.H. Pandith, L.A. Malik, A. Qureashi, F.A. Ganaie, G.N. Dar, Magnetically recyclable L-cysteine capped Fe3O4 nanoadsorbent: a promising pH guided removal of Pb(II), Zn(II) and HCrO4- contaminants, J. Environ. Chem. Eng. 9 (2021), 105880, https://doi.org/10.1016/j.jece.2021.105880.
[48] S. Ghaedi, K. Seifpanahi-Shabani, M. Sillanpää, Waste-to-Resource: new application of modified mine silicate waste to remove Pb2+ ion and methylene blue dye, adsorption properties, mechanism of action and recycling, Chemosphere 292 (2022), https://doi.org/10.1016/j.chemosphere.2021.133412.
[49] Y. Zhang, C. Hui, R. Wei, Y. Jiang, L. Xu, Y. Zhao, L. Du, H. Jiang, Study on anionic and cationic dye adsorption behavior and mechanism of biofilm produced by Bacillus amyloliquefaciens DT, Appl. Surf. Sci. 573 (2022), 151627, https://doi.org/10.1016/j.apsusc.2021.151627.
[50] A. Pettignano, N. Tanchoux, T. Cacciaguerra, T. Vincent, L. Bernardi, E. Guibal, F. Quignard, Sodium and acidic alginate foams with hierarchical porosity: preparation, characterization and efficiency as a dye adsorbent, Carbohydr. Polym. 178 (2017) 78–85, https://doi.org/10.1016/j.carbpol.2017.09.022.
[51] N.U. Alamin, A.S. Khan, A. Nasrullah, J. Iqbal, Z. Ullah, I.U. Din, N. Muhammad, S. Z. Khan, Activated carbon-alginate beads impregnated with surfactant as sustainable adsorbent for efficient removal of methylene blue, Int. J. Biol. Macromol. 176 (2021) 233–243, https://doi.org/10.1016/j.ijbiomac.2021.02.017.
[52] C. Jiao, T. Li, J. Wang, H. Wang, X. Zhang, X. Han, Z. Du, Y. Shang, Y. Chen, Efficient removal of dyes from aqueous solution by a porous sodium alginate/gelatin/graphene oxide triple-network composite aerogel, J. Polym. Environ. 28 (2020) 1492–1502, https://doi.org/10.1007/s10924-020-01702-1.
[53] S. Wang, Q. Zhang, Z. Wang, J. Pu, Facile fabrication of an effective nanocellulose-based aerogel and removal of methylene blue from aqueous system, J. Water Process Eng. 37 (2020), 101511, https://doi.org/10.1016/j.jwpe.2020.101511.
[54] X. Wei, T. Huang, J. Nie, J. hui Yang, X. dong Qi, Z. wan Zhou, Y. Wang, Bio-inspired functionalization of microcrystalline cellulose aerogel with high adsorption performance toward dyes, Carbohydr. Polym. 198 (2018) 546–555, https://doi.org/10.1016/j.carbpol.2018.06.112.
[55] Q. Liu, H. Yu, F. Zeng, X. Li, J. Sun, C. Li, H. Lin, Z. Su, HKUST-1 modified ultrastability cellulose/chitosan composite aerogel for highly efficient removal of methylene blue, Carbohydr. Polym. 255 (2021), 117402, https://doi.org/10.1016/j.carbpol.2020.117402.
[56] T.E. Ma D., S. Yang, X. Hao, Graphene oxide-montmorillonite/sodium alginate aerogel beads for selective adsorption of methylene blue in wastewater, J. Alloy. Compd. 832 (2020), 154833, https://doi.org/10.1016/j.jallcom.2020.154833.
[57] Y. Shi, G. Song, A. Li, J. Wang, H. Wang, Y. Sun, G. Ding, Graphene oxide-chitosan composite aerogel for adsorption of methyl orange and methylene blue: effect of pH in single and binary systems, Colloids Surf. A Physicochem. Eng. Asp. 641 (2022), 128595, https://doi.org/10.1016/j.colsurfa.2022.128595.
[58] T. Maimaiti, R. Hu, H. Yuan, C. Liang, F. Liu, Q. Li, S. Lan, B. Yu, S.T. Yang, Magnetic Fe3O4/TiO2/graphene sponge for the adsorption of methylene blue in aqueous solution, Diam. Relat. Mater. 123 (2022), 108811, https://doi.org/10.1016/j.diamond.2021.108811.
[59] L. Jiang, Y. Wen, Z. Zhu, X. Liu, W. Shao, A Double cross-linked strategy to construct graphene aerogels with highly efficient methylene blue adsorption performance, Chemosphere 265 (2021), 129169, https://doi.org/10.1016/j.chemosphere.2020.129169.
[60] Y. Chen, M. Hanshe, Z. Sun, Y. Zhou, C. Mei, G. Duan, J. Zheng, S.E. Jiang S., Lightweight and anisotropic cellulose nanofibril/rectorite composite sponges for efficient dye adsorption and selective separation, Int. J. Biol. Macromol. 207 (2022) 130–139, https://doi.org/10.1016/j.ijbiomac.2022.03.011.
[61] X. Wei, T. Huang, J. hui Yang, N. Zhang, Y. Wang, Z. wan Zhou, Green synthesis of hybrid graphene oxide/microcrystalline cellulose aerogels and their use as superabsorbents, J. Hazard. Mater. 335 (2017) 28–38, https://doi.org/10.1016/j.jhazmat.2017.04.030.
[62] M. Borowicz, J. Paciorek-Sadowska, J. Lubczak, B. Czupryński, Biodegradable, flame-retardant, and bio-based rigid polyurethane/polyisocyanurate foams for thermal insulation application, Polymers 11 (2019), https://doi.org/10.3390/polym11111816.
[63] M. Borowicz, J. Paciorek-Sadowska, M. Isbrandt, Ł. Grzybowski, B. Czupryński, Glycerolysis of poly(lactic acid) as away to extend the "life cycle" of this material, Polymers 11 (2019), https://doi.org/10.3390/polym11121963.

4.4. Gum Hydrocolloids Reinforced Silver Nanoparticle Sponge for Catalytic Degradation of Water Pollutants

Abstract: The accumulation of organic contaminants including dyes in aquatic systems is of significant environmental concern, necessitating the development of affordable and sustainable materials for the treatment/elimination of these hazardous pollutants. Here, a green synthesis strategy has been used to develop a self-assembled gum kondagogu-sodium alginate bioconjugate sponge adorned with silver nanoparticles, for the first time. The properties of the nanocomposite sponge were then analyzed using FTIR, TGA, SEM, and MicroCT. The ensued biobased sponge exhibited a hierarchical microstructure, open cellular pores, good shape memory, and mechanical properties. It merges the attributes of an open cellular porous structure with metal nanoparticles and is envisaged to be deployed as a sustainable catalytic system for reducing contaminants in the aqueous environment. This nanocomposite sponge showed enhanced catalytic effectiveness (k_m values up to 37 min^{-1} g^{-1} and 44 min^{-1} g^{-1} for methylene blue and 4-nitrophenol, respectively), antibacterial properties, reusability, and biodegradability (65% biodegradation in 28 days).

Citation: R.K. Ramakrishnan, V.V.T. Padil, M. Černík, S. Wacławek, R.S. Varma, Gum Hydrocolloids Reinforced Silver Nanoparticle Sponge for Catalytic Degradation of Water Pollutants, Polymers (Basel). 13 (2022) 1–21

polymers

MDPI

Article

Gum Hydrocolloids Reinforced Silver Nanoparticle Sponge for Catalytic Degradation of Water Pollutants

Rohith K. Ramakrishnan [1], Daniele Silvestri [1], Nechikkottil S. Sumitha [2], Nhung H. A. Nguyen [1], Karel Havlíček [1], Dariusz Łukowiec [3], Stanisław Wacławek [1], Miroslav Černík [1], Diwakar Tiwari [4], Vinod V. T. Padil [1,*] and Rajender S. Varma [5,*]

[1] Institute for Nanomaterials, Advanced Technologies and Innovation (C × I), Technical University of Liberec (TUL), Studentská 1402/2, 461 17 Liberec, Czech Republic; rohith.kunjiparambil.ramakrishnan@tul.cz (R.K.R.); daniele.silvestri@tul.cz (D.S.); nhung.nguyen@tul.cz (N.H.A.N.); karel.havlicek@tul.cz (K.H.); stanislaw.waclawek@tul.cz (S.W.); miroslav.cernik@tul.cz (M.Č.)

[2] Department of Polymer Science and Rubber Technology, Cochin University of Science and Technology, Kochi 682 022, Kerala, India; sumithans93@gmail.com

[3] Materials Research Laboratory, Faculty of Mechanical Engineering, Silesian University of Technology, Konarskiego 18 a St., 44-100 Gliwice, Poland; dariusz.lukowiec@polsl.pl

[4] Department of Chemistry, Mizoram University (A Central University), Aizawal 796004, Mizoram, India; diwakarmzu@gmail.com

[5] Regional Centre of Advanced Technologies and Materials, Czech Advanced Technology and Research Institute, Palacký University in Olomouc, Šlechtitelů 27, 783 71 Olomouc, Czech Republic

* Correspondence: vinod.padil@tul.cz (V.V.T.P.); varma.rajender@epa.gov (R.S.V.)

Abstract: The accumulation of organic contaminants including dyes in aquatic systems is of significant environmental concern, necessitating the development of affordable and sustainable materials for the treatment/elimination of these hazardous pollutants. Here, a green synthesis strategy has been used to develop a self-assembled gum kondagogu-sodium alginate bioconjugate sponge adorned with silver nanoparticles, for the first time. The properties of the nanocomposite sponge were then analyzed using FTIR, TGA, SEM, and MicroCT. The ensued biobased sponge exhibited hierarchical microstructure, open cellular pores, good shape memory, and mechanical properties. It merges the attributes of an open cellular porous structure with metal nanoparticles and are envisaged to be deployed as a sustainable catalytic system for reducing contaminants in the aqueous environment. This nanocomposite sponge showed enhanced catalytic effectiveness (k_m values up to 37 min^{-1} g^{-1} and 44 min^{-1} g^{-1} for methylene blue and 4-nitrophenol, respectively), antibacterial properties, reusability, and biodegradability (65% biodegradation in 28 days).

Keywords: biodegradation; biosponge; catalysis; green synthesis; silver nanoparticles; tree gum kondagogu

Citation: Ramakrishnan, R.K.; Silvestri, D.; Sumitha, N.S.; Nguyen, N.H.A.; Havlíček, K.; Łukowiec, D.; Wacławek, S.; Černík, M.; Tiwari, D.; Padil, V.V.T.; et al. Gum Hydrocolloids Reinforced Silver Nanoparticle Sponge for Catalytic Degradation of Water Pollutants. *Polymers* **2022**, *14*, 3120. https://doi.org/10.3390/polym14153120

Academic Editor: Shiyong Liu

Received: 18 June 2022
Accepted: 29 July 2022
Published: 31 July 2022

1. Introduction

The release of a huge quantity of organic contaminants from the agricultural field, pharmaceutical, and chemical industries creates severe environmental pollution that directly causes a significant threat to the health of human beings and all other living organisms [1,2]. The treatment and removal of most pollutants in water have become incredibly challenging due to their water solubility and stability in the environment [3,4]. Although adsorption, biological treatment, solvent extraction, distillation, and chemical oxidation are some conventional methods for removing contaminants from water, catalytic hydrogenation is a highly efficient and convenient technique for degrading contaminants, producing fewer harmful effects [5]. For practical applications, the catalyst must meet the conditions of availability, low cost, high efficiency, reusability, and environmental friendliness [6].

Metal nanoparticles have garnered tremendous attention from researchers owing to their excellent selectivity and outstanding reactivity for catalytic destruction of contaminants [7]. Among them, silver nanoparticles (AgNPs) have been extensively applied as catalysts for reducing organic pollutants because of relatively abundant resources [8]. Capturing AgNPs on polymer templates minimizes the oxidation and aggregation of nanoparticles and simultaneously improves their catalytic activity [9]. The metal nanoparticles are well supported by an open-cellular sponge, which may be readily retrieved and reused after being utilized in catalytic reactions. Recently, NPs have been successfully decorated on chitosan, cellulose, and alginate-based materials for diverse applications [10,11]. However, these biopolymers require toxic chemicals, expensive equipment, and sophisticated technologies for extraction and purification [12]. In contrast, tree gums are non-toxic and sustainable alternatives which offer abundant functionalities, and advantages in terms of gel-forming capacity as well as degradability. Consequently, comprehensive research on these materials with promising features is necessary. An efficient and recyclable catalyst developed with a renewable material is environmentally and economically viable [10–12].

Gum kondagogu is a non-toxic polysaccharide extracted from the plant *Cochlospermum Gossypium* (Bixaceae family) [13]. It is a composition of arabinose, mannose, D-glucuronic acid, α-D galacturonic acid, β-D-galacturonic acid, α-D glucose, β-D-glucose, galactose, rhamnose, and fructose with an average molecular weight of 7.23×10^6 g mol^{-1} [14]. It also contains proteins, tannin, and soluble fibers. Although template-assisted green synthesis may be conducted to generate nanoparticles making use of tree gums, their delicate nature makes three-dimensional fabrication and application problematic. On the other hand, gum functional groups can be coupled with other biopolymers to aid conjugate sponge formation with better characteristics and targeted application potential [15,16]. In this way, gum kondagogu combines with another polysaccharide, sodium alginate, derived from marine algae. Sodium alginate is a polysaccharide composed of two functional units β-D-mannuronic acid and α-L-guluronic acid joined by 1→4 bonds [17]. In addition, several free hydroxyl and carboxyl groups are distributed in the alginate structure, allowing them to form conjugate with other polymers. These conjugations convert the fragile and lower compressible tree gum sponge to a compressible composite sponge with structural integrity, hierarchical porosity, and low density [18]. Despite the benefits outlined above, only a few studies have been reported on gum sponges containing metal nanoparticles.

In the current work, AgNPs are green synthesized via an in-situ reduction process and uniformly decorated onto the gum kondagogu-sodium alginate conjugate sponge (Ag@KS) for the first time. The abundant functional groups in the gum and alginate facilitate conjugate formation and provide mechanical integrity. The remaining functionalities are further used for the green synthesis and stabilization of AgNPs to form a sustainable nanocomposite sponge. The reduction efficiency of the sponge for the nanoparticles' synthesis has been assessed, and the optimum sponge-Ag precursor ratio has been identified for further examination. The physico-chemical and morphological characterization was then conducted to understand the properties of nanocomposite sponges. Both Gram-positive and Gram-negative bacteria were used to examine the antibacterial efficiency of the sponge.

Moreover, the post-degradation profile of the nanocomposite sponge shows its eco-friendly nature. The ligation of AgNPs onto the microporous sponge is anticipated to enhance the catalytic reduction of contaminants (4-Nitrophenol (4-NP) and Methyleneblue (MB) as examples) in an aqueous environment by allowing diffusion of polluted water to the interior of the porous network and at the same time preventing the AgNPs' oxidation, aggregation, and leach out. The intriguing structural durability, good antibacterial and catalytic properties, and biodegradability would make it a rapid and sustainable solution to environmental pollution.

2. Materials and Methods

2.1. Materials

Gum kondagogu was supplied by Girijan cooperative society, Andhra pradesh, India. Sodium alginate, Silver nitrate ($AgNO_3$, 99.8%), Calcium chloride ($CaCl_2$, ≥93.0%), Sodium borohydride ($NaBH_4$, ≥96.0%), Sodium hydroxide (NaOH, ≥98%), 4-Nitrophenol (4-NP, ≥99%), and Methylene blue (MB) were procured from Sigma-Aldrich, Darmstadt, Germany. The supernatant of the settled sludge from a municipal waste-water treatment facility (the Liberec WWTP, Czech R.) was used as an activated sludge for biodegradation experiments. All the chemicals purchased were of analytical grade and used as such without purification. In all the experiments, deionized water was used.

2.2. Preparation of Ag@KS Sponge

Gum kondagogu and sodium alginate were added in 1:1 ratio (*w*/*w*) to different concentrations of $AgNO_3$ solution (4 mM, 6 mM, 8 mM, and 10 mM). The final polymer concentration in the resulting composite solution is maintained at 1.5 wt% [19]. The mixtures were then continuously stirred at 85 °C for 45 min to complete the reduction of nanoparticles under alkaline condition (pH = 10) using 0.1 N NaOH. The unreacted $AgNO_3$ and excess NaOH after the reduction were removed through dialysis, the solutions were poured into the mould, and lyophilized at −52 °C for 24 h to obtain the Ag@KS sponges. Furthermore, post-synthesis crosslinking was performed using 5% $CaCl_2$ solution, followed by washing with water to eliminate excess $CaCl_2$, and lyophilized again. The pristine sample without AgNPs is referred to as KS sponge.

2.3. Characterization

UV–visible absorption spectra (UV-Vis) were recorded using UV Spectrophotometer (Hach DR 3900, Loveland, CO, USA) to monitor the reduction of Ag^+ solution by the conjugate. The size and morphology of AgNPs were observed by transmission electron microscopy (TEM, Titan 80–300, FEI Company, Hillsboro, OR, USA). Silver concentration on sponge and leaching in water were evaluated using ICP-MS (Elan 6000, PerkinElmer, Akron, OH, USA). The X-ray diffraction (XRD) spectrum was recorded using a Rigaku MiniFlex, Austin, TX, USA, 600 X-ray powder diffractometer with a copper tube, Cu K_α (λ = 0.15406 nm), a tube voltage of 40 kV, and a current of 15 mA). Fourier transform infrared spectroscopy (FTIR) was performed on an infrared spectrophotometer (Nicolet iZ10, Thermo Scientific, Waltham, MA, USA), and thermal stability under a nitrogen atmosphere (at a flow rate of 50 mL min^{-1}) was studied using Q500 Thermogravimetric Analyzer (TA instruments, New Castle, DE, USA) from 30 to 600 °C with a heating rate of 20 °C min^{-1}. The morphology and porous architecture of sponges were observed by scanning electron microscope (SEM, Carl Zeiss, Ultra/Plus, Munich, Germany) equipped with energy dispersive X-ray spectroscopy (EDS). X-ray computed tomography (MicroCT, Skyscan 1272, Bruker, Billerica, MA, USA) was used to characterize the composite microstructure and porosity. A universal testing machine (Shimadzu Autograph AG-I series, Kyoto, Japan) was used to analyze the mechanical properties of the sponges in terms of compressive strength at a test speed of 5 mm min^{-1} for up to 80% compression. The sample dimensions were of 10 mm diameter and 20 mm length. The compressive strength was taken as the highest value of compressive stress, and the elastic moduli were calculated from the initial linear region (up to 1.5% strain) of the stress−strain curves. Bulk densities of the sponges were calculated from the weight (taken on an analytical balance SAB 124e, ADAM, Oxford, CT, USA) and volume of the sponges, where a digital calliper measured the dimensions of the sponges at five different positions.

2.4. Catalytic Degradation

Catalytic reduction of MB dye was performed with minor modifications of the previously reported procedure [20]. Briefly, 1.5, 1.9, and 3.1 mg of Ag@KS sponge were immersed separately in a mixture of $NaBH_4$ (1 mL, 50 mM) and MB dye (4 mL, 30 µM) and stirred

at room temperature for 60 min. The discoloration process was monitored using UV–Vis absorption spectroscopy at the MB maximum absorbance (λmax = 664 nm) at predefined time intervals of 0, 0.5, 1, 2, 3, 4, 5, 10, 15, 20, 30, 40, and 60 min.

Similarly, catalytic reduction of 4-NP was also accomplished as per the procedure reported earlier [21]. For this purpose, 1.0, 1.8, and 3.6 mg of Ag@KS sponge was immersed separately into an aqueous solution mixture of 4-NP (1 mM, 10 mL) and $NaBH_4$ (0.3 M, 5 mL) at room temperature for 60 min. The reduction of 4-NP was monitored by UV–Vis spectroscopy at the 4-NP maximum absorbance (λ_{max} = 400 nm) at a predetermined time interval as that for MB.

The kinetics of the catalytic performance of the Ag@KS sponge were fitted to the pseudo-first order kinetic model. The kinetic rate constants were calculated using Equation (1):

$$ln\frac{A_t}{A_0} = -k_{app}t \quad (1)$$

where A_0 and A_t are the measured absorbance at $t = 0$ and at time t, respectively, and k_{app} is the apparent rate constant of pseudo-first order kinetics.

For comparison of catalytic efficacy, the activity parameter (k_m) was calculated according to Equation (2):

$$k_m = \frac{k_{app}}{m} \quad (2)$$

where m is the total mass of the catalyst (g).

2.5. Reusability

The reusability of the Ag@KS Sponge for degradation of MB and 4-NP was investigated for five cycles. For MB, the first cycle was performed by immersing 1.0 mg of Ag@KS sponge in a mixture of $NaBH_4$ (1 mL, 50 mM) and MB dye (4 mL, 30 µM), followed by stirring at room temperature for 60 min. From the second cycle onwards, the sponge was washed with water several times, freeze dried for the next cycle, and repeated the catalysis procedure for 60 min. A similar procedure was followed for 4-NP, where 1.0 mg of the Ag@KS sponge was immersed in a mixture of 4-NP (1 mM, 10 mL) and $NaBH_4$ (0.3 M, 5 mL) at room temperature for 60 min.

The reusability of the sponge was calculated by means of UV-visible spectroscopy (664 nm for MB and 400 nm for 4-NP). The degradation percentage was calculated using Equation (3):

$$\text{Degradation of pollutants } (\%) = \frac{C_0 - C_t}{C_0} \times 100 \quad (3)$$

where C_0 is the initial concentration of pollutant, and C_t is the pollutant concentration at time t.

2.6. Antibacterial Properties

The Gram-positive *Staphylococcus aureus* (CCM 3953) and Gram-negative *Escherichia coli* (CCM 3954) bacterial strains used in this analysis were procured from the Czech Collection of Microorganisms (Masaryk University, Brno, Czech Republic). Bacterial suspensions were freshly prepared in a nutrient broth (agar) by growing a single colony at 37 °C, overnight. The obtained bacterial culture was centrifuged into a pellet, which was further washed and resuspended in physiological solution (0.85% NaCl) and adjusted to an optical density of 0.1 at 600 nm. The bacteria were dispersed homogeneously on nutrient broth agar plates [23.5 g L^{-1}, Plate Count Agar (M091), Himedia, India]. Sponges (KS and Ag@KS) were cut into a thickness of 3 mm and diameter of 5 mm, and placed onto the agar plates covered with bacteria. All the plates were inoculated for 24 h at 37 °C. The antibacterial activity was expressed in terms of zone of inhibition, which was determined as the total diameter (mm) of each sample plus the halo zone where bacterial growth was inhibited. The samples were tested in triplicates, and the average values are presented.

2.7. Biodegradation

The biodegradation of the KS and Ag@KS sponges in aqueous solutions under aerobic circumstances was evaluated using the technique described elsewhere [22]. The experiments were run in a Micro-Oxymax respirometer (Columbus Instruments International, Columbus, OH, USA). Approximately 2 g of the tested material were added to 95 mL of the biological medium (reference on ISO 14851:1999) and 5 mL of inoculum (activated sludge) into a 250 mL respiration cell and kept in a dark room at 20 ± 1 °C for 28 days. The oxygen consumption for an aerobic biodegradability was measured. The percentage of degradation was calculated based on the weight difference [23] using Equation (4):

$$\text{Weight loss } (\%) = \frac{W_f - W_d}{W_d} \times 100 \quad (4)$$

where W_f is the initial weight (g), while W_d represents the residual weight of the sponge (g).

3. Results

3.1. Characterization of AgNPs

A green pathway for converting Ag^+ ions to AgNPs and the fabrication of Ag@KS sponge is schematically represented in Figure 1. The negatively charged surface functional groups in the conjugate, particularly the carboxylic and hydroxyls groups, were exposed to the Ag^+ precursor solution. These groups have high affinity and binding capability towards Ag^+ ions through electrostatic interaction, resulting in Ag^+ ions being reduced to AgNPs. The large number of active functional groups distributed along the backbone of the conjugate serve a dual role as a reducer and stabilizer for AgNPs.

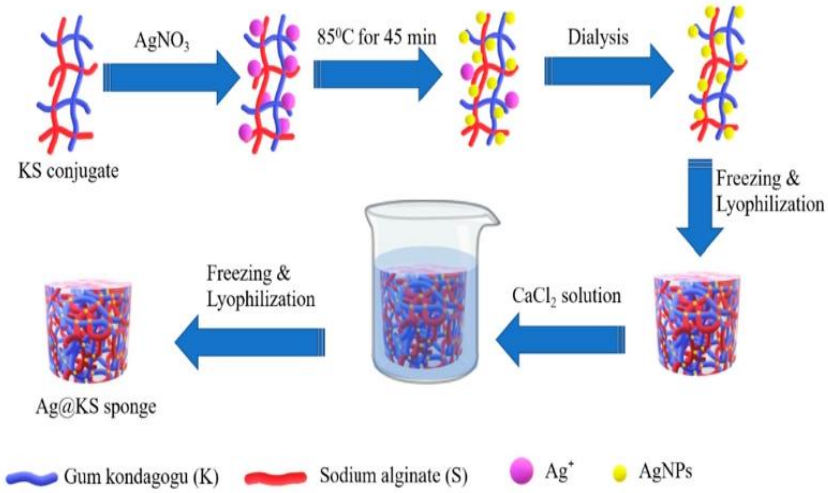

Figure 1. Schematic illustration of the Ag@KS sponge fabrication.

A visible color change from off-white to yellowish-brown (Figure 2a,b) and UV-visible absorption spectra were used to monitor the conversion of Ag^+ ions to AgNPs. The functional groups of the conjugate firmly bind and stabilize the nanoparticles, as observed from the highly colloidal and homogeneous solution after the formation of AgNPs. The color of the solution intensified with increasing $AgNO_3$ concentration, indicating the generation of more AgNPs and their deposition on the surface of the conjugate at higher Ag precursor concentrations; similar findings have been reported previously [24,25]. The UV-visible spectra of AgNPs synthesized using varying $AgNO_3$ concentrations are shown in Figure 2c, where increasing $AgNO_3$ concentrations resulted in enhanced absorption peak strength at 420 nm. At 10 mM $AgNO_3$ concentration, 90 ± 2% of Ag^+ content in the precursor solution was retained in the Ag@KS sponge, as per the ICP-MS analysis (Table S1). Similarly, 90% conversion of Ag^+ ions to AgNPs has been reported in the green

synthesis using plant leaf broth [26]. At concentrations higher than 10 mM, nanoparticle aggregation would compromise structural robustness and increase leaching. Therefore, 10 mM concentration was considered for further study as an optimal value for further experiments.

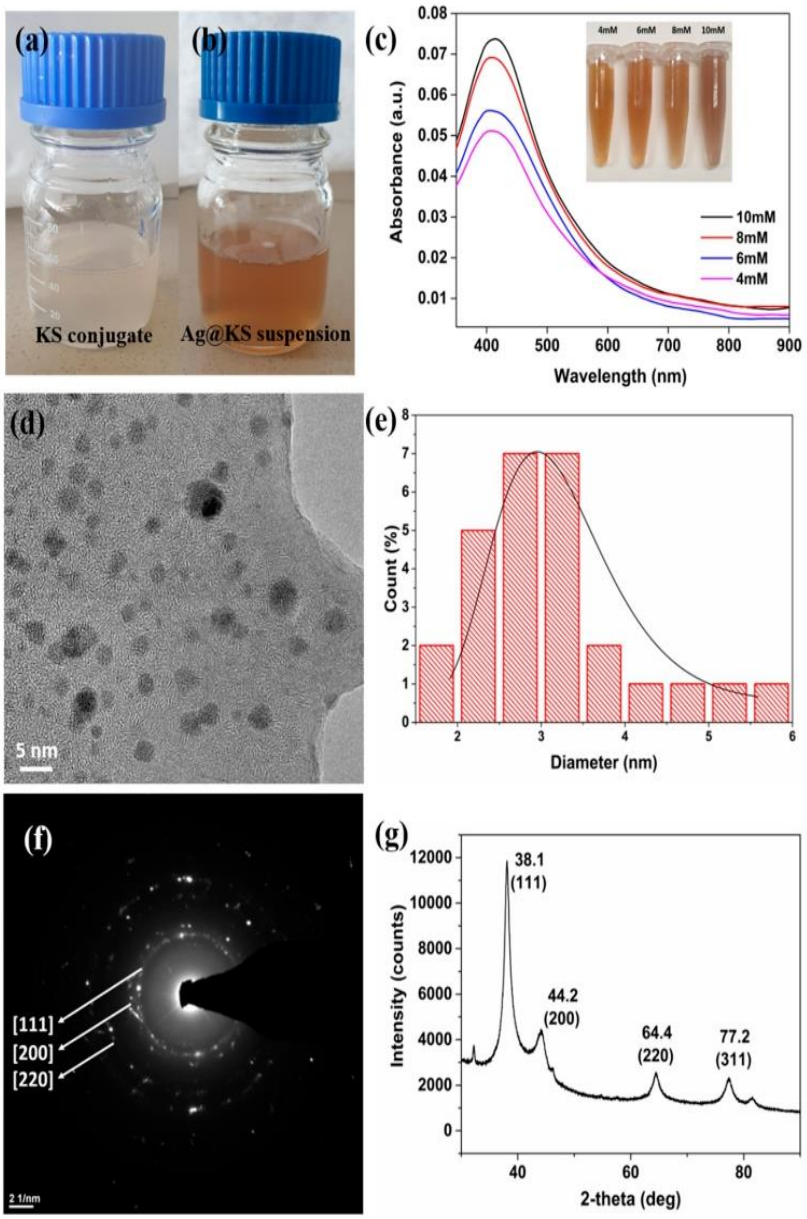

Figure 2. (**a**) Digital photograph of KS conjugate solution and (**b**) Ag@KS suspension, (**c**) UV–visible spectra of the AgNPs synthesized from various concentrations of $AgNO_3$, the insert is a photograph of Ag@KS suspension at various $AgNO_3$ concentrations, (**d**) TEM image of Ag@KS suspension at 10 mM $AgNO_3$, (**e**) histogram representing the particle size distribution for 10 mM $AgNO_3$ precursor, (**f**) SAED pattern, and (**g**) XRD spectrum of Ag@KS sponge.

The predominantly spherical AgNPs in the size range of 1.5–6 nm are well disseminated in the conjugate solution, as shown by TEM imaging (Figure 2d). The particle size histogram of AgNPs, calculated using ImageJ software, shows the average diameter as 2.9 ± 0.5 nm (Figure 2e), which is lower than the AgNPs formed by porous lignocellulose hydrogel [27]. The lower size enhances the surface area and thereby catalytic performance. The functional groups on the conjugate serve as capping agents, preventing AgNPs from

clumping together to ensure their uniform distribution on the sponge surface [28,29]. The SAED pattern (Figure 2f) implies a highly crystalline nature of nanoparticles, which was further confirmed by the XRD spectrum (Figure 2g). Four distinctive diffraction peaks were detected at 38.1°, 44.2°, 64.4°, and 77.2°, respectively, corresponding to (111), (200), (220), and (311) planes of face-centered cubic (fcc) crystal structure of metallic silver. The interplanar spacing ($d_{h\ k\ l}$) values (2.352, 2.048 and 1.447 Å) determined from the XRD spectrum correlate well with the standard values [28,30]. The above results clearly show that the silver nanoparticles thus synthesized using the green method are nanocrystalline [31,32].

3.2. Ag@KS Sponge Characterization

The Ag@KS sponge developed by green synthesis has a low density (22 ± 0.5 mg/cm^3) and 6.2 wt% silver content as AgNPs. The digital photographs of KS and Ag@KS sponges on a dandelion flower, exposing their low density, are represented in Figure S1a,b.

Figure 3a shows the thermogravimetric analysis and the derivative curves of the KS and Ag@KS sponges. The initial (at temperature below 150 °C) weight loss of about 10% is associated with the desorption of physisorbed water on the samples. Both KS and Ag@KS sponges begin to disintegrate at around 200 °C, beyond which the thermograms take on different features. Because of the higher thermal stability conferred by strong interaction between AgNPs and the conjugate, the curve of Ag@KS is shifted towards the higher temperature. At 274 °C, the KS sponge degrades at a maximum rate, and the overall weight loss reached 38% of the initial weight. Ag@KS, on the other hand, exhibits a lower degradation rate and registers the highest degradation temperature (282 °C), and the corresponding weight loss is 31%. The thermogram of Ag@KS also presents a higher remnant weight of 40.6% at 600 °C compared to 35% for KS sample. This weight difference of 5.6% shows the silver content in the sponge. As in previously reported studies, Ag@KS sponges show better temperature stability than KS sponges due to the shielding effect induced by AgNPs [33].

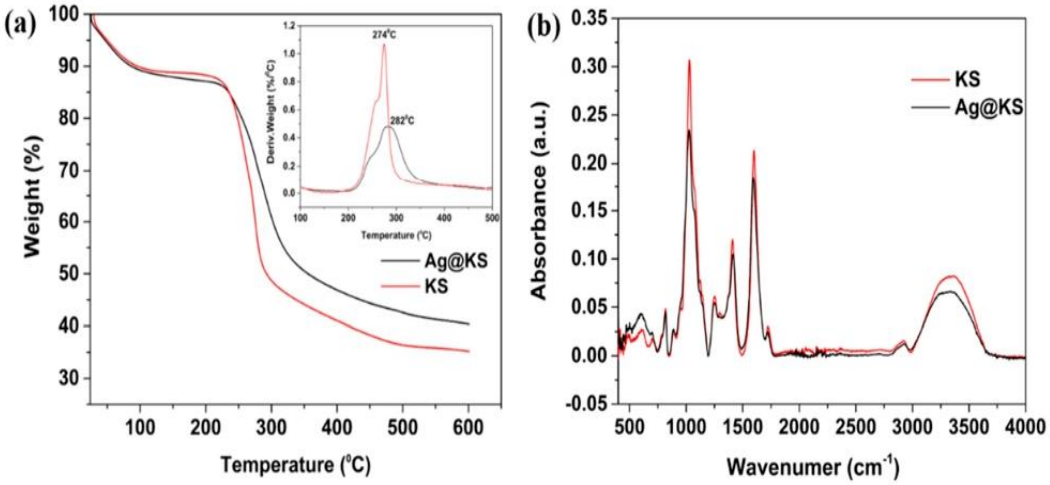

Figure 3. (**a**) Thermogravimetric profile of KS and Ag@KS sponge (derivative curve is inserted), (**b**) FTIR spectra of KS and Ag@KS sponge.

FTIR spectra of KS and Ag@KS sponge are depicted in Figure 3b. Both sponges show peaks at 3280 cm^{-1}, 1600 cm^{-1}, and 1410 cm^{-1} corresponding to OH stretching, C=O stretching, and OH bending, respectively [34]. The intensity of these peaks in Ag@KS sponge declines due to the interactions between the conjugate and in-situ generated AgNPs [33]. The change of intensities confirms that the conjugate offers multiple sites to reduce Ag^+ ions and simultaneously supports/stabilizes the ensued AgNPs.

The water-activated shape memory property of the tree gum conjugate sponge has not been well explored previously. The Ag@KS sponge exhibited excellent shape restoration

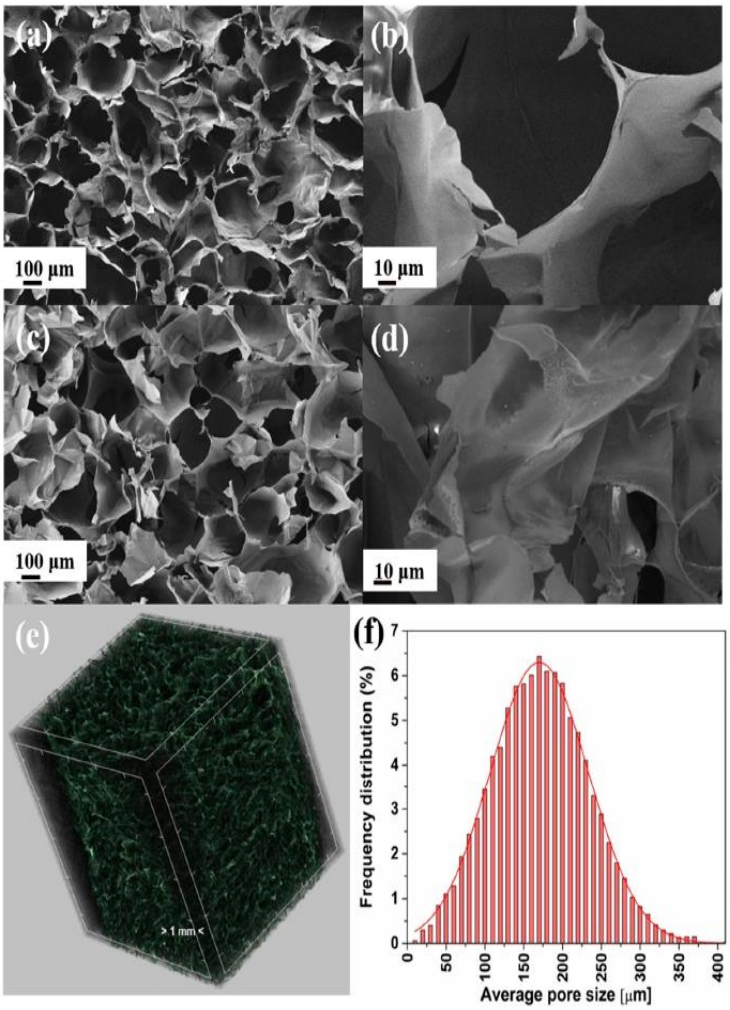

Figure 4. (**a**,**b**) SEM micrographs of KS sponge and (**c**,**d**) Ag@KS sponge at different magnifications, (**e**) 3D micro-CT image of Ag@KS sponge, (**f**) the pore size distribution of the Ag@KS sponge.

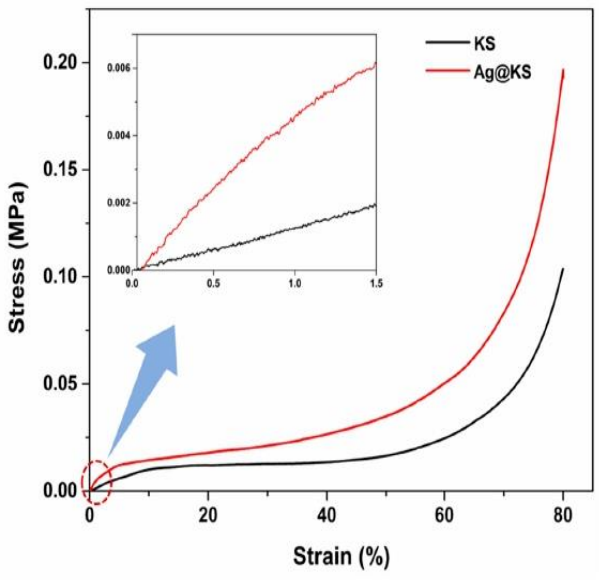

Figure 5. The compressive stress–strain curves of the KS and Ag@KS sponges (the initial linear region is inserted).

3.3. Catalytic Reduction of MB and 4-NP

The model contaminants, 4-NP and MB dye, were used to evaluate the catalytic potential of the Ag@KS sponge. These pollutants have a strong absorption peak in visible light, making them easier to detect by UV-visible spectroscopy. Hence, they are commonly deployed for evaluating the catalytic potential of different materials [38,39].

The linear dependency of the logarithm of absorbance on time confirmed the catalytic degradation of both toxic organic dyes following the pseudo-first-order kinetics (Equation (1)). As shown in Figure 6a, MB's apparent rate constants (k_{app}) are 0.041, 0.058, and 0.116 min^{-1} for 1.5, 1.9, and 3.1 mg of sponge, respectively. An increasing tendency could be observed in the k_{app} values as the catalyst amount increased (Figure 6c). For comparing catalytic performance, the activity parameter of k_m, which equals 37 min^{-1} g^{-1}, was used, which is the ratio of rate constant to the weight of catalyst (3.1 mg) [40,41]. The k_m parameter was compared with other catalysts reported in the literature (Table S2), which revealed that the Ag@KS sponge has more excellent MB conversion rates than most catalysts used.

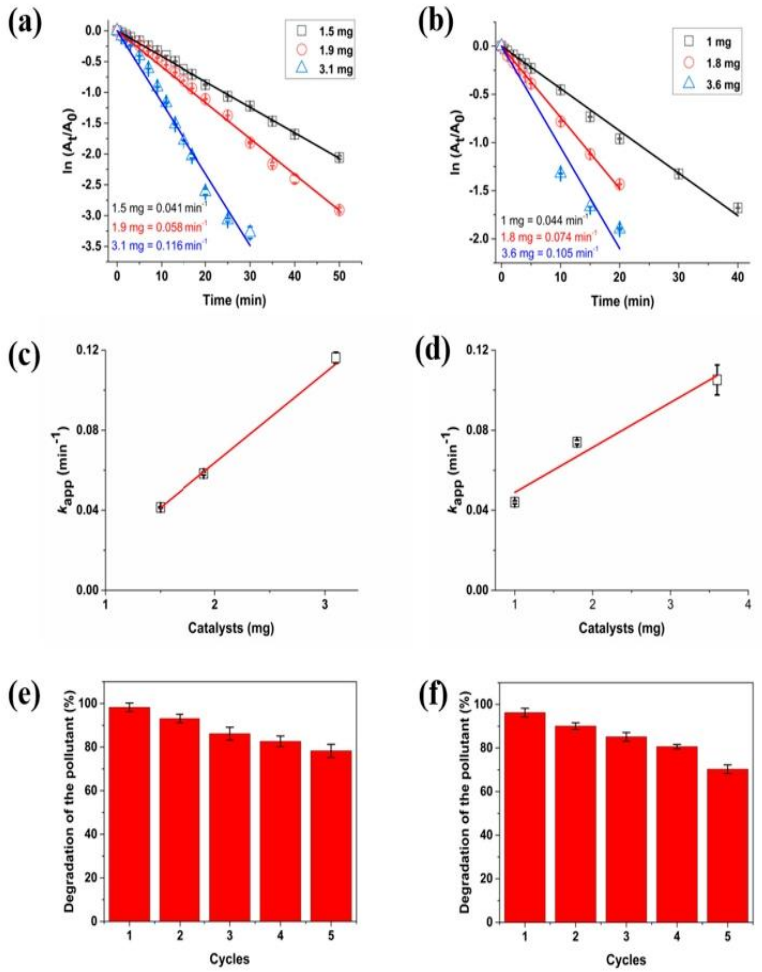

Figure 6. The pseudo-first-order kinetic curves of the catalytic reduction of (**a**) MB and (**b**) 4-NP, k_{app} values of (**c**) MB and (**d**) 4-NP under different Ag@KS concentrations; and degradation percentage of (**e**) MB and (**f**) 4-NP over five reduction cycles.

When KS sponge was utilised, no catalytic reduction of MB to leucomethylene blue (LMB) was detected (data not shown), indicating the potential of AgNPs as a catalyst. The reusability of catalyst is of important concern in the environmental and economic perspectives and, therefore, the reusability of Ag@KS sponge for MB degradation was

investigated. The results showed retention of catalytic activity over five cycles, though a slight reduction (78% degradation from 98%) was observed (Figure 6e). As previously reported by Kamal et al., the decrease in pollutant degradation during repeated cycles could be attributed to the catalyst poisoning by S atoms [42].

Figure 6b shows the catalytic reduction of 4-NP, which follows pseudo-first-order kinetics with apparent rate constants of 0.044, 0.074, and 0.105 min^{-1} for 1.0, 1.8, and 3.6 mg of sponge, respectively. Here, the k_{app} values continued to rise as the catalyst amount increased (Figure 6d), and the k_m values of 44 min^{-1} g^{-1} are calculated from 1.0 mg weight of catalyst. In this case too, a comparison of the activity parameter (k_m) with that of other documented sponges in the literature (Table S3) indicates that Ag@KS performed better for catalytic degradation of 4-NP to 4-Aminophenol (4-AP) amongst many reported examples. The reusability of Ag@KS sponge for 4-NP catalytic reduction was also determined (Figure 6f), wherein, after five cycles, 75% of pollutants are degraded, demonstrating steady catalytic performance and remarkable durability of the Ag@KS sponge, endowed by strong capping capacity of the functional groups of the conjugate.

3.4. Catalysis Mechanism of Ag@KS Sponge

Figure 7 depicts the proposed pathway for contaminants removal using the Ag@KS sponge. The sponge has many micropores and open channels, while AgNPs are immobilized on the sponge surface walls. The presence of AgNPs induces BH_4^- (of $NaBH_4$) oxidation with a release of electrons, resulting in a negatively charged layer on the sponge's surface [41]. When the contaminant molecules (MB or 4-NP) contact the charged sponge surface, AgNPs facilitate the electron relay from BH_4^- to MB/4-NP, leading to the disruption of pollutant's chromophore structure. The 4-NP is reduced to 4-Aminophenol and MB to leucomethylene blue.

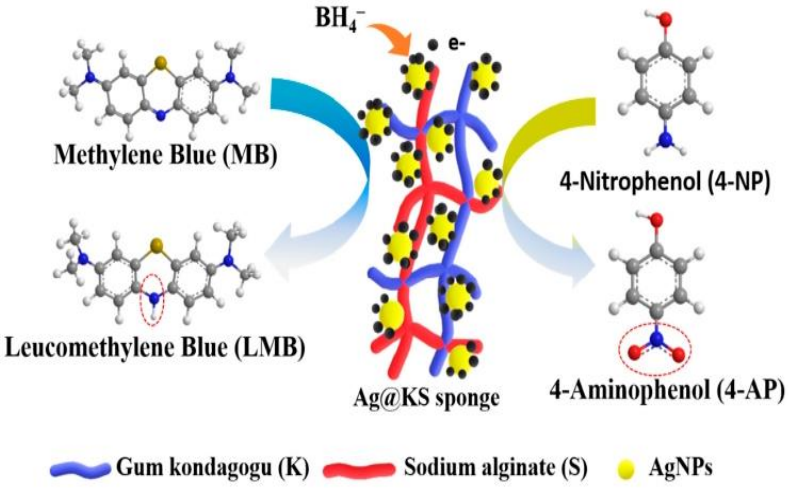

Figure 7. Proposed catalytic reduction mechanism of MB and 4-NP in the Ag@KS sponge network, using $NaBH_4$.

3.5. Antibacterial Properties

The antibacterial activity of KS and Ag@KS sponges were evaluated against *Escherichia coli* and *Staphylococcus aureus* by measuring the zone of inhibition of bacterial growth around discs placed on agar medium (Figure 8). Figure 8a,c show no inhibition zone around the KS sponge in both bacterial media. In contrast, the Ag@KS sponge showed a prominent zone of inhibition of diameter 11.2 mm ± 0.2 mm and 11.0 mm ± 0.2 mm, respectively, for *Escherichia coli* and *Staphylococcus aureus*, indicating excellent antibacterial activity (Figure 8b,d). AgNPs with a size of less than 10 nm have the ability to penetrate bacterial cell walls and subsequently change the structure and cause cell damage [43]. Overall, our findings indicate that AgNPs decorated on this sustainable sponge have a

distinct inhibitory effect on the microbial growth of *Staphylococcus aureus* (Gram-positive) and *Escherichia coli* (Gram-negative), thus widening their applications in the environmental field [44].

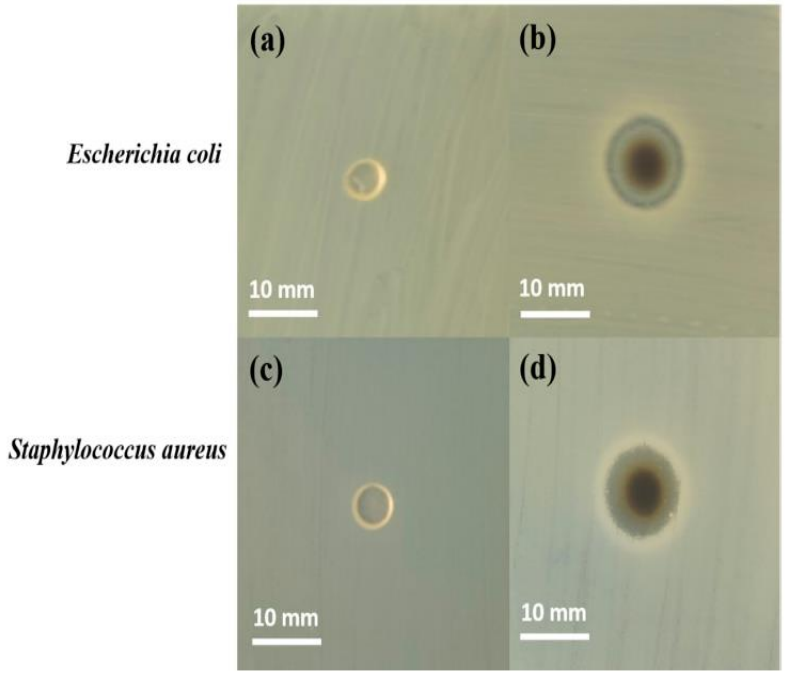

Figure 8. Formation of inhibition zone around KS (**a**,**c**) and Ag@KS (**b**,**d**) sponge discs against *E. coli* and *S. aureus* after 24 h incubation.

3.6. Biodegradation of the Sponge

The biodegradability of the sponges was tested under aerobic conditions with an inoculum taken from WWTP. Figure 9 shows the biochemical oxygen demand (BOD) for KS and Ag@KS sponges. Aerobic microbial species disintegrate the sponges into smaller molecules during the degradation process through metabolic or enzymatic activities. In the case of the KS sponge, after the initial phase without BOD, the degradation profile goes linearly upwards. For Ag@KS, the reluctant phase is significantly longer (to around 150 h), and the slope of the degradation phase is also smaller. Hence, the KS degradation rate is higher than that of Ag@KS. After 28 days (672 h), the final BOD value for the KS sponge is 1566 ± 16 mg O_2 L^{-1}, while that for the Ag@KS sponge is 535 ± 35 mg O_2 L^{-1}. By comparing the weight loss, 90% of KS and 65% of Ag@KS were degraded in 28 days. The rapid deterioration of the KS sponge implies that the microorganisms present in the sludge could act on it faster, but the presence of AgNPs on the Ag@KS sponge slows down the activity of microorganisms in the material and thereby reduces the rate of degradation.

The bio-based nanocomposite sponges have gained popularity as a greener choice for reducing waste generation and lowering production costs. The results presented here suggest that the green synthesized sponges can be biologically degraded by the microbes, thus minimizing the secondary contamination of the environment.

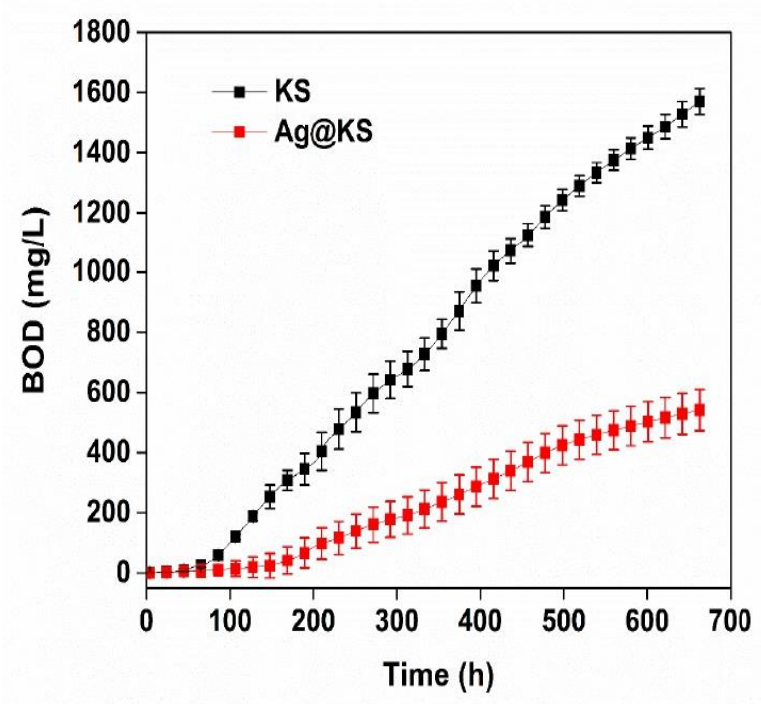

Figure 9. Biochemical oxygen demand of KS and Ag@KS sponges for a period of 28 days of enzymatic degradation.

4. Discussion

In this study, we have developed a conjugate of gum kondagogu and sodium alginate that overwhelms the components individually in terms of hydrophilicity and mechanical strength. In addition to being an affordable and renewable biopolymer source, tree gum conjugate simultaneously aids the generation and stabilization of AgNPs with greater than 90% retention of NPs. The AgNPs immobilized conjugate sponge with low density and high porosity are then crosslinked with Ca^{2+} ions. The structural stability, surface morphology, and compressive strength can be tailored both by the decoration of AgNPs on the sponge and ionic crosslinking. As the NPs are evenly distributed along the surface of the Ag@KS sponge, the oxidation, aggregation, and leach out of AgNPs are effectively minimized, leading to enhanced efficiency towards the catalytic reduction of MB and 4-NP from aqueous media. When compared to previously published catalyst systems, the nanocomposite sponge used in this study demonstrated impressive catalytic activity. The shape recovery property of the sponges in water is of much significance since it enables the repeated usage of the material without compromising structural integrity. The reusability study of the sponge showed retention of catalytic activity of 78% and 75% for MB and 4-NP, respectively, even after five cycles. Additionally, it effectively reacted with both Gram-positive and Gram-negative bacteria during the antibacterial study. Finally, the biodegradability of the sponge (65% within 28 days) affirms its eco-friendliness and at the same time offers numerous opportunities for environmental remediation applications.

5. Conclusions and Future Perspectives

In conclusion, AgNPs immobilized on tree gum based sustainable sponges represent a new class of catalyst carrier systems. The preparation of Ag@KS sponges is facile with the deployment of renewable and earth-abundant materials and can therefore be converted to many other green synthesized nanoparticle-based catalyst systems with excellent catalytic efficiency. The combination of high macroporosity (92%) and low density (22 ± 0.5 mg/cm^3) allows the effective mass transfer of the contaminants to the catalytic sites (AgNPs). The observed negligible leaching of Ag nanoparticles (<0.2 wt %) from Ag@KS sponge supports its use for long-term water remediation operations. The novelty of this model sponge

catalyst is the exploitation of greener synthesis and biodegradability aspects in the design of newer sustainable materials. Furthermore, they display excellent antibacterial properties against *Escherichia coli* and *Staphylococcus aureus*. The catalysis was achieved with an activity parameter of 37 min^{-1} g^{-1} and 44 min^{-1} g^{-1} for MB and 4-NP, respectively. The prepared Ag@KS sponge shows excellent reusability even after five cycles of usage. These findings will pave the way to exploit the enormous potential of tree gum-based sponge systems in a vast variety of applications in environmental, industrial, and medicinal fields.

Supplementary Materials: The following supporting information can be downloaded at: https://www.mdpi.com/article/10.3390/polym14153120/s1, Figure S1: (a) and (b) Digital photograph of KS and Ag@KS sponge on a dandelion flower, respectively; Figure S2: Photographs taken when the hydrated Ag@KS sponge was fully recovered by compressive squeezing; Figure S3: The leaching percentage of AgNPs from Ag@KS sponge, calculated using ICP-MS analysis for seven days of immersion in water Figure S4: (a) SEM image and (b) Energy-dispersive X-ray spectra of Ag@KS sponge. Elemental distribution of (c) C, (d) O, (e) Ca, (f) Na, (g) Ag, and (h) Cl, respectively; Table S1: ICP-MS analysis result of silver nanoparticles immobilized sponge using various precursor concentrations; Table S2: Comparison of the catalytic activity of different catalysts for MB catalytic degradation; Table S3: Comparison of the catalytic activity of different catalysts for 4-NP catalytic degradation.

Author Contributions: Formal analysis, Data Curation, Writing—Original Draft, Investigation, R.K.R.; Formal analysis, Data Curation, D.S., N.S.S., N.H.A.N. and K.H.; Formal analysis, Data Curation, S.W.; Investigation, Formal analysis, Experimental, D.Ł., Formal analysis, Data Curation, Writing—Review and Editing, M.Č. and D.T.; Conceptualization, Formal analysis, supervision, Writing—Review, V.V.T.P.; Formal analysis, Resources, Writing—Review, R.S.V. All authors have read and agreed to the published version of the manuscript.

Funding: The work funded by Inter Excellence Action Program within the framework of the project "Bio-based Porous 2D Membranes and 3D Sponges Based on Functionalized Tree Gum Polysaccharides and their Environmental Application" (registration number LTAUSA19091)—TUL internal No.: 18309/136, supported by the Ministry of Education, Youth and Sports of the Czech Republic. This work was also supported by the Student Grant Scheme at the Technical University of Liberec through project number SGS-2022-3027.

Institutional Review Board Statement: Not applicable.

Informed Consent Statement: Not applicable.

Data Availability Statement: Not applicable.

Acknowledgments: The authors would like to acknowledge the assistance provided by the Research Infrastructure NanoEnviCz (Project No. LM2018124) and the "Inter Excellence Action Programme" within the framework of the project "Bio-based Porous 2D Membranes and 3D Sponges Based on Functionalized Tree Gum Polysaccharides and their Environmental Application" (registration number LTAUSA19091)—TUL internal No.: 18309/136, supported by the Ministry of Education, Youth, and Sports of the Czech Republic. This work was also supported by the project- Hybrid Materials for Hierarchical Structures (HyHi, Reg. No. CZ.02.1.01/0.0/0.0/16_019/0000843) financed by the Ministry of Education, Youth, and Sports of the Czech Republic, and the European Union-European Structural and Investment Funds in the framework of the Operational Program Research, Development and Education.

Conflicts of Interest: The authors declare no conflict of interest.

References

1. Wacławek, S.; Lutze, H.V.; Grübel, K.; Padil, V.V.T.; Černík, M.; Dionysiou, D.D. Chemistry of persulfates in water and wastewater treatment: A review. *Chem. Eng. J.* **2017**, *330*, 44–62. [CrossRef]
2. Yaqoob, A.A.; Parveen, T.; Umar, K.; Nasir, M.; Nasir, I. Role of Nanomaterials in the Treatment of waste water. *Water* **2020**, *12*, 495. [CrossRef]
3. Adeola, A.O.; Nomngongo, P.N. Advanced Polymeric Nanocomposites for Water Treatment Applications: A Holistic Perspective. *Polymers* **2022**, *14*, 2462. [CrossRef]

4. Choi, W.S.; Lee, H.-J. Nanostructured Materials for Water Purification: Adsorption of Heavy Metal Ions and Organic Dyes. *Polymers* **2022**, *14*, 2183. [CrossRef]
5. Kudaibergenov, S.E.; Dzhardimalieva, G.I. Flow-through catalytic reactors based on metal nanoparticles immobilized within porous polymeric gels and surfaces/hollows of polymeric membranes. *Polymers* **2020**, *12*, 572. [CrossRef] [PubMed]
6. Nghiem, T.L.; Coban, D.; Tjaberings, S.; Gröschel, A.H. Recent advances in the synthesis and application of polymer compartments for catalysis. *Polymers* **2020**, *12*, 2190. [CrossRef] [PubMed]
7. Yaqoob, A.A.; Ahmad, H.; Parveen, T.; Ahmad, A.; Oves, M.; Ismail, I.M.I.; Qari, H.A.; Umar, K.; Mohamad Ibrahim, M.N. Recent Advances in Metal Decorated Nanomaterials and Their Various Biological Applications: A Review. *Front. Chem.* **2020**, *8*, 1–23. [CrossRef]
8. Ali, A.; Khalid, Y.; Mohamad, U.; Mohamad, N. Silver nanoparticles: Various methods of synthesis, size affecting factors and their potential applications—A review. *Appl. Nanosci.* **2020**, *10*, 1369–1378.
9. Cao, H.; Liu, C.; Cai, F.; Qiao, X. In situ immobilization of ultra- fine AgNPs onto magnetic Ag@RF@Fe3O4 core-satellite nanocomposites for the rapid catalytic reduction of nitrophenols. *Water Res.* **2020**, *179*, 115882. [CrossRef]
10. Umar, K.; Yaqoob, A.A.; Ibrahim, M.N.M.; Parveen, T.; Safian, M.T.U. Environmental applications of smart polymer composites. In *Smart Polymer Nanocomposites Biomedical and Environmental Applications*; Woodhead Publishing: Cambridge, UK, 2021; pp. 295–312.
11. Sumitha, N.S.; Prakash, P.; Nair, B.N.; Sailaja, G.S. Degradation-Dependent Controlled Delivery of Doxorubicin by Glyoxal Cross-Linked Magnetic and Porous Chitosan Microspheres. *ACS Omega* **2021**, *6*, 21472–21484. [CrossRef] [PubMed]
12. Sumitha, N.S.; Sreeja, S.; Varghese, P.J.G.; Sailaja, G.S. A dual functional superparamagnetic system with pH-dependent drug release and hyperthermia potential for chemotherapeutic applications. *Mater. Chem. Phys.* **2021**, *273*, 125108. [CrossRef]
13. Kumar, A.; Ahuja, M. Carboxymethyl gum kondagogu: Synthesis, characterization and evaluation as mucoadhesive polymer. *Carbohydr. Polym.* **2012**, *90*, 637–643. [CrossRef] [PubMed]
14. Vinod, V.T.P.; Sashidhar, R.B.; Sarma, V.U.M.; Vijaya Saradhi, U.V.R. Compositional analysis and rheological properties of gum kondagogu (*Cochlospermum gossypium*): A tree gum from India. *J. Agric. Food Chem.* **2008**, *56*, 2199–2207. [CrossRef] [PubMed]
15. Janaki, B.; Sashidhar, R.B. Physico-chemical analysis of gum kondagogu (*Cochlospermum gossypium*): A potential food additive. *Food Chem.* **1998**, *61*, 2–7. [CrossRef]
16. Akshay Kumar, K.P.; Ramakrishnan, R.K.; Cerník, M.; Padil, V.V.T. Tree gum-based nanostructures and their biomedical applications. In *Micro and Nano Technologies*; Elesvier: Amsterdam, The Netherlands, 2022; pp. 383–407.
17. Ramakrishnan, R.K.; Cernik, M.; Padil, V.V.T.; Wacławek, S. Biomacromolecule assembly based on gum kondagogu-sodium alginate composites and their expediency in flexible packaging films. *Int. J. Biol. Macromol.* **2021**, *177*, 526–534. [CrossRef]
18. Ngece, K.; Aderibigbe, B.A.; Ndinteh, D.T.; Fonkui, Y.T.; Kumar, P. Alginate-gum acacia based sponges as potential wound dressings for exuding and bleeding wounds. *Int. J. Biol. Macromol.* **2021**, *172*, 350–359. [CrossRef] [PubMed]
19. Ramakrishnan, R.K.; Padil, V.V.T.; Škodová, M.; Wacławek, S.; Černík, M.; Agarwal, S. Hierarchically Porous Bio-Based Sustainable Conjugate Sponge for Highly Selective Oil/Organic Solvent Absorption. *Adv. Funct. Mater.* **2021**, *31*, 2100640. [CrossRef]
20. Liu, N.; Zhang, W.; Li, X.; Qu, R.; Zhang, Q.; Wei, Y.; Feng, L.; Jiang, L. Fabrication of robust mesh with anchored Ag nanoparticles for oil removal and: In situ catalytic reduction of aromatic dyes. *J. Mater. Chem. A* **2017**, *5*, 15822–15827. [CrossRef]
21. Silvestri, D.; Wacławek, S.; Sobel, B.; Torres-Mendieta, R.; Novotný, V.; Nguyen, N.H.A.; Ševců, A.; Padil, V.V.T.; Müllerová, J.; Stuchlík, M.; et al. A poly(3-hydroxybutyrate)-chitosan polymer conjugate for the synthesis of safer gold nanoparticles and their applications. *Green Chem.* **2018**, *20*, 4975–4982. [CrossRef]
22. Padil, V.V.T.T.; Senan, C.; Waclawek, S.; Černík, M.; Agarwal, S.; Varma, R.S. Bioplastic Fibers from Gum Arabic for Greener Food Wrapping Applications. *ACS Sustain. Chem. Eng.* **2019**, *7*, 5900–5911. [CrossRef]
23. Stepczyńska, M.; Rytlewski, P. Enzymatic degradation of flax-fibers reinforced polylactide. *Int. Biodeterior. Biodegrad.* **2018**, *126*, 160–166. [CrossRef]
24. Yu, Z.; Hu, C.; Guan, L.; Zhang, W.; Gu, J. Green Synthesis of Cellulose Nanofibrils Decorated with Ag Nanoparticles and Their Application in Colorimetric Detection of l-Cysteine. *ACS Sustain. Chem. Eng.* **2020**, *8*, 12713–12721. [CrossRef]
25. Yang, Y.; Chen, Z.; Wu, X.; Zhang, X.; Yuan, G. Nanoporous cellulose membrane doped with silver for continuous catalytic decolorization of organic dyes. *Cellulose* **2018**, *25*, 2547–2558. [CrossRef]
26. Song, J.Y.; Kim, B.S. Rapid biological synthesis of silver nanoparticles using plant leaf extracts. *Bioprocess Biosyst. Eng.* **2009**, *32*, 79–84. [CrossRef] [PubMed]
27. Zhang, L.; Lu, H.; Chu, J.; Ma, J.; Fan, Y.; Wang, Z.; Ni, Y. Lignin-Directed Control of Silver Nanoparticles with Tunable Size in Porous Lignocellulose Hydrogels and Their Application in Catalytic Reduction. *ACS Sustain. Chem. Eng.* **2020**, *8*, 12655–12663. [CrossRef]
28. Kora, A.J.; Sashidhar, R.B.; Arunachalam, J. Gum kondagogu (*Cochlospermum gossypium*): A template for the green synthesis and stabilization of silver nanoparticles with antibacterial application. *Carbohydr. Polym.* **2010**, *82*, 670–679. [CrossRef]
29. Zhao, X.H.; Li, Q.; Ma, X.M.; Xiong, Z.; Quan, F.Y.; Xia, Y.Z. Alginate fibers embedded with silver nanoparticles as efficient catalysts for reduction of 4-nitrophenol. *RSC Adv.* **2015**, *5*, 49534–49540. [CrossRef]
30. Garibo, D.; Borbón-Nuñez, H.A.; de León, J.N.D.; García Mendoza, E.; Estrada, I.; Toledano-Magaña, Y.; Tiznado, H.; Ovalle-Marroquin, M.; Soto-Ramos, A.G.; Blanco, A.; et al. Green synthesis of silver nanoparticles using Lysiloma acapulcensis exhibit high-antimicrobial activity. *Sci. Rep.* **2020**, *10*, 12805. [CrossRef]

31. Jeeva, K.; Thiyagarajan, M.; Elangovan, V.; Geetha, N.; Venkatachalam, P. Caesalpinia coriaria leaf extracts mediated biosynthesis of metallic silver nanoparticles and their antibacterial activity against clinically isolated pathogens. *Ind. Crops Prod.* **2014**, *52*, 714–720. [CrossRef]
32. Kumar, V.; Yadav, S.K. Plant-mediated synthesis of silver and gold nanoparticles and their applications. *J. Chem. Technol. Biotechnol.* **2009**, *84*, 151–157. [CrossRef]
33. Zhou, S.; Wang, M.; Chen, X.; Xu, F. Facile Template Synthesis of Microfibrillated Cellulose/Polypyrrole/Silver Nanoparticles Hybrid Aerogels with Electrical Conductive and Pressure Responsive Properties. *ACS Sustain. Chem. Eng.* **2015**, *3*, 3346–3354. [CrossRef]
34. Guo, M.; Zhang, Y.; Du, F.; Wu, Y.; Zhang, Q.; Jiang, C. Silver nanoparticles/polydopamine coated polyvinyl alcohol sponge as an effective and recyclable catalyst for reduction of 4-nitrophenol. *Mater. Chem. Phys.* **2019**, *225*, 42–49. [CrossRef]
35. Moghim, M.H.; Keshavarz, M.; Zebarjad, S.M. Effect of SiO_2 nanoparticles on compression behavior of flexible polyurethane foam. *Polym. Bull.* **2019**, *76*, 227–239. [CrossRef]
36. Venkatesan, J.; Lee, J.Y.; Kang, D.S.; Anil, S.; Kim, S.K.; Shim, M.S.; Kim, D.G. Antimicrobial and anticancer activities of porous chitosan-alginate biosynthesized silver nanoparticles. *Int. J. Biol. Macromol.* **2017**, *98*, 515–525. [CrossRef]
37. Lv, P.; Tang, X.; Zheng, R.; Ma, X.; Yu, K.; Wei, W. Graphene/Polyaniline Aerogel with Superelasticity and High Capacitance as Highly Compression-Tolerant Supercapacitor Electrode. *Nanoscale Res. Lett.* **2017**, *12*, 630. [CrossRef]
38. Silvestri, D.; Wacławek, S.; Venkateshaiah, A.; Krawczyk, K.; Sobel, B.; Padil, V.V.T.; Černík, M.; Varma, R.S. Synthesis of Ag nanoparticles by a chitosan-poly(3-hydroxybutyrate) polymer conjugate and their superb catalytic activity. *Carbohydr. Polym.* **2020**, *232*, 115806. [CrossRef]
39. Subhan, F.; Aslam, S.; Yan, Z.; Yaseen, M. Unusual Pd nanoparticle dispersion in microenvironment for p-nitrophenol and methylene blue catalytic reduction. *J. Colloid Interface Sci.* **2020**, *578*, 37–46. [CrossRef]
40. Baruah, B.; Gabriel, G.J.; Akbashev, M.J.; Booher, M.E. Facile synthesis of silver nanoparticles stabilized by cationic polynorbornenes and their catalytic activity in 4-nitrophenol reduction. *Langmuir* **2013**, *29*, 4225–4234. [CrossRef]
41. An, Q.; Yu, M.; Zhang, Y.; Ma, W.; Guo, J.; Wang, C. Fe_3O_4@carbon microsphere supported Ag-Au bimetallic nanocrystals with the enhanced catalytic activity and selectivity for the reduction of nitroaromatic compounds. *J. Phys. Chem. C* **2012**, *116*, 22432–22440. [CrossRef]
42. Kamal, T.; Asiri, A.M.; Ali, N. Catalytic reduction of 4-nitrophenol and methylene blue pollutants in water by copper and nickel nanoparticles decorated polymer sponges. *Spectrochim. Acta Part A Mol. Biomol. Spectrosc.* **2021**, *261*, 120019. [CrossRef] [PubMed]
43. Virk, K.; Sharma, K.; Kapil, S.; Kumar, V.; Sharma, V.; Pandey, S.; Kumar, V. Synthesis of gum acacia-silver nanoparticles based hydrogel composites and their comparative anti-bacterial activity. *J. Polym. Res.* **2022**, *29*, 118. [CrossRef]
44. Praveen; Suzuki, S.; Carson, C.F.; Saunders, M.; Clode, P.L.; Myers, M.; Chirila, T.V.; Baker, M.V. Poly(2-Hydroxyethyl Methacrylate) Sponges Doped with Ag Nanoparticles as Antibacterial Agents. *ACS Appl. Nano Mater.* **2020**, *3*, 1630–1639. [CrossRef]

5. Conclusions

In the present study, GK-SA conjugate sponges were synthesized and their environmental remediation performance was subsequently enriched by various functional modifications. Initially, the best suited composition of GK and SA was optimized by fabricating their films at different w/w ratios. The conjugate sponge was then prepared by the FD method, which was then functionalized using silylation, ionic crosslinking, and silver nanoparticle decoration. The silylated conjugate sponge exhibited highly efficient oil/organic solvent absorption, while the ionically crosslinked sponges were utilized for methylene blue dye absorption from an aqueous environment. The hydroxyl and carboxyl functionalities on the conjugate sponge surface simultaneously aid the synthesis and stabilization of silver nanoparticles. The silver nanoparticle embedded nanoconjugate sponge was then employed for the catalytic degradation of two model pollutants, i.e., methylene blue and 4-nitrophenol. Altogether, the properties of the conjugate sponges may be modulated by adopting different functionalization techniques so as to develop materials with a high potential for environmental remediation applications.

6. Future Prospects

The future prospects associated with the developed systems extend to a wide variety of applications, including energy storage devices, food packaging, EMI shielding, sensors, tissue engineering, wound healing, and drug delivery, etc.

The unique features of exudate gums make them an attractive material for producing biodegradable and sustainable 3D materials. The potential ability of tree gums to build 3D structures with extraordinary qualities is one of the most significant findings of the current research. However, the study provided in this thesis was undertaken on a laboratory scale, and a scaling up of the procedure is still necessary.

Developing conducting sponges from tree gum polysaccharides is an additional application with considerable potential. The electrical conductivity of tree gum sponges can be obtained by combining them with conducting materials, such as carbon nanotubes, graphene, and MXenes. More sustainable and biodegradable EMI shielding materials may be fabricated.

Furthermore, 3D printing using tree gums can be explored for biomedical applications. Their non-toxicity and biocompatibility enhance scaffold preparation. Nanoparticle embedded tree gum sponges have an enormous potential for sensor applications.

7. Publications

Thesis related publications:

1. **R.K. Ramakrishnan**, M. Cernik, V.V.T. Padil, S. Wacławek, "*Biomacromolecule assembly based on gum kondagogu-sodium alginate composites and their expediency in flexible packaging films", Int. J. Biol. Macromol.* 177 (2021) 526–534.

2. **R.K. Ramakrishnan**, V.V.T. Padil, M. Škodová, S. Wacławek, M. Černík, S. Agarwal, "*Hierarchically Porous Bio-Based Sustainable Conjugate Sponge for Highly Selective Oil/Organic Solvent Absorption", Adv. Funct. Mater*. 31 (2021) 2100640.

3. **R.K. Ramakrishnan,** V.V.T. Padil, S. Wacławek, M. Černík, D. Tiwari, "*Sustainable, biodegradable, and recyclable bio-sponge for rapid and practical bioremediation of dye from water", J. Environ. Chem. Eng.* (2022) 108285.

4. **R.K. Ramakrishnan**, D. Silvestri, N.S. Sumitha, N.H.A. Nguyen, K. Havlíček, D. Łukowiec, S. Wacławek, M. Černík, D. Tiwari, V.V.T. Padil, R.S. Varma, "*Gum Hydrocolloids Reinforced Silver Nanoparticle Sponge for Catalytic Degradation of Water Pollutants", Polymers (Basel).* 14 (2022).

Additional publications:

5. **R.K. Ramakrishnan**, V.V.T. Padil, M. Černík, S. Wacławek, R.S. Varma, "*Eco-Friendly and Economic, Adsorptive Removal of Cationic and Anionic Dyes by Bio-Based Karaya Gum—Chitosan Sponge", Polymers (Basel).* 13 (2021) 1–21.

6. A. Venkateshaiah, D. Silvestri, S. Wacławek, **R.K. Ramakrishnan**, K. Krawczyk, P. Saravanan, M. Pawlyta, V. V. Vinod, M. Černík, D.D. Dionysiou, "*A comparative study of the degradation efficiency of chlorinated organic compounds by bimetallic zero-valent iron nanoparticles", Environ. Sci. Water Res. Technol.* 8 (2022) 162–172.

7. D. Silvestri, S. Wacławek, **R.K. Ramakrishnan**, A. Venkateshaiah, K. Krawczyk, V.V.T. Padil, B. Sobel, M. Cernik, "*The Use of a Biopolymer Conjugate for an Eco-Friendly One-Pot Synthesis of Palladium-Platinum Alloys", Polymers (Basel).* 11 (2019) 1–14.

8. A. Venkateshaiah, D. Silvestri, **R.K. Ramakrishnan**, S. Wacławek, V.V.T. Padil, M. Cernik, R.S. Varma, "*Gum Kondagoagu / Reduced Graphene Oxide Framed Platinum Nanoparticles and Their Catalytic Role", Molecules*. 24 (2019) 1–11.

Book chapter:

1. K.P. Akshay Kumar, **R.K. Ramakrishnan**, M. Cerník, V.V.T. Padil, "*Tree gum-based nanostructures and their biomedical applications", Micro- Nanoeng. Gum-Based Biomater. Drug Deliv. Biomed. Appl*. (2022) 383–407

Active participation on international Conferences

1. **R.K. Ramakrishnan**, Vinod V. Padil, Miroslav Černík. "Ultra-flexible film based on tree gum biowaste for high-performance electromagnetic interference shielding". NANOCON 2022, 17-19 October 2022, Brno, Czech Republic.

2. **R.K. Ramakrishnan**, Abhilash Venkateshaiah, Klaudiusz Grübel, Edyta Kudlek, Daniele Silvestri, Vinod V. Padil, Miroslav Černík, Stanisław Wacławek. "Impact of UV-activated PDS and MPS oxidation on an organic dye removal in water and ecotoxicological assessment". American chemical society (ACS) FALL2022, Sustainability in a changing world, 21-25 August 2022, Chicago, Illinois, USA.

3. **R.K. Ramakrishnan**, Vinod V. Padil, Miroslav Černík. "Fabrication of ''Green" Sponges Based on Natural Polysaccharides for Dyes Removal from Water". NANOCON 2018, 17-19 October 2018, Brno, Czech Republic.

8. References

[1] H. Han, W. Wei, Z. Jiang, J. Lu, J. Zhu, and J. Xie, "Removal of cationic dyes from aqueous solution by adsorption onto hydrophobic/hydrophilic silica aerogel," *Colloids Surfaces A Physicochem. Eng. Asp.*, vol. 509, pp. 539–549, 2016, doi: 10.1016/j.colsurfa.2016.09.056.

[2] M. B. Wu *et al.*, "Compressible Carbon Sponges from Delignified Wood for Fast Cleanup and Enhanced Recovery of Crude Oil Spills by Joule Heat and Photothermal Effect," *Adv. Funct. Mater.*, vol. 2006806, pp. 1–8, 2020, doi: 10.1002/adfm.202006806.

[3] F. Liu and T. S. Seo, "A controllable self-assembly method for large-scale synthesis of craphene sponges and free-standing craphene films," *Adv. Funct. Mater.*, vol. 20, no. 12, pp. 1930–1936, 2010, doi: 10.1002/adfm.201000287.

[4] C. Simón-herrero, X. Chen, M. Luz, A. Romero, J. L. Valverde, and L. Sánchez-silva, "Linear and crosslinked polyimide aerogels : synthesis and characterization," *Integr. Med. Res.*, vol. 8, no. 3, pp. 2638–2648, 2019, doi: 10.1016/j.jmrt.2019.02.016.

[5] Z. Zhang, Y. Pan, L. Gong, X. Yao, X. Cheng, and Y. Deng, "Mechanically strong polyimide aerogels cross-linked with low-cost polymers," *RSC Adv.*, vol. 11, no. 18, pp. 10827–10835, 2021, doi: 10.1039/d0ra10633j.

[6] S. Ghaffari-Mosanenzadeh *et al.*, "Recent advances in tailoring and improving the properties of polyimide aerogels and their application," *Adv. Colloid Interface Sci.*, vol. 304, no. February, p. 102646, 2022, doi: 10.1016/j.cis.2022.102646.

[7] P. Lin, L. Meng, Y. Huang, and L. Liu, "Synthesis of porous polyurea monoliths assisted by centrifugation as adsorbents for water purification," *Colloids Surfaces A Physicochem. Eng. Asp.*, vol. 506, pp. 87–95, 2016, doi: 10.1016/j.colsurfa.2016.06.017.

[8] N. Zhang, X. Yang, Y. Wang, Y. Qi, P. Cui, and W. Jiang, "Hierarchically porous superhydrophobic sponge for oil-water separation," *J. Water Process Eng.*, vol. 46, no. January, p. 102590, 2022, doi: 10.1016/j.jwpe.2022.102590.

[9] H. Gu, H. Lou, D. Ling, B. Xiang, and Z. Guo, "Polystyrene controlled growth of zerovalent nanoiron/magnetite on a sponge-like carbon matrix towards effective Cr(VI) removal from polluted water," *RSC Adv.*, vol. 6, no. 111, pp. 110134–110145, 2016, doi: 10.1039/c6ra22709k.

[10] L. Liang, Y. Xue, Q. Wu, Y. Dong, and X. Meng, "Self-assembly modification of polyurethane sponge for application in oil/water separation," *RSC Adv.*, vol. 9, no. 69, pp. 40378–40387, 2019, doi: 10.1039/c9ra05855a.

[11] H. Bin Yao *et al.*, "A flexible and highly pressure-sensitive graphene-polyurethane sponge based on fractured microstructure design," *Adv. Mater.*, vol. 25, no. 46, pp. 6692–6698, 2013, doi: 10.1002/adma.201303041.

[12] N. Cao, B. Yang, A. Barras, S. Szunerits, and R. Boukherroub, "Polyurethane sponge functionalized with superhydrophobic nanodiamond particles for efficient oil/water separation," *Chem. Eng. J.*, vol. 307, pp. 319–325, 2017, doi: 10.1016/j.cej.2016.08.105.

[13] Q. Zhu *et al.*, "Robust superhydrophobic polyurethane sponge as a highly

reusable oil-absorption material," *J. Mater. Chem. A*, vol. 1, no. 17, pp. 5386–5393, 2013, doi: 10.1039/c3ta00125c.

[14] W. Wei, J. Liu, Z. Bin Peng, M. Liang, Y. S. Wang, and X. Q. Wang, "Gellable silk fibroin-polyethylene sponge for hemostasis," *Artif. Cells, Nanomedicine Biotechnol.*, vol. 48, no. 1, pp. 28–36, 2020, doi: 10.1080/21691401.2019.1699805.

[15] L. Zhang *et al.*, "Treatment capability of an up-flow anammox column reactor using polyethylene sponge strips as biomass carrier," *J. Biosci. Bioeng.*, vol. 110, no. 1, pp. 72–78, 2010, doi: 10.1016/j.jbiosc.2009.12.005.

[16] A. Alassod, S. R. Islam, A. Farooq, and G. Xu, "Fabrication of polypropylene/lignin blend sponges via thermally induced phase separation for the removal of oil from contaminated water," *SN Appl. Sci.*, vol. 2, no. 9, pp. 1–10, 2020, doi: 10.1007/s42452-020-03372-z.

[17] G. Wang and H. Uyama, "Facile synthesis of flexible macroporous polypropylene sponges for separation of oil and water," *Sci. Rep.*, vol. 6, no. February, pp. 1–6, 2016, doi: 10.1038/srep21265.

[18] A. Karimi, M. Navidbakhsh, and R. Razaghi, "An experimental-finite element analysis on the kinetic energy absorption capacity of polyvinyl alcohol sponge," *Mater. Sci. Eng. C*, vol. 39, no. 1, pp. 253–258, 2014, doi: 10.1016/j.msec.2014.03.009.

[19] M. Guo, Y. Zhang, F. Du, Y. Wu, Q. Zhang, and C. Jiang, "Silver nanoparticles / polydopamine coated polyvinyl alcohol sponge as an effective and recyclable catalyst for reduction of 4-nitrophenol," *Mater. Chem. Phys.*, vol. 225, no. December 2018, pp. 42–49, 2019, doi: 10.1016/j.matchemphys.2018.12.049.

[20] H.-Y. Mi, X. Jing, H. X. Huang, X. F. Peng, and L. S. Turng, "Superhydrophobic Graphene/Cellulose/Silica Aerogel with Hierarchical Structure as Superabsorbers for High Efficiency Selective Oil Absorption and Recovery," *Ind. Eng. Chem. Res.*, vol. 57, no. 5, pp. 1745–1755, 2018, doi: 10.1021/acs.iecr.7b04388.

[21] S. Gupta and N. H. Tai, "Carbon materials as oil sorbents: A review on the synthesis and performance," *J. Mater. Chem. A*, vol. 4, no. 5, pp. 1550–1565, 2016, doi: 10.1039/c5ta08321d.

[22] S. S. Kistler, "Coherent expanded aerogels and jellies [5]," *Nature*, vol. 127, no. 3211. Nature Publishing Group, p. 741, 1931, doi: 10.1038/127741a0.

[23] C. A. García-González, M. Alnaief, and I. Smirnova, "Polysaccharide-based aerogels - Promising biodegradable carriers for drug delivery systems," *Carbohydr. Polym.*, vol. 86, no. 4, pp. 1425–1438, 2011, doi: 10.1016/j.carbpol.2011.06.066.

[24] P. Van De Witte, P. J. Dijkstra, J. W. A. Van Den Berg, and J. Feijen, "Phase separation processes in polymer solutions in relation to membrane formation," *J. Memb. Sci.*, vol. 117, no. 1–2, pp. 1–31, Aug. 1996, doi: 10.1016/0376-7388(96)00088-9.

[25] S. Iannace and C. B. Park, *Biofoams: Science and Applications of Bio-Based Cellular and Porous Materials, CRC Press*. 2015.

[26] A. Barbetta, E. Barigelli, and M. Dentini, "Porous alginate hydrogels: Synthetic methods for tailoring the porous texture," *Biomacromolecules*, vol. 10, no. 8, pp. 2328–2337, 2009, doi: 10.1021/bm900517q.

[27] M. Sjöqvist and P. Gatenholm, “The effect of starch composition on structure of foams prepared by microwave treatment,” *J. Polym. Environ.*, vol. 13, no. 1, pp. 29–37, 2005, doi: 10.1007/s10924-004-1213-8.

[28] H. Zhang *et al.*, “Versatile fabrication of a superhydrophobic and ultralight cellulose-based aerogel for oil spillage clean-up,” *Phys. Chem. Chem. Phys.*, vol. 18, no. 40, pp. 28297–28306, 2016, doi: 10.1039/c6cp04932j.

[29] M. Nofar, A. Ameli, and C. B. Park, “A novel technology to manufacture biodegradable polylactide bead foam products,” *Mater. Des.*, vol. 83, pp. 413–421, 2015, doi: 10.1016/j.matdes.2015.06.052.

[30] M. Nofar, W. Zhu, and C. B. Park, “Effect of dissolved CO2 on the crystallization behavior of linear and branched PLA,” *Polymer (Guildf).*, vol. 53, no. 15, pp. 3341–3353, 2012, doi: 10.1016/j.polymer.2012.04.054.

[31] B. Li, G. Zhao, G. Wang, L. Zhang, and J. Gong, “Fabrication of high-expansion microcellular PLA foams based on pre-isothermal cold crystallization and supercritical CO2 foaming,” *Polym. Degrad. Stab.*, vol. 156, pp. 75–88, 2018, doi: 10.1016/j.polymdegradstab.2018.08.009.

[32] S. A. Poursamar, J. Hatami, A. N. Lehner, C. L. Da Silva, F. C. Ferreira, and A. P. M. Antunes, “Gelatin porous scaffolds fabricated using a modified gas foaming technique: Characterisation and cytotoxicity assessment,” *Mater. Sci. Eng. C*, vol. 48, pp. 63–70, 2015, doi: 10.1016/j.msec.2014.10.074.

[33] I. Smirnova and P. Gurikov, “Aerogel production: Current status, research directions, and future opportunities,” *J. Supercrit. Fluids*, vol. 134, no. October 2017, pp. 228–233, 2018, doi: 10.1016/j.supflu.2017.12.037.

[34] S. S. Silva, A. R. C. Duarte, A. P. Carvalho, J. F. Mano, and R. L. Reis, “Green processing of porous chitin structures for biomedical applications combining ionic liquids and supercritical fluid technology,” *Acta Biomater.*, vol. 7, no. 3, pp. 1166–1172, 2011, doi: 10.1016/j.actbio.2010.09.041.

[35] J. J. Yoon and T. G. Park, “Degradation behaviors of biodegradable macroporous scaffolds prepared by gas foaming of effervescent salts,” *J. Biomed. Mater. Res.*, vol. 55, no. 3, pp. 401–408, 2001, doi: 10.1002/1097-4636(20010605)55:3<401::AID-JBM1029>3.0.CO;2-H.

[36] H. R. Lin, C. J. Kuo, C. Y. Yang, S. Y. Shaw, and Y. J. Wu, “Preparation of macroporous biodegradable PLGA scaffolds for cell attachment with the use of mixed salts as porogen additives,” *J. Biomed. Mater. Res.*, vol. 63, no. 3, pp. 271–279, 2002, doi: 10.1002/jbm.10183.

[37] Y. S. Nam, J. J. Yoon, and T. G. Park, “A novel fabrication method of macroporous biodegradable polymer scaffolds using gas foaming salt as a porogen additive,” *J. Biomed. Mater. Res.*, vol. 53, no. 1, pp. 1–7, 2000, doi: 10.1002/(SICI)1097-4636(2000)53:1<1::AID-JBM1>3.0.CO;2-R.

[38] A. G. Mikos *et al.*, “Preparation and characterization of poly(l-lactic acid) foams,” *Polymer (Guildf).*, vol. 35, no. 5, pp. 1068–1077, 1994, doi: 10.1016/0032-3861(94)90953-9.

[39] F. Fischer, A. Rigacci, R. Pirard, S. Berthon-Fabry, and P. Achard, “Cellulose-

based aerogels," *Polymer (Guildf).*, vol. 47, no. 22, pp. 7636–7645, Oct. 2006, doi: 10.1016/j.polymer.2006.09.004.

[40] A. Zaman, F. Huang, M. Jiang, W. Wei, and Z. Zhou, "Preparation , Properties , and Applications of Natural Cellulosic Aerogels : A Review," *Energy Built Environ.*, vol. 1, no. 1, pp. 60–76, 2020, doi: 10.1016/j.enbenv.2019.09.002.

[41] S. Zhang, J. Feng, J. Feng, and Y. Jiang, "Formation of enhanced gelatum using ethanol/water binary medium for fabricating chitosan aerogels with high specific surface area," *Chem. Eng. J.*, vol. 309, pp. 700–707, Feb. 2017, doi: 10.1016/j.cej.2016.10.098.

[42] G. Duan *et al.*, "Ultralight, soft polymer sponges by self-assembly of short electrospun fibers in colloidal dispersions," *Adv. Funct. Mater.*, vol. 25, no. 19, pp. 2850–2856, 2015, doi: 10.1002/adfm.201500001.

[43] N. Reddy, R. Reddy, and Q. Jiang, "Crosslinking biopolymers for biomedical applications," *Trends Biotechnol.*, vol. 33, no. 6, pp. 362–369, Jun. 2015, doi: 10.1016/J.TIBTECH.2015.03.008.

[44] K. Liu, L. Chen, L. Huang, and Y. Lai, "Evaluation of ethylenediamine-modified nanofibrillated cellulose/chitosan composites on adsorption of cationic and anionic dyes from aqueous solution," *Carbohydr. Polym.*, vol. 151, pp. 1115–1119, Oct. 2016, doi: 10.1016/j.carbpol.2016.06.071.

[45] J. Liu, S. Willför, and C. Xu, "A review of bioactive plant polysaccharides: Biological activities, functionalization, and biomedical applications," *Bioact. Carbohydrates Diet. Fibre*, vol. 5, no. 1, pp. 31–61, 2015, doi: 10.1016/j.bcdf.2014.12.001.

[46] V. López Durán, J. Erlandsson, L. Wågberg, and P. A. Larsson, "Novel, Cellulose-Based, Lightweight, Wet-Resilient Materials with Tunable Porosity, Density, and Strength," *ACS Sustain. Chem. Eng.*, vol. 6, no. 8, pp. 9951–9957, 2018, doi: 10.1021/acssuschemeng.8b01165.

[47] S. Jiang, S. Agarwal, and A. Greiner, "Low-Density Open Cellular Sponges as Functional Materials," *Angew. Chemie - Int. Ed.*, vol. 56, no. 49, pp. 15520–15538, 2017, doi: 10.1002/anie.201700684.

[48] A. Mumtaz, I. Ahmed, and N. Ahmad, "Sources , structure , properties and health benefits of plant gums : A review," *Int. J. Biol. Macromol.*, vol. 135, pp. 46–61, 2019, doi: 10.1016/j.ijbiomac.2019.05.103.

[49] V. D. Prajapati, G. K. Jani, B. S. Zala, and T. A. Khutliwala, "An insight into the emerging exopolysaccharide gellan gum as a novel polymer," *Carbohydr. Polym.*, vol. 93, no. 2, pp. 670–678, 2013, doi: 10.1016/j.carbpol.2013.01.030.

[50] P. Kanmani and J. W. Rhim, "Properties and characterization of bionanocomposite films prepared with various biopolymers and ZnO nanoparticles," *Carbohydr. Polym.*, vol. 106, no. 1, pp. 190–199, 2014, doi: 10.1016/j.carbpol.2014.02.007.

[51] E. Nazarzadeh Zare, P. Makvandi, A. Borzacchiello, F. R. Tay, B. Ashtari, and V. T. V. Padil, "Antimicrobial gum bio-based nanocomposites and their industrial and biomedical applications," *Chem. Commun.*, vol. 55, no. 99, pp. 14871–14885, 2019, doi: 10.1039/c9cc08207g.

[52] V. T. P. Vinod and R. B. Sashidhar, “Surface morphology, chemical and structural assignment of gum Kondagogu (Cochlospermum gossypium DC.): An exudate tree gum of India,” *Indian J. Nat. Prod. Resour.*, vol. 1, no. 2, pp. 181–192, 2010.

[53] S. Malik, A. Kumar, and M. Ahuja, “Synthesis of gum kondagogu-g-poly(N-vinyl-2-pyrrolidone) and its evaluation as a mucoadhesive polymer,” *Int. J. Biol. Macromol.*, vol. 51, no. 5, pp. 756–762, 2012, doi: 10.1016/j.ijbiomac.2012.07.009.

[54] V. G. M. Naidu *et al.*, “Polyelectrolyte complexes of gum kondagogu and chitosan, as diclofenac carriers,” *Carbohydr. Polym.*, vol. 76, no. 3, pp. 464–471, 2009, doi: 10.1016/j.carbpol.2008.11.010.

[55] A. J. Kora, R. B. Sashidhar, and J. Arunachalam, “Gum kondagogu (Cochlospermum gossypium): A template for the green synthesis and stabilization of silver nanoparticles with antibacterial application,” *Carbohydr. Polym.*, vol. 82, no. 3, pp. 670–679, 2010, doi: 10.1016/j.carbpol.2010.05.034.

[56] G. B. Reddy, A. Madhusudhan, D. Ramakrishna, D. Ayodhya, M. Venkatesham, and G. Veerabhadram, “Green chemistry approach for the synthesis of gold nanoparticles with gum kondagogu: characterization, catalytic and antibacterial activity,” *J. Nanostructure Chem.*, vol. 5, no. 2, pp. 185–193, 2015, doi: 10.1007/s40097-015-0149-y.

[57] L. Rastogi, D. Karunasagar, R. B. Sashidhar, and A. Giri, “Peroxidase-like activity of gum kondagogu reduced/stabilized palladium nanoparticles and its analytical application for colorimetric detection of glucose in biological samples,” *Sensors Actuators, B Chem.*, vol. 240, pp. 1182–1188, 2017, doi: 10.1016/j.snb.2016.09.066.

[58] P. Saravanan, V. T. P. Vinod, B. Sreedhar, and R. B. Sashidhar, “Gum kondagogu modified magnetic nano-adsorbent: An efficient protocol for removal of various toxic metal ions,” *Mater. Sci. Eng. C*, vol. 32, no. 3, pp. 581–586, 2012, doi: 10.1016/j.msec.2011.12.015.

[59] A. Venkateshaiah *et al.*, “Alkenyl succinic anhydride modified tree-gum kondagogu: A bio-based material with potential for food packaging,” *Carbohydr. Polym.*, vol. 266, p. 118126, Aug. 2021, doi: 10.1016/j.carbpol.2021.118126.

[60] V. V. T. Padil, C. Senan, S. Wacławek, and M. Černík, “Electrospun fibers based on Arabic, karaya and kondagogu gums,” *Int. J. Biol. Macromol.*, vol. 91, pp. 299–309, 2016, doi: 10.1016/j.ijbiomac.2016.05.064.

[61] M. Ranjbar-Mohammadi, M. P. Prabhakaran, S. H. Bahrami, and S. Ramakrishna, “Gum tragacanth/poly(l-lactic acid) nanofibrous scaffolds for application in regeneration of peripheral nerve damage,” *Carbohydr. Polym.*, vol. 140, pp. 104–112, 2016, doi: 10.1016/j.carbpol.2015.12.012.

[62] K. R. Aadil, A. Nathani, C. S. Sharma, N. Lenka, and P. Gupta, “Investigation of poly(vinyl) alcohol-gellan gum based nanofiber as scaffolds for tissue engineering applications,” *J. Drug Deliv. Sci. Technol.*, vol. 54, no. September, p. 101276, 2019, doi: 10.1016/j.jddst.2019.101276.

[63] L. Parwani, M. Bhatnagar, A. Bhatnagar, V. Sharma, and V. Sharma, “Gum acacia-PVA hydrogel blends for wound healing,” *Vegetos*, vol. 32, no. 1, pp. 78–91, 2019, doi: 10.1007/s42535-019-00009-4.

[64] K. K. Mali, S. C. Dhawale, and R. J. Dias, “Synthesis and characterization of hydrogel films of carboxymethyl tamarind gum using citric acid,” *Int. J. Biol. Macromol.*, vol. 105, pp. 463–470, 2017, doi: 10.1016/j.ijbiomac.2017.07.058.

[65] S. Kundu, A. Das, A. Basu, D. Ghosh, P. Datta, and A. Mukherjee, “Carboxymethyl guar gum synthesis in homogeneous phase and macroporous 3D scaffolds design for tissue engineering,” *Carbohydr. Polym.*, vol. 191, no. October 2017, pp. 71–78, 2018, doi: 10.1016/j.carbpol.2018.03.007.

[66] D. Sakloetsakun *et al.*, “Chitosan–gum arabic polyelectrolyte complex films: physicochemical, mechanical and mucoadhesive properties,” *Pharm. Dev. Technol.*, vol. 21, no. 5, pp. 590–599, 2016, doi: 10.3109/10837450.2015.1035727.

[67] S. Sethi, B. S. Kaith, M. Kaur, N. Sharma, and S. Khullar, “Study of a cross-linked hydrogel of Karaya gum and Starch as a controlled drug delivery system,” *J. Biomater. Sci. Polym. Ed.*, vol. 30, no. 18, pp. 1687–1708, 2019, doi: 10.1080/09205063.2019.1659710.

[68] V. V. Alange, R. P. Birajdar, and R. V. Kulkarni, “Functionally modified polyacrylamide-graft-gum karaya pH-sensitive spray dried microspheres for colon targeting of an anti-cancer drug,” *Int. J. Biol. Macromol.*, vol. 102, pp. 829–839, 2017, doi: 10.1016/j.ijbiomac.2017.04.023.

[69] S. Lankalapalli and R. M. Kolapalli, “Biopharmaceutical evaluation of diclofenac sodium controlled release tablets prepared from gum karaya-chitosan polyelectrolyte complexes,” *Drug Dev. Ind. Pharm.*, vol. 38, no. 7, pp. 815–824, 2012, doi: 10.3109/03639045.2011.630006.

[70] R. Y. Tsai *et al.*, “Chitosan/pectin/gum Arabic polyelectrolyte complex: Process-dependent appearance, microstructure analysis and its application,” *Carbohydr. Polym.*, vol. 101, no. 1, pp. 752–759, 2014, doi: 10.1016/j.carbpol.2013.10.008.

[71] M. Li *et al.*, “A Bioinspired Alginate-Gum Arabic Hydrogel with Micro-/Nanoscale Structures for Controlled Drug Release in Chronic Wound Healing,” *ACS Appl. Mater. Interfaces*, vol. 9, no. 27, pp. 22160–22175, 2017, doi: 10.1021/acsami.7b04428.

[72] Y. Du *et al.*, “Development of antimicrobial packaging materials by incorporation of gallic acid into Ca 2 + crosslinking konjac glucomannan / gellan gum fi lms,” *Int. J. Biol. Macromol.*, vol. 137, pp. 1076–1085, 2019, doi: 10.1016/j.ijbiomac.2019.06.079.

[73] H. Lee, B. Rukmanikrishnan, and J. Lee, “Rheological , morphological , mechanical , and water-barrier properties of agar / gellan gum / montmorillonite clay composite fi lms,” *Int. J. Biol. Macromol.*, vol. 141, pp. 538–544, 2019, doi: 10.1016/j.ijbiomac.2019.09.021.

[74] B. Rukmanikrishnan, F. Rigana, M. Ismail, R. Kumar, S. Soo, and J. Lee, “Blends of gellan gum / xanthan gum / zinc oxide based nanocomposites for packaging application : Rheological and antimicrobial properties,” *Int. J. Biol. Macromol.*, vol. 148, pp. 1182–1189, 2020, doi: 10.1016/j.ijbiomac.2019.11.155.

[75] L. Ge, X. Li, R. Zhang, T. Yang, X. Ye, and D. Li, “Development and characterization of dialdehyde xanthan gum crosslinked gelatin based edible fi lms incorporated with amino-functionalized montmorillonite,” *Food Hydrocoll.*, vol. 51, pp.

129–135, 2015, doi: 10.1016/j.foodhyd.2015.04.029.

[76] M. Alizadeh-sani, J. Rhim, M. Azizi-lalabadi, M. Hemmati-dinarvand, and A. Ehsani, “Preparation and characterization of functional sodium caseinate / guar gum / TiO 2 / cumin essential oil composite film,” *Int. J. Biol. Macromol.*, vol. 145, pp. 835–844, 2020, doi: 10.1016/j.ijbiomac.2019.11.004.

[77] X. Tian, G. Chengcheng, F. Xiao, H. Meigui, Y. Yuling, and S. Xinchun, “Cinnamon and clove essential oils to improve physical , thermal and antimicrobial properties of chitosan-gum arabic polyelectrolyte complexed fi lms,” *Carbohydr. Polym.*, vol. 217, no. February, pp. 116–125, 2019, doi: 10.1016/j.carbpol.2019.03.084.

[78] Z. Tahsiri, H. Mirzaei, S. Mohammad, and H. Hosseini, “Gum arabic improves the mechanical properties of wild almond protein fi lm,” *Carbohydr. Polym.*, vol. 222, no. June, p. 114994, 2019, doi: 10.1016/j.carbpol.2019.114994.

[79] A. Amalraj, J. T. Haponiuk, S. Thomas, and S. Gopi, “Preparation, characterization and antimicrobial activity of polyvinyl alcohol/gum arabic/chitosan composite films incorporated with black pepper essential oil and ginger essential oil,” *Int. J. Biol. Macromol.*, vol. 151, pp. 366–375, 2020, doi: 10.1016/j.ijbiomac.2020.02.176.

[80] M. Qianyun, D. Lin, Y. Yang, and W. Lijuan, “Rheology of film-forming solutions and physical properties of tara gum film reinforced with polyvinyl alcohol (PVA),” *Food Hydrocoll.*, vol. 63, pp. 677–684, 2017, doi: 10.1016/j.foodhyd.2016.10.009.

[81] J. Antoniou, F. Liu, H. Majeed, and F. Zhong, “Characterization of tara gum edible films incorporated with bulk chitosan and chitosan nanoparticles : A comparative study,” *Food Hydrocoll.*, vol. 44, pp. 309–319, 2015, doi: 10.1016/j.foodhyd.2014.09.023.

[82] V. Trinetta, C. N. Cutter, and J. D. Floros, “Effects of ingredient composition on optical and mechanical properties of pullulan film for food-packaging applications,” *LWT - Food Sci. Technol.*, vol. 44, no. 10, pp. 2296–2301, 2011, doi: 10.1016/j.lwt.2011.07.015.

[83] C. Arismendi *et al.*, “Optimization of physical properties of xanthan gum / tapioca starch edible matrices containing potassium sorbate and evaluation of its antimicrobial effectiveness,” *LWT - Food Sci. Technol.*, vol. 53, no. 1, pp. 290–296, 2013, doi: 10.1016/j.lwt.2013.01.022.

[84] A. Kurt, O. Said, and F. Tornuk, “Effect of xanthan and locust bean gum synergistic interaction on characteristics of biodegradable edible film,” *Int. J. Biol. Macromol.*, vol. 102, pp. 1035–1044, 2017, doi: 10.1016/j.ijbiomac.2017.04.081.

[85] Y. Tang, X. Zhang, R. Zhao, D. Guo, and J. Zhang, “Preparation and properties of chitosan / guar gum / nanocrystalline cellulose nanocomposite fi lms,” *Carbohydr. Polym.*, vol. 197, no. January, pp. 128–136, 2018, doi: 10.1016/j.carbpol.2018.05.073.

[86] A. Bahrami, R. Rezaei, M. Sowti, B. Ghanbarzadeh, and R. Salehi, “Physico-mechanical and antimicrobial properties of tragacanth / hydroxypropyl methylcellulose / beeswax edible films reinforced with silver nanoparticles,” *Int. J. Biol. Macromol.*, vol. 129, pp. 1103–1112, 2019, doi: 10.1016/j.ijbiomac.2018.09.045.

[87] P. Bidarakatte Krishnappa and V. Badalamoole, “Karaya gum-graft-poly(2-

(dimethylamino)ethyl methacrylate) gel: An efficient adsorbent for removal of ionic dyes from water," *Int. J. Biol. Macromol.*, vol. 122, pp. 997–1007, 2018, doi: 10.1016/j.ijbiomac.2018.09.038.

[88] H. Mittal, A. Maity, and S. S. Ray, "Gum karaya based hydrogel nanocomposites for the effective removal of cationic dyes from aqueous solutions," *Appl. Surf. Sci.*, vol. 364, no. 2016, pp. 917–930, 2016, doi: 10.1016/j.apsusc.2015.12.241.

[89] B. K. Preetha and V. Badalamoole, "Modification of Karaya gum by graft copolymerization for effective removal of anionic dyes," *Sep. Sci. Technol.*, vol. 54, no. 16, pp. 2638–2652, 2019, doi: 10.1080/01496395.2018.1549079.

[90] H. Mittal, A. Maity, and S. S. Ray, "Synthesis of co-polymer-grafted gum karaya and silica hybrid organic-inorganic hydrogel nanocomposite for the highly effective removal of methylene blue," *Chem. Eng. J.*, vol. 279, pp. 166–179, 2015, doi: 10.1016/j.cej.2015.05.002.

[91] A. M. Elbedwehy and A. M. Atta, "Novel superadsorbent highly porous hydrogel based on arabic gum and acrylamide grafts for fast and efficient methylene blue removal," *Polymers (Basel).*, vol. 12, no. 2, 2020, doi: 10.3390/polym12020338.

[92] V. Hasija, K. Sharma, V. Kumar, S. Sharma, and V. Sharma, "Green synthesis of agar / Gum Arabic based superabsorbent as an alternative for irrigation in agriculture," *Vacuum*, vol. 157, no. September, pp. 458–464, 2018, doi: 10.1016/j.vacuum.2018.09.012.

[93] A. Akkineni, T. Ahlfeld, A. Funk, A. Waske, A. Lode, and M. Gelinsky, "Highly Concentrated Alginate-Gellan Gum Composites for 3D Plotting of Complex Tissue Engineering Scaffolds," *Polymers (Basel).*, vol. 8, no. 5, p. 170, 2016, doi: 10.3390/polym8050170.

[94] D. S. Seeli, S. Dhivya, N. Selvamurugan, and M. Prabaharan, "Guar gum succinate-sodium alginate beads as a pH-sensitive carrier for colon-specific drug delivery," *Int. J. Biol. Macromol.*, vol. 91, pp. 45–50, 2016, doi: 10.1016/j.ijbiomac.2016.05.057.

[95] B. Singh, A. Kumar, and Rohit, "Synthesis and characterization of alginate and sterculia gum based hydrogel for brain drug delivery applications," *International Journal of Biological Macromolecules*, vol. 148. pp. 248–257, 2020, doi: 10.1016/j.ijbiomac.2020.01.147.

[96] A. L. de Farias, A. B. Meneguin, H. da Silva Barud, and F. L. Brighenti, "The role of sodium alginate and gellan gum in the design of new drug delivery systems intended for antibiofilm activity of morin," *Int. J. Biol. Macromol.*, vol. 162, pp. 1944–1958, 2020, doi: 10.1016/j.ijbiomac.2020.08.078.

[97] M. Chintha, S. R. Obireddy, P. Areti, S. Marata Chinna Subbarao, C. R. Kashayi, and J. K. Rapoli, "Sodium alginate/locust bean gum-g-methacrylic acid IPN hydrogels for 'simvastatin' drug delivery," *J. Dispers. Sci. Technol.*, vol. 41, no. 14, pp. 2192–2202, 2019, doi: 10.1080/01932691.2019.1677247.

[98] D. Huang, Q. Quan, Y. Zheng, W. Tang, Z. Zhang, and X. Qiang, "Dual-network design to enhance the properties of agar aerogel adsorbent by incorporating in situ ion cross-linked alginate," *Environ. Chem. Lett.*, vol. 18, no. 1, pp. 251–255, 2020, doi: 10.1007/s10311-019-00932-7.

[99] K. Dong, K. Xu, N. Wei, Y. Fang, and Z. Qin, “Three-dimensional porous sodium alginate/gellan gum environmentally friendly aerogel: preparation, characterization, adsorption, and kinetics studies,” *Chem. Eng. Res. Des.*, 2022, doi: 10.1016/j.cherd.2022.01.027.